The effect of GABRB3 polymorphisms on brain function and structure in healthy male volunteers assessed by multimodal imaging

The Effect of GABRB3 Polymorphisms on Brain Function and Structure in Healthy Male Volunteers Assessed by Multimodal Imaging

DISSERTATION

to obtain the degree of Doctor at Maastricht University
and Université de Liège,
on the authorities of the Rectores Magnifici,
Prof. dr. Rianne M. Letschert and Professor Albert Corhay
in accordance with the decision of the Board of Deans,
to be defended in public
on Wednesday 12th of July 2017 at 16.00 hours in Masstricht

by

Jorge Andrés Arrubla Martínez

Supervisors

Prof. Dr. N. Jon Shah, Maastricht University

Prof. Dr. André Luxen, Université de Liège

Co-supervisor

Prof. Dr. Irene Neuner, Forschungszentrum Jülich GmbH

Assessment Committee

Ir. Dr. Christophe Phillips, Université de Liège (Chairman)

Prof. Dr. Eric Salmon, Université de Liège

Prof. Dr. Koen Schruers, Maastricht University

Prof. Dr. Kamil Uludag, Maastricht University

The work presented in this thesis was funded by the EU within the PEOPLE Programme (FP7): Initial Training Networks (FP7-PEOPLE-ITN-2008), Grant Agreement No. 238593 NEUROPHYSICS, in which Maastricht University, Université de Liège, Forschungszentrum Jülich GmbH and GlaxoSmithKline Ltd. were network partners. The PhD was mainly conducted at the Forschungszentrum Jülich.

With the greatest admiration for my wife Carolina, my father Jorge and my uncle Álvaro.

Abstract

The combination of genetic information and data provided by magnetic resonance imaging (MRI) techniques is commonly referred as *imaging genetics*, an interesting approach with the potential to investigate the mechanisms linked to genetic variation. The gene that codifies the beta–3 subunit of the GABA-A receptor (GABRB3) is of great interest due to its early expression during embryonic stages, its role in neurodevelopment and its relationship with neurologic diseases such as epilepsy and autism. In order to investigate the possible effects of GABRB3 on brain structure and function, a sample of 63 healthy young male volunteers was measured using multimodal imaging techniques including: structural imaging, diffusion-weighted imaging, resting state fMRI, magnetic resonance spectroscopy and electroencephalography (EEG). Inter-group differences in brain function and structure were tested on the basis of frequency and prevalence of G2, the most frequent allele of GABRB3 in the population. The results showed that there were significant differences in diffusion parameters among the different subgroups on the basis of the G2 allelic prevalence and frequency. Non-carrier volunteers exhibited significantly increased axial diffusivity in the right superior longitudinal fasciculus, right corticospinal tract and body of the corpus callosum compared to homozygote carriers of the G2 allele. Initially, such differences in diffusion parameters were only evident for axial diffusivity, although when a focused region-of-interest analysis was performed, differences in fractional anisotropy and mean diffusivity emerged. A statistically significant higher *delta* voltage in the global activity of EEG was also found in homozygote carriers of the G2 allele compared to heterozygote carries. The results presented here confirm the importance of the expression of GABRB3 gene in brain structure, particularly in defining the features of the white matter microstructure. Differences in EEG were also found to depend on the frequency of the G2 allele, which confirms the conclusions of previous investigations in which the expression of GABRB3 was crucial for the activity of EEG.

Résumé

La combinaison de l'information génétique et les données obtenues par les différentes techniques d'imagerie par résonance magnétique (IRM), est communément appelée *imagerie génétique*. Cette dernière représente une approche particulièrement appropriée pour l'étude des mécanismes liés à la variation génétique. Le gène qui codifie le beta-3 sous-unité du récepteur GABA-A (GABRB3) est d'un très grand intérêt en raison de son expression précoce au cours des étapes embryonnaires, son rôle dans le développement neurologique ainsi que sa relation avec les maladies neurologiques telles que l'épilepsie et l'autisme. Afin d'étudier les possibles effets du gène GABRB3 sur la structure et le fonctionnement du cerveau, un échantillon de 63 jeunes volontaires sains et de sexe masculin a été mesuré en utilisant des techniques d'imagerie multimodales, comprenant: l'imagerie structurelle, l'IRM de diffusion, l'imagerie fonctionnelle au repos, la spectroscopie par résonance magnétique nucléaire et l'électroencéphalographie (EEG). Des différences structurelles et fonctionnelles du cerveau entre les groupes ont été évaluées en se basant sur la fréquence et la prévalence du G2, l'allèle du gène GABRB3 le plus fréquent dans la population. Les résultats obtenus ont montré qu'il y avait des différences significatives dans les paramètres de diffusions entre les différents sous-groupes dépendant principalement de la prévalence de l'allèle G2 et de sa fréquence. Les volontaires non porteurs présentaient une augmentation significative de la diffusion axiale dans le fascicule longitudinal supérieur droit, le faisceau corticospinal droit et le corps calleux comparé aux porteurs homozygotes de l'allèle G2. Initialement, une telle différence dans les paramètres de diffusion était observée que pour une diffusion axiale, bien que lorsqu'une analyse de région d'intérêt bien ciblée est effectuée, des différences apparaissent dans la fraction anisotropique et la diffusion moyenne. Une augmentation statistiquement significative de la différence de tension dans l'activité globale *delta* de l'EEG a été également observée à travers les porteurs homozygotes de l'allèle G2 comparé aux porteurs hétérozygotes. Les résultats présentés dans cette étude confirment l'importance de l'expression du gène GABRB3 dans la structure du cerveau, en particulier lors de la définition des caractéristiques microstructurales de la matière blanche. Les différences en EEG dépendent également de la fréquence de l'allèle G2, ce qui confirme les conclusions des études précédentes concernant l'expression du gène GABRB3 comme étant cruciale pour l'activité de l'EEG.

Curriculum Vitae

Name: Jorge Andrés Arrubla Martínez

Date and place of birth: 4th of June 1986, Medellín, Colombia

1997 – 2002: Secondary education. Colegio San José de Calasanz , Medellín, Colombia. Grade achieved: "Bachiller Académico".

2003 – 2010: Study of human medicine. Universidad de Antioquia, Colombia. Grade achieved: "Médico y Cirujano".

2011 – 2015: PhD Candidate. Institute for Medicine and Neuroscience 4, Research Centre Jülich, Germany.

2012: Recognition of the university degree to equivalet in Spain: "Licenciado en Medicina".

2012: Recognition of the university degree to equivalent in Germany: "Arzt", with medical license.

2015: Degree obtained: "Doktor der Medizin" from the RWTH Aachen University, Germany.

Acknowledgements

The help from Dr. Desmond Tse and Dr. Ezequiel Farrher during the acquisition and analysis of the spectroscopy data is gratefully acknowledged. Dr. Farrher also helped with the performing of additional corrections to the diffusion data.

The author would like to thank Mr. David Hahn, Ms. Christin Amkreutz and Ms. Johanna Strippelmann for their help during the recruitment of the volunteers and the acquisition of the data.

The help from Prof. Dr. Thomas Eggermann, Prof. Dr. Klaus Zerres and the Institute of Human Genetics of the RWTH Aachen University is gratefully acknowledged. They performed the analysis of the blood samples.

The author gratefully acknowledges the help from Prof. Dr. Irene Neuner in the planning of the project and the general support given.

The supervision of Prof. André Luxen is gratefully acknowledged.

The author would like to acknowledge Prof. N. Jon Shah for the general support given during the entire production of this study.

The support from Christophe Phillips, Peter de Weerd and Ermo Daniels during all the administrative processes is gratefully acknowledged.

Contents

Chapter 1

Introduction

1.1 The evolution of genetics and its related concepts

The earliest notion of heredity was held by Hippocrates. The first observations suggested that the features of an individual could be inherited, and such a concept became a matter of discussion that puzzled a number of thinkers such as Aristotle and Darwin. There was traditionally some resistance to these ideas; Darwin, for example, formulated a heredity theory, namely 'pangenesis', which was generally not well received by the scientific community of the time (Sturtevant 1965). The work of Mendel with peas in 1866, which was undoubtedly a breakthrough in the history of genetics, remained utterly ignored until 1900, sixteen years after his death in 1884, when it was rescued from oblivion. In his work, the notion of genes appearing in pairs was implied, although not completely explained. From that point, a group of scientists interested in heredity started to replicate and extend the experiments of Mendel, and over time the introduction of a new terminology became a necessity. The concept of *genetics* was first introduced in 1902 by William Bateson (Sturtevant 1965). Bateson also introduced the concepts of *zygote*, *homozygote*, *heterozygote* and *allele*; the related terms *genotype*, *phenotype* and *gene* were later introduced in 1909 by Wilhelm Johannsen (Sturtevant 1965). The term *gene* gained notoriety, and was initially equivalent to the concept of *factor* as formulated in the work of Batenson, or *Merkmal* (from the German, translated in English as *attribute*), as it was formulated in the work of Mendel. Subsequent studies demonstrated that the genes were organised in chromosomes, and with the work of Walter Sutton

in 1903, the role of chromosomes in segregation became clear, also introducing the notion of randomness to heredity.

Great advances were made in the field of genetics with the study of the Drosophila fly; it was particularly helpful in discovering the role of chromosomes in sex determination. These studies also permitted a better understanding of how the genes are present in pairs of both paternal and maternal origin, i.e. *alleles*. An improved theory of how the alleles exhibit dominance, co-dominance and recessiveness was formulated together with the idea of multiple alleles (Sturtevant 1965).

The concept of genetic variation was rapidly linked to the study of evolution, although this was related more to the changes in populations rather than in individuals. Nowadays it is accepted that variation in alleles occurs both within and among populations, moreover it became possible to recognise the genetic variation by examining phenotypes, traits and even enzymes and proteins. Ultimately, genetic variation was demonstrated to be caused by variation in the order of bases in the nucleotides of the genes. Genetic studies have benefited from the new technologies which permit deoxyribonucleic acid (DNA) sequencing and from the successful characterisation of the nucleotide base-pair order that represents the human genome (Lander et al. 2001; Venter et al. 2001).

The discussion about the genetic variation gave rise to the concepts of *phenotype* and *genotype*. The phenotype refers to the observable characteristics or traits of an individual, such as its morphology, development, biochemical or physiological properties, behaviour, and products of behaviour. On the other hand, the genotype refers to the inherited instructions that an individual carries within the genetic code. This genotype-phenotype distinction was initially proposed by Wilhelm Johannsen in 1911 in order to provide clarity in the difference between the heredity of an individual and what such heredity actually produces in terms of observable characteristics. In the case where there are two or more clearly different phenotypes in a species, such a characteristic is defined as polymorph, and in terms of genotype implies the existence of polymorphic genes. It was suggested that the phenotypes are controlled by the expression of 'discrete genes', which produce characteristics and exclude their counterpart; on the other hand continuous traits are those that have a range of phenotypic variation. Francis Galton and Karl Pearson investigated largely the discrete traits, and were the

pioneers in demonstrating that a number of quantitative traits, such as height, were inherited. Moreover, they invented the statistical tools of correlation and regression analysis in order to study the inheritance of traits that fall into smooth distributions.

The study of mutations was the driving force of genetics in the twentieth century. The process by which mutation produces alleles that differ from the 'wild-type' permitted the identification of how several aspects of the phenotype are under genetic control. This process would be ultimately responsible for the evolution process as described by Darwin. Mutation processes could be beneficial in some species in which a better adaptation to the environment is developed. On the other hand, mutations could also be fatal in the cases where they give rise to individuals not able to survive with their existing genetic configuration. Mutations are responsible in humans for a large number of genetic diseases. Some of the first studies of heredity in human disease were precisely those related to metabolic diseases. The first description of an inherited disease was provided by British physician Archibald Edward Garrod. He concluded that alkaptonuria was an inherited condition in which an alternative pathway in the metabolism of nitrogenous materials led to the excretion of homogentisic acid. This work was rapidly recognised as of great magnitude, and led later to the conclusion that genes are responsible for the production of enzymes (and also proteins), and that any disturbance in the genetic material could result in a change of specificity and/or effectiveness of the enzymes. The event in which a mutant gene occasionally produces an abnormal, and therefore dysfunctional protein (*missense* variant), is a well demonstrated fact (Cooper et al. 2013). In some cases such mutations result in relatively mild abnormalities, leading to diseases with less severe symptoms; in other cases, the disruption of the protein integrity is of such magnitude that all functionality is lost, and eventually leads to 'non-viable' individuals, a situation often referred as 'lethal mutation', highlighting the fact that such situation is incompatible with life. From this perspective, one might assert that the smallest variation in a gene could result in the production of a protein with different functional profiles when compared to the 'original' ones, even though the main function remains.

Another important development in the field of genetics was the explanation of the mechanisms of DNA and ribonucleic acid (RNA) synthesis, described in 1956 by Severo Ochoa and his student Arthur Kornberg, a work for which they were

awarded with the Nobel Prize in Physiology–Medicine in 1959 (Karlson 1960). This work permitted the understanding of how a messenger RNA is translated into the amino acid sequence of a protein in the ribosomes of the cells. With this development it became clear that the flow of information from the genes determines the protein composition and thereby the functions of the cell.

1.2 Neurogenetics

The term *neurogenetics* refers to the study of genetics in the development, structure and function of the nervous system. It is based on the observation that the nervous system of individuals might not be identical despite belonging to the same species. Based on the evidence provided by neurogenetic studies, it is possible now to assert that genetic expression is determinant of the structure and function of brain, as in many other organs.

The brain is the most complex of all organs. Its individual cells are quite different from each other in their transcriptomes, proteomes, and phenotypes and also in the thousands of connections and interactions (Figure 1.1). Dissimilar cellular conditions result in differences on the biochemical and epigenetic levels (Gottesman & Gould 2003). Anatomic aspects of the brain have been found to be determined by diverse genetic factors. Studies in non-human primates demonstrated the existence of genetic control over morphological variability of primary sulci and gyri (Kochunov et al. 2010b). Other features of the brain, such as size, have been found to be determined by genetic factors (Bartley et al. 1997). In an interesting study by Bryant et al. (2011), the researchers took a step further, and described a neuroanatomical phenotype of Klinefelter syndrome, a genetic disorder characterised by a supernumerary X chromosome.

The notion that the genetic factors determine the function and structure of brain was not completely unfamiliar in the beginning of neurogenetics. The first evidence was thrown by the observation of heritability in psychiatric and neurological diseases (Goldman et al. 2008; Goldman et al. 2009; Honea et al. 2008; McDonald et al. 2006; van der Schot et al. 2009). Within the investigation of heredity in mental illness the term *endophenotype* was born. This concept was first introduced by John and Lewis (1966), and is used to classify some behavioural symptoms into more stable phenotypes with a clear genetic connection.

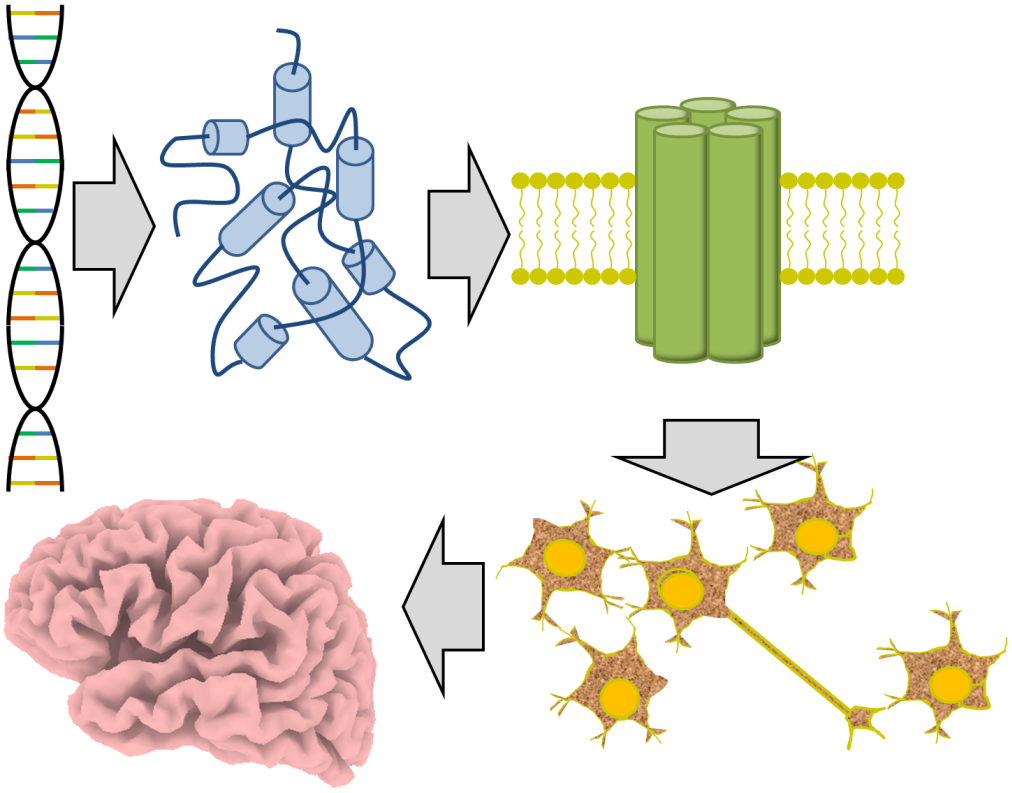

FIGURE 1.1: Flow of information from the genome, to the proteins, to receptors, cells and finally organs. (Source: own creation)

Other terms have been used as synonyms, such as 'intermediate phenotype', 'biological marker', 'subclinical trait', and 'vulnerability marker'. This concept has been extensively applied to psychiatric diseases such as schizophrenia and bipolar disorder. The idea that some endophenotypes bear a closer relationship to the processes that give rise to psychiatric illness has gained significant interest, and consequently, much effort has been dedicated to find such endophenotypes, which could define predisposition to mental illness (Flint & Munafò 2007).

The methods available nowadays for endophenotype analysis include neurophysiological, biochemical, endocrinological, neuroanatomical, cognitive, and neuropsychological measures (Leboyer et al. 1998). Advanced neuroimaging tools can be also used to investigate endophenotypes; methods such as functional magnetic resonance imaging (fMRI), morphometric MRI, diffusion-weighted imaging (DWI), single photon emission computed tomography (SPECT), and positron

emission tomography (PET) promise to expand the possibilities even more (Callicott & Weinberger 2003; Diwadkar & Keshavan 2002; Glahn et al. 2007; Martinez et al. 2001). With the new neuroimaging techniques, it now becomes feasible to elucidate the neural mechanisms responsible for the behavioural differences seen in populations holding diverse genetic information (Honea et al. 2012).

Although there is still controversy about the real impact of neurogenetics (Abbott 2008; Bartley et al. 1997; Winkler et al. 2010), there is little resistance in the research community to accept the idea that its study will ultimately improve our understanding of neurodevelopment and disease.

1.3 Genotypes in disease

Genotypes are useful as probabilistic prognosticators of disease. In contrast to phenotypes, which are not helpful because they represent observable characteristics of an organism, and they are the joint product of both genotypic and environmental influences (Cooper et al. 2013). Nevertheless, the fact that an individual with a certain pathological mutation does not always develop a disease highlights the complexity of genetics and disease. An explanation for this situation is provided by the concept of *penetrance*, defined as the proportion of individuals harbouring a particular pathogenic genotype who exhibit clinical signs of the associated disorder. In the case where this proportion is 100%, the disease genotype is said to exhibit *complete penetrance*. If not, they are said to exhibit reduced (or incomplete) penetrance (Cooper et al. 2013). Reduced penetrance is not uncommon, and therefore, most individual carriers of the risk alleles would most likely never develop the disease in question; this is because such genetic variants only contribute partially to the multifactorial aetiology of the condition, which has been confirmed by genome-wide association studies (Cooper et al. 2013). Such discussion has given rise to models in which the environmental stressors also play an important role in the aetiology of genetic-related diseases (Barros & Offenbacher 2009).

There is substantial evidence that a number of psychiatric illnesses such as schizophrenia, bipolar disorder, autism, and alcoholism have a strong genetic basis (Cowan et al. 2002). In schizophrenia, for example, numerous genetic

variants have been identified as risk factors; it is said that schizophrenia exhibits a heritability near to 80% (Jones & Cannon 1998). The polygenic model of schizophrenia (Gottesman & Shields 1967), suggests that many genetic variants in combination could explain the observed heritability. For example, it was demonstrated that subjects with a mutation in a specific gene, called COMT, have worse working memory and lower activity in the prefrontal cortex (Weinberger et al. 2001). The same gene was found in parents whose progeny had schizophrenia. The effect is due to the two forms of the enzyme differing in how efficiently they break down dopamine, and thus, children with the mutant variant of the gene exhibit increased susceptibility to schizophrenia.

A number of neurologic diseases such as dementias, epilepsies, dystonias, Parkinson's disease, ataxias, polyneurophaties, dystrophies and phakomatoses have also been associated with genetic factors (Rosenberg 2007). In the case of diseases exhibiting mendelian genetics as their distal causes, the existence of a genotype usually suggests the existence of a concomitant phenotype. However, this degree of genetic certainty does not exist for diseases with complex genetics (Province, Shannon, & Rao, 2001). The case of epilepsy, for example, is particularly interesting for the reason that the epileptic state represents a dramatic change in balance between excitatory and inhibitory activity; it implies the existence of failures in several regulatory systems. Studies in animals and humans have suggested that seizure activity results from altered expression of GABA type A receptors (GABAA-Rs) (Benarroch 2007; Coulter 2001). For example, solid evidence suggests the role of two particular genes in the aetiology of epileptic encephalopathies, a sub-type of epileptic states: the beta-3 subunit of the GABA-A receptor (GABRB3), and the ALG13 (Allen et al. 2013). Although it is widely accepted that epilepsies have a strong hereditary basis, their exact causes remain obscure. The reason could reside in the fact that epilepsy and other neuropsychiatric disorders have their origins in neurodevelopment, and this is where epigenetic mechanisms, or even chance, play a greater role (Shorvon 2011).

As previously mentioned, genes involved in neurodevelopment might have a crucial role in the generation of diseases such as epilepsy. Development describes the process of gradual change that produces increasing complexity during the growth of an organism. The fact that development and particularly neurodevelopment are under genetic control is very well-described (Hogart et al. 2008). Furthermore, the genes that are expressed during neurodevelopment might greatly

contribute to the generation of particular neuroanatomical phenotypes.

1.4 Neuroimaging genetics

Imaging studies in genetic disorders have also contributed to the understanding of how genetic expression contributes to the structure of the human brain. Furthermore, the magnetic resonance imaging (MRI) techniques are tools with the potential to identify the 'neuroanatomical phenotype' of an individual, a concept implicitly carrying the notion of heritability in the particularities of the nervous system. The search for the genetic bases of psychiatric and neurological illnesses has a more practical motivation rather than the improving of our understanding, since elucidating such genetic bases could reveal unknown molecular targets, exploitable in the development of new and more effective therapies (Cowan et al. 2002).

The combination of genetic information and data provided by MRI techniques is commonly referred as *imaging genetics* (Hariri & Weinberger 2003), an interesting approach with the potential to investigate the mechanisms linked to genetic variation. Derived from this is the concept of *neuroimaging genetics*.

Neuroimaging genetics is an emerging field in which different imaging modalities are used to elucidate the possible effect of specific genes in the structure and function of the brain (Thompson et al. 2010). Given the complexity of heredity, the investigation of genetics by the means of imaging techniques would extend our knowledge of brain function, structure and development by identifying the intrinsic roles of the different genes and their expression. The search for genes that influence brain-related traits could be improved by choosing imaging phenotypes that are closest to a single gene action. In this sense defining candidate genes could be extremely useful for the investigation of the neurogenetics, and at this point, investigating a candidate gene is a similar source of controlled variance system as the use of a pharmacological manipulation (Meyer-Lindenberg 2012).

As it has been common in the study of human genetics, one of the first studies including a neuroimaging approach was in schizophrenic patients, where a familial phenotype for schizophrenia comprising increased ventricle-to-brain ratio was

described (Weinberger et al. 1981). Numerous subsequent neuroimaging studies confirmed the notion of a brain phenotype in schizophrenia (Baaré et al. 2001; Cannon et al. 2002; Cannon et al. 2006; Hulshoff Pol, Schnack, Mandl, et al. 2006; Job et al. 2003; Job et al. 2005; Lawrie et al. 2001; Reveley et al. 1982; Reveley et al. 1984; Rijsdijk et al. 2005; Suddath et al. 1990). Nevertheless, the neuroimaging studies have not focused only on pathological conditions, but have extended their scope to the normal brain. Several neuroimaging studies have investigated the effect of specific genetic variants in the structure of the brain. MRI studies in twins have revealed significant genetic effects in several brain areas (Furman et al. 2011; Markett et al. 2013; Yoon et al. 2011). For example, the oxytocin receptor gene has been found to define the volume of amygdala (Furman et al. 2011), and the dopamine receptor D2 gene has been related to the volume of grey matter in putamen (Markett et al. 2013).

The microstructure of the brain has also been shown to be controlled by genetic factors (Chiang et al. 2011; Dietsche et al. 2014; Forde et al. 2014; Kochunov et al. 2010a). In a study of twins and their siblings, genes were found to affect fibre integrity (Chiang et al. 2011). The same study showed that the effects of such genes varied with age, sex, socioeconomic status and intelligence quotient (Chiang et al. 2011). Structural differences in white matter paths have been found to be linked to some genetic variants (Forde et al. 2014). For example, genes involved in the expression of calcium channels were found to be related to the microstructure of the hippocampal formation (Dietsche et al. 2014).

According to recent studies, specific patterns of brain function exhibit a close relationship with genetics. A number of fMRI studies have revealed that patterns of task-related activation are heritable (Blokland et al. 2008; Koten et al. 2009). For example, significant genetic influence was found on brain activation of neural networks supporting working memory tasks (Koten et al. 2009). Similarly, in an fMRI study using a N-back working memory task it was demonstrated that the individual variation in brain activation related to working memory is influenced by genes (Blokland et al. 2014). A number of genetic variants have been analysed in meta-analyses, some of which have concluded that fMRI is capable of showing the effects of the studied genetic variants with a high degree of consistency and penetrance at the behavioural level (Mier et al. 2010; Munafò et al. 2008).

The resting state activity also seems to be controlled by genetic factors. The default-mode network (DMN) connectivity pattern of 333 individuals was found to be influenced by genetic factors, and despite the neuroanatomic variation in this network is heritable, the genetic factors that influence default-mode functional connectivity and grey matter density seem to be distinct, suggesting that unique genes influence the structure and function of the network (Glahn et al. 2010). More evidence for the idea of the resting activity being governed by genetic factors emerged from studies of polymorphisms (Clemens et al. 2014; El-Hage et al. 2013; Filippini et al. 2009; Rao et al. 2007; Tian et al. 2013). The genetic variation in a serotonin transporter, for example, was found to alter the resting brain function of healthy individuals (Rao et al. 2007). The same gene seemed to modulate the resting state cerebral blood flow in the amygdala (El-Hage et al. 2013). Similarly, it was found that the monoamine oxidase A genotype influences the activity within the common resting state networks (Clemens et al. 2014). Interestingly, a genetic variation of the KIBRA gene, which has been linked to episodic memory, executive function, and Alzheimer's disease, was associated with different patterns of synchronisation within the default-mode and executive control networks (Wang et al. 2013). Furthermore, carriers of a variant of this gene also showed a smaller grey matter volume in the medial prefrontal cortex and bilateral anterior cingulated cortices (Wang et al. 2013). The gene that codifies for the apolipoprotein E (APOE) has been often investigated in fMRI studies. Carriers of the APOE4 allele exhibit different patterns of brain activity within the DMN (Filippini et al. 2009). In a different study, it was found that the same allele affects complexity and functional connectivity of the resting brain activity (Yang et al. 2014). Additionally, the APOE4 allele has been found to have a negative impact on regional neural synchronisation and inter-regional neural interaction measured by EEG (Lee et al. 2012a; Lehtovirta et al. 1996).

EEG studies have also shown the existence of a close relationship between brain function and genetic factors. A number of studies in twins and their siblings found that some patterns of EEG activity are heritable (Loo et al. 2003; Smit et al. 2008; Wacker & Gatt 2010). The presence of some polymorphisms appears to influence some brain features measurable through EEG. The dopamine transporter gene (DAT1) allele, for example, appears to influence the cortical activity in children suffering from attention deficit hyperactivity disorder (Loo

et al. 2003). Similarly, a functional polymorphism of the enzyme catechol-O-methyltransferase has been associated with increased *delta/theta* in the scalp EEG (Wacker & Gatt 2010).

MRI studies are being directed towards the investigation of a variety of diseases in the quest for the genetic variants that explain or predict some features of the disturbances observed. Family history of Alzheimer's disease, for example, has been associated with reduced resting state functional connectivity between the posterior cingulate and the medial temporal cortex (Wang et al. 2012). In a similar fashion, MRI is being used to investigate the complex genetics of neuropsychiatric illness by generating quantitative and qualitative brain phenotypes (Callicott & Weinberger 1999). These studies have been motivated by the possibilities of identifying genetic variants which provide increased risk of mental illness before it arises. That kind of studies could also indicate new biochemical pathways where to direct novel treatments (Cooper et al. 2013).

1.5 Summary

The field of genetics has grown spectacularly in complexity over the last hundred years and permits nowadays the understanding of several mechanisms of heredity. New fields such as neurogenetics focus their efforts to elucidate the effect of genes on brain structure and function, and the imaging tools play an important role to that end. Imaging genetics studies have yielded interesting results, and have demonstrated for the first time that some features of the brain are influenced by genetic factors. Interestingly, investigations of the structure and function of the brain under the scope of genetics have also provided hints of how all these factors interact and define behavioural traits, resulting in an increased risk for a disease, or even resulting in the disease itself. Unquestionably, variations in the linear sequence of the genetic code, such as single nucleotide polymorphisms (SNPs), might play a key role in explaining inter-individual differences in structure and function of the brain, as well as explain phenomena such as susceptibility and resistance in a wide range of diseases.

In the following chapters a classic imaging genetics study will be summarised. This study was feasible thanks to optimised routines of imaging acquisition, including structural imaging, diffusion-weighted imaging, resting state fMRI,

magnetic resonance spectroscopy and electroencephalography. Thanks to this routine the acquisition of such amount of data in a limited time is possible. The methodological approach of this study was similar to the one used in other imaging genetics studies, in which a cohort is screened and grouped according to their allelic status. Hence, the comparisons are similar to a study in which a cohort of subjects is exposed to a factor and there is a control group without the exposition.

A candidate gene was chosen to this end and investigated individually, using the advantages of multimodal imaging. The results of differences based on the allelic prevalence and frequency were expected to point at the crucial aspects of gene expression. Chapter 2 will support the choice of the candidate gene, which is based on the current literature. Each of chapters 3 to 7 is dedicated to a specific imaging modality, and as such, comprises different methods for acquisition and analysis. As a result each of chapters 3 to 7 has its own background, methods, results and discussion. An integrative overview and the final conclusions are given in the last chapter.

Chapter 2

Screening and genotypification of the GABRB3 gene

2.1 The role of the GABRB3 gene in disease

In the previous chapter, it was explained how large-scale sequencing and genotyping studies of healthy individuals represent a powerful new approach that could be used to understand the penetrance of pathological mutations/genotypes, as well as its possible influence on brain structure and function. The results of such studies would potentially predict the likelihood that a given disease will manifest itself in an individual who carries a specific genotype (Cooper et al. 2013).

As mentioned in Chapter 1, the GABRB3 gene is of great interest due to its early expression during embryonic stages, its role in neurodevelopment (Al-Jaberi et al. 2013) and its relationship to neurological diseases such as epilepsy and autism (Allen et al. 2013; Buxbaum et al. 2002; DeLorey 2005). *De novo* mutations of the GABRB3 gene have shown a clear association with two classical epileptic encephalopathies in humans: infantile spasms and Lennox-Gastaut syndrome (Allen et al. 2013), a complex neurodevelopmental disorder. *In vivo* studies suggest that GABRB3 haploinsufficiency is one of the causes of epilepsy in Angelman syndrome (DeLorey et al. 1998). A complementary study found that mice with disruptions in the GABRB3 gene exhibit abnormalities in electroencephalography (EEG), seizures, and behavioural characteristics typically associated with Angelman syndrome (DeLorey & Olsen 1999). Furthermore, there is evidence in

humans that Angelman syndrome and autism both exhibit reduced expression of GABRB3 (Tanaka et al. 2012). Angelman syndrome is a neurogenetic disorder characterised by severe intellectual disability, absent speech, seizures, and outbursts of laughter. Diffusion tensor imaging (DTI) studies in patients suffering from Angelman syndrome suggest decreased myelination, decreased axonal density and aberrant axonal organisation in the whole brain (Peters et al. 2011; Tiwari et al. 2012). Punctual morphological changes have also been observed in the arcuate fasciculus in patients suffering from Angelman syndrome (Wilson et al. 2011). Based on the evidence of the functional and structural abnormalities found in mice and humans when abnormal expression of the GABRB3 occurs, as well as the association with Angelman syndrome, the role of GABRB3 gene expression in neurodevelopment becomes evident. Moreover, functional variants of this gene, even those changes that do not cause a lack of function, might lead to changes in the neurodevelopmental processes and therefore in the resulting neuroanatomical phenotypes.

Alterations in the expression of GABRB3 exhibit a high degree of association with autism spectrum conditions, which are highly heritable (Hallmayer et al. 2011; Klei et al. 2012). Autism spectrum conditions are characterised by impairments in social interaction and communication along with abnormally narrow interests and repetitive behaviour. Variation of the GABRB3 gene in humans has been implicated in empathy-related behaviour (Chakrabarti et al. 2009) and autism (Buxbaum et al. 2002; Fatemi et al. 2009; Pizzarelli & Cherubini 2011; Schroer et al. 1998). A study by Warrier et al. (2013) confirmed the role of the GABRB3 gene as an important candidate for causing both autism spectrum conditions and normative variation in related endophenotypes. The study by Delahanty et al. (2011) provided direct evidence that a variant of the GABRB3 gene from maternal origin causes a synaptic dysfunction that is relevant in autism. Put together, all these findings are supported by the evidence found in GABRB3 knockout mice, which exhibit deficits in social behaviour along with a number of structural abnormalities (DeLorey et al. 2008).

Polymorphic variants of the GABRB3 are also associated with the pathogenesis of non-syndromic cleft lip and/or palate (Filézio et al. 2013). Cleft lip (cheiloschisis) and cleft palate (palatoschisis) are types of congenital deformity with clear genetic associations.

Mutations of the GABRB3 gene have been associated with epilepsy (Allen et al. 2013; DeLorey et al. 1998; Tanaka et al. 2012), particularly with childhood absence epilepsy, in which punctual mutations alter receptor expression and channel gating (Gurba et al. 2012; Lachance-Touchette et al. 2010; Feucht et al. 1999). Some of these mutations affect the expression of GABAA-Rs by altering receptor function and/or by impairing receptor biogenesis by multiple mechanisms including reducing subunit mRNA transcription or stability; impairing subunit folding, stability or oligomerisation and by inhibiting receptor trafficking (Macdonald et al. 2010).

Apart from the possible morphological factors directed by the expression of GABRB3, the expression of normal variants of such a gene (*polymorphisms*) could lead to changes in a wide range of functional aspects. Conformational changes in this protein, even those due to SNPs, might lead to changes in sensitivity profiles to neurotransmitters, drugs or even in the coupling with other molecules or proteins. Such conformational changes, which again might not imply a lack of function, would result in different patterns of measurable brain activity, such as EEG activity, resulting from the bulk postsynaptic activity of neurons and neurotransmitters.

2.2 The GABA-A receptor and the GABRB3 gene

Gamma-aminobutyric acid (GABA), acting via GABAA-Rs, mediates the bulk of rapid inhibitory neurotransmission in the adult mammalian central nervous system (for a review see Jacob, Moss, & Jurd, 2008). GABA activates synaptic and extrasynaptic GABAA-Rs, producing phasic and tonic inhibitory chloride currents that result in the stabilisation of the neuron near the resting potential, and therefore in inhibition of the neuronal action potentials (Olsen & Sieghart 2008).

GABAA-Rs are pentameric chloride channels assembled from 18 different subunits, alpha (1–6), beta (1–3), gamma (1–3), delta, epsilon (1–3), pi, and theta (Barnard et al. 1998). Most native receptors are formed by two alpha, two beta, and one gamma or delta subunits (Tretter et al. 1997). The different subunit compositions of GABAA-Rs have different physiological and pharmacological properties; they are also differently expressed throughout the brain and

are targeted at different subcellular regions. GABAA-Rs are assembled from their component subunits in the endoplasmic reticulum, from where they are trafficked to the Golgi apparatus and segregated into vesicles for transport and insertion into the neuronal cell surface. GABAA-Rs on the neuronal cell surface exist as diffuse populations or as synaptic or extrasynaptic clusters. GABAA-Rs containing the beta–3 subunit, for example, are more likely diffuse and/or extrasynaptic (Danglot et al. 2003; Jacob et al. 2005). A study by Kash et al. (2004) documented how domains in the subunits of the GABAA-Rs are responsible for receptor assembly, receptor trafficking, binding to GABA, and channel gating. Consequently, the diverse functions of GABA in the central nervous system are matched not just by the heterogeneity of GABAA-Rs, but also by the complex trafficking mechanisms and protein-protein interactions that generate and maintain an appropriate receptor cell-surface localisation (Jacob et al. 2008). GABAA-Rs control activity at the network and the cellular level. GABAA-Rs are clinically relevant drug targets for anti-convulsant, anxiolytic and hypnotic agents. Deficits in the functional expression of GABAA-Rs are critical in epilepsy (Benarroch 2007), anxiety disorders (Rudolph & Möhler 2004), cognitive deficits, schizophrenia (Lewis & Gonzalez-Burgos 2006), depression and substance abuse (Krystal et al. 2006).

As previously mentioned, the beta–3 subunits of the GABAA-Rs are of particular interest because their expression has been linked to neurodevelopmental disorders (Saitoh et al. 1992; Wagstaff et al. 1991) and autism spectrum disorder (Buxbaum et al. 2002; DeLorey 2005; Shao et al. 2003). GABAA-R containing beta–3 are also a crucial site of action for intravenous anaesthetics (Jurd et al. 2003; Zeller et al. 2007b; Zeller et al. 2007a) and ethanol (Wallner et al. 2003). Importantly, the expression of the GABRB3 is also an essential factor involved in developmental processes such as neuronal migration (Culiat et al. 1995; Dellovade et al. 2001).

The GABRB3 gene is located on the chromosome 15, locus q11.2–q12 (Figure 2.1), and its expression is regulated by non-Mendelian processes, epigenetic modulation, and sex-specific transcription with deviation of parental gene expression (Glatt et al. 1997).

Much of the knowledge about the function of GABAergic elements arise from mice models. In the developing rodent the beta–3 subunit is widely expressed in

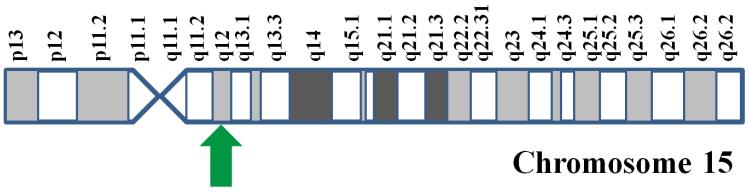

FIGURE 2.1: Representation of chromosome 15. The green arrow points to the locus where the GABRB3 gene is located. (Source: own creation)

brain and spinal cord (Laurie et al. 1992). The GABRB3 gene is expressed at embryonic days 14–17 in rat, and reaches its strongest expression at the perinatal stage, which is about 150% of the level expressed in the adult (Laurie et al. 1992). After birth, GABRB3 levels decrease to moderate levels in adult cortex, while falling rapidly in most thalamic nuclei, except in the reticular thalamic nucleus. In the adult rodent, the highest levels of beta–3 expression occur in the hippocampus, cortex, olfactory bulb and striatum (Miralles et al. 1999; Pirker et al. 2000). Given its location, GABRB3 is of particular importance in thalamocortical circuits, and since these circuits are essential to sensory processing, it is not surprising that disruptions of the GABRB3 gene in mice elicit somatosensory disturbances (DeLorey et al. 2011). Ferguson et al. (2007) successfully created a mutant beta–3 mouse that exhibited various alterations. Beta–3 knockout mice exhibited a high frequency (55%) of cleft palate in agreement with a previous publication (Homanics et al. 1997), and with evidence in humans suggesting that GABAergic signalling and system integrity is critical for the normal development of the palate (Filézio et al. 2013). Similarly, Dellovade et al. (2001) conducted a study with beta–3 knockout mice, and observed alterations in neuronal migration in the ventromedial nucleus of the hypothalamus, which further supports that the GABRB3 gene plays a crucial role in neurodevelopment. Another study conducted by Homanics et al. (1997) found various alterations in the beta–3 knockout mice, such as motor alterations, frequent myoclonus, epileptic seizures, hyperactivity and lack of coordination. Put together, all these findings suggest that alterations of the beta–3 subunit result in reduced presynaptic inhibition in the spinal cord, as well as impaired inhibition in the higher cortical centres. These findings also suggest that the normal functioning of GABAergic elements is important for neurodevelopment, particularly for the cellular topography in specific regions.

2.3 The effect of GABRB3 polymorphisms on brain function and structure

In Chapter 1 it was explained how, through MRI techniques, it is possible to investigate the contribution of genetic expression to structure and function of the human brain. MRI is a mature, non-invasive technique with enormous developmental prospects and the advantage of a widespread clinical availability (Shah et al. 2013). Multimodal imaging, referring to the combination of imaging techniques, fits well in the imaging genetics approaches, since it is desirable to measure different aspects of the brain under the same physiological conditions (Neuner et al. 2013). By using multimodal approaches the relationship between the different techniques could be assessed and new dimensions of brain genetics might be revealed.

As previously discussed, GABRB3 is an important gene in neurodevelopment (Tanaka et al. 2012; DeLorey et al. 2011), and it is associated with epilepsy and other pathological entities (Gurba et al. 2012; Tanaka et al. 2012; DeLorey & Olsen 1999). Therefore, it is an interesting candidate gene for explaining the inter-subject differences in brain function and structure observed among healthy individuals. To that end, this text has as general aim to summarise the investigation of the effect of GABRB3 polymorphisms in brain function and structure in a homogeneous sample of healthy young male volunteers.

2.4 Screening and experimental procedure

Subjects were recruited in Cologne, Jülich, Aachen and the surrounding areas. Subjects were recruited by Internet alerts, newsletters and flyers and were financially compensated for participation. Written, informed consent was obtained from all subjects and the study was approved by the Ethics Committee of the Medical Faculty of the Rheinisch-Westfälischen Technischen Hochschule Aachen (RWTH Aachen University, Germany). The study was conducted in accordance with the Declaration of Helsinki. In an initial assessment, MRI compatibility exclusion criteria were applied: incorporated metal, retainers, pacemakers, tattoos, etc. Study-specific inclusion criteria were: males aged 18–35 years old and right-handedness according to the Edinburgh Inventory of Handedness (Oldfield

1971). A second assessment included a medical interview and examination to exclude psychiatric and neurological conditions. Drug abuse, smoking status and medication intake were assessed using the DIA-X questionnaire (Diagnostisches Expertensystem für Psychische Störungen, Wittchen & Pfister 1997). Finally, 10 ml venous blood was extracted using tubes with EDTA as anticoagulant.

A multimodal EEG-MRI data acquisition was performed in a third assessment at the Research Centre Jülich (Jülich, Germany). Only volunteers who completed all the steps and fulfilled all criteria were included in the final sample. Volunteers with incomplete datasets or with deficient data quality were excluded from the study.

A total of 67 volunteers completed the study. One volunteer was excluded due to an incidental finding of neuroanatomical abnormalities. Two volunteers were excluded due to poor MR data quality. One volunteer was excluded due to failure in the determination of the genotypes.

The final sample consisted of 63 volunteers (mean age = 25.57, SD = 3.38).

Importantly, this study only included a homogeneous sample of male subjects in a certain age range and right-handed. This was performed to assure that the differences observed could be attributed to the presence of the gene and not to other factors. In this study female subjects were excluded in order to avoid factors related to variable hormonal levels, particularly important for the spectroscopy measurements.

2.5 Determination of the GABRB3 alleles

Genomic DNA was isolated from peripheral lymphocytes with a routine salting-out procedure. For the determination of the GABRB3 genotypes standard polymerase chain reaction (PCR) amplifications were performed in a 25-μl volume containing 80 ng of genomic DNA, 1 unit of recombinant Taq polymerase (Life Technologies, Darmstadt/Germany), PCR buffer (10 mM Tris-HCl, 50 mM KCl, 2.5 mM $MgCl_2$, pH 8.3), 200 mM deoxynucleotides (dNPTs), and 20 pmol of each primer. The GABRB3 primer sequences were obtained from dinucleotide repeat polymorphism at GABRB3 locus in the Angelman/Prader-Willi region of chromosome 15 (Mutirangura et al., 1992). The forward primer was FAM-labeled.

The PCR was run on an MJ PTC200 Temperature Cycler (Biozym, Germany). PCR products were run on an automated sequencing system (AB3130, Applied Biosystems, USA), and the electropherograms were analysed with gene mapping software (Applied Biosystems, USA).

Twelve CA repeat alleles were found, here designated as: G1 (171 bp), G2 (179 bp), G3 (181 bp), G4 (183 bp), G5 (185 bp), G6 (187 bp), G7 (189 bp), G8 (191 bp), G9 (193 bp), G10 (195 bp), G11 (197 bp) and G12 (199 bp). The frequencies of the CA repeat alleles are presented in Table 2.1

Allele	**bp**	**Frequency**	**Carriers**	**Homozygotes**	**Heterozygotes**
G1	171	0.016	2	0	2
G2	179	0.365	34	12	22
G3	181	0.056	7	0	7
G4	183	0.198	20	5	15
G5	185	0.048	6	0	6
G6	187	0.032	4	0	4
G7	189	0.016	2	0	2
G8	191	0.159	18	2	16
G9	193	0.016	2	0	2
G10	195	0.048	6	0	6
G11	197	0.024	3	0	3
G12	199	0.024	3	0	3

TABLE 2.1: Frequencies of the CA repeat alleles.

For the GABRB3 genotypes, comparisons among the groups were made between the most common CA repeat allele (G2) and the combined CA repeat alleles (G1 and G3 – G12), hereafter 'Non–G2'. This was done also on the basis of G2 allelic prevalence (G2 presence = G2+, or absence = G2–) and allelic frequency (G2 and Non–G2 alleles), similarly as in the study by Noble et al. (1998). The GABRB3 genotype distributions on the basis of G2 allelic frequency and G2 prevalence are presented in Tables 2.2 and 2.3 respectively.

Genotype	***n***	**Age (years)**
G2/G2	12	24.79 (SD 2.70)
G2/Non–G2	22	26.95 (SD 3.35)
Non–G2/Non–G2	29	24.84 (SD 3.41)

TABLE 2.2: GABRB3 genotype distribution on the basis of G2 allelic frequency.

A one-way ANOVA showed that there were no differences in age among the groups based on the G2 allelic frequency (G2/G2, G2/Non–G2 and Non–G2/Non–G2); $F(2,60) = 3.034$, $p = 0.056$.

Genotype	***n***	**Age (years)**
G2+	34	26.19 (SD 3.26)
G–	29	24.84 (SD 3.41)

TABLE 2.3: GABRB3 genotype distribution on the basis of G2 prevalence.

An independent-samples t-test revealed that there were no statistically significant differences in age between the groups based on the G2 prevalence (G2+ and G2–); $t(61) = –1.604$, $p = 0.114$.

2.6 Significance of the genotype results

A given gene can have more than two alleles. Although any particular individual can have only two, many alleles of a given gene may exist in a population. In fact, multiple alleles are the rule rather than the exception. This is also the case in GABRB3, where all studies are consistent in describing 11–12 alleles. The frequencies of the GABRB3 CA alleles were first described in the study of Mutirangura et al. (1992), where 11 alleles were found, and the frequency of G2 (A11 in that study) was 0.325. Other studies have found similar frequencies of the G2 allele (Noble et al. 1998; Inoue et al. 2008; Scapoli et al. 2002). In a study by Noble et al. (1998), for example, different G2 (G1 in that study) allelic prevalences were found in alcoholics and non-alcoholics.

The results presented here are in line with the previous observations of the G2 allelic frequency and, therefore, provide the opportunity to assess differences in carriers and non-carriers of the G2 allele. Based on the various functions of GABRB3, the expression of different variants of such a gene could influence neurodevelopment and therefore the adult brain could exhibit functional and/or structural features resulting from the genetic expression mechanisms. Consequently, the following chapters will include the assessment of the different aspects of the brain on the basis of the different imaging techniques used for this study. For that purpose the carrier status of the most frequent CA allele will be used for the comparisons, which are expected to represent the structural and functional aspects where the expression of the GABRB3 variants is critical.

Chapter 3

Investigation of the effect of GABRB3 polymorphisms on grey matter using voxel-based morphometry

3.1 Background

Voxel-based morphometry (VBM, Ashburner & Friston 2000) refers to a method in which the local volume of grey matter is measured to be later statistically compared in different populations. A number of brain morphometry studies have been carried out on several populations and with several purposes, such as the investigation of ageing (Good et al. 2001), cognitive deficit (Abell et al. 1999) and neurodegenerative diseases (Baron et al. 2001). The importance of the VBM approach is that it is not subjective to one particular structure and gives a relatively unbiased and complete assessment of anatomical differences throughout the brain (Ashburner & Friston 2000; Wright et al. 1995).

VBM studies have been successful in characterising structural brain differences in a variety of diseases including schizophrenia (Cooper et al. 2014), autism spectrum disorder (Chen et al. 2011), bipolar disorder (Selvaraj et al. 2012),

epilepsy (Kakeda & Korogi 2010; Keller & Roberts 2008; Li et al. 2012), Parkinson's disease (Price et al. 2004) and Alzheimer's disease (Fox et al. 1999; Karas et al. 2004; Yang et al. 2012). In all these studies, the differences in grey matter volume were linked to the physiopathology of the conditions and, thus, offered morphological explanations of the symptoms and the signs characterising the diseases.

VBM has also been used in genetic studies. Genetic control over the morphology of the brain has been already demonstrated in non-human primates (Kochunov et al. 2010b). Moreover, there are studies in humans suggesting that the size of the brain, as well as the pattern of gyri and sulci are strongly determined by genetic factors (Bartley et al. 1997). Other studies have shown that the volume of most brain structures is highly heritable, meanwhile other structures, such as the cerebellum, are more environmentally influenced (Hulshoff Pol, Schnack, Posthuma, et al. 2006). VBM studies in twins have revealed significant genetic effects in several brain structures and suggest the existence of biological markers for inherited traits (Yoon et al. 2011).

A number of genetic studies used the VBM approach to find significant differences in groups of populations relatively 'homogenous', differing solely in the variant expressed of a specific gene (Furman et al. 2011; Markett et al. 2013); such potential differences could be attributed to the presence of the genetic variant in question. For example, it has been demonstrated that women homozygous for a polymorphism of the oxytocin receptor gene have smaller volumes of both left and right amygdala (Furman et al. 2011). Similarly, differences in the volume of grey matter in the putamen have been found in carriers of a polymorphism of the dopamine receptor D2 (Markett et al. 2013). Although all these findings correspond to structural differences, they could have a degree of correspondence with behavioural differences giving rise to the observable endophenotypes. Nevertheless, such conclusion requires more detailed observation of the relationship between the behavioural and structural aspects.

Voxel-based morphometry of MRI structural data involves normalising all the images to the same stereotactic space, extracting the grey matter from the normalised images, smoothing, and finally performing a statistical analysis to make inferences about group differences (Ashburner & Friston 2000). The statistical analysis is based on the general linear model (GLM), and is used to identify

regions of grey matter volume which are significantly related to the particular effect under study. The GLM approach uses the theory of Gaussian random fields (Friston et al. 1996; Worsley et al. 1996) to assess the significance of any difference found. GLM has been extensively used in imaging statistics, particularly after it was proposed for the analysis of functional images (Friston et al. 1994). The flexibility of GLM provides useful solutions for the modelling of hemodynamic response functions in fMRI data (Poline & Brett 2012), as well as for the implementation of several statistical tests, such as t-test, ANOVA, ANCOVA and linear regression.

Given the important association of GABRB3 in neurodevelopment (Tanaka et al. 2012) described in Chapter 2, and the associations with epilepsy and other pathological entities, this sub-study aims at investigating whether differences in the local grey matter volume exist among the groups of healthy male volunteers on the basis of G2 allelic prevalence and G2 frequency. As it was described in Chapter 2, alterations in hippocampus have been observed in beta–3 knockout mice (Dellovade et al. 2001); in addition, adult rodents exhibit high expression of this gene in the same area (Miralles et al. 1999; Pirker et al. 2000). Consequently, this study will have as well as a whole-brain approach, a parallel approach directed to investigate the possible differences in grey matter volume in hippocampus.

3.2 Methods

3.2.1 Subjects and data acquisition

Data from the 63 volunteers (mean age = 25.57, SD = 3.38) were included in this sub-study. Details about the samples are presented in Chapter 2. Anatomical (T1-weighted) images were acquired for every subject by means of a Magnetisation-Prepared, Rapid Acquisition Gradient-Echo (MP-RAGE) sequence (TR = 2250 ms, TE = 3.03 ms, voxel-size = $1 \times 1 \times 1$ mm^3, matrix size = $256 \times 256 \times 176$, sagittal slices, flip angle = 9° and GRAPPA factor of 2 with 70 autocalibration signal lines) in a 3 T Siemens Magnetom Trio scanner (Erlangen, Germany).

3.2.2 Data analysis

Structural data were analysed with FSL-VBM (Douaud et al. 2007, http://fsl.-fmrib.ox.ac.uk/fsl/fslwiki/FSLVBM), an optimised VBM protocol (Good et al. 2001) carried out in FMRIB software library (FSL, v5.0. Smith et al. 2004, http://fsl.fmrib.ox.ac.uk/fsl/fslwiki/). First, structural images were brain-extracted and grey matter-segmented before being registered to the MNI152 standard space using non-linear registration (FNIRT, http://fsl.fmrib.ox.ac.uk/fsl/fslwiki/-FNIRT). The resulting images were averaged and flipped along the x-axis to create a left-right symmetric, study-specific grey matter template. Second, all native grey matter images were non-linearly registered to this study-specific template and 'modulated' to correct for local expansion (or contraction) due to the non-linear component of the spatial transformation. The modulated grey matter images were then smoothed with an isotropic Gaussian kernel with a sigma of 4 mm. Finally, a voxel-wise statistical analysis was performed using GLM and permutation-based testing, corrected for multiple comparisons across space. A graphical representation of the analysis steps is presented in Figure 3.1.

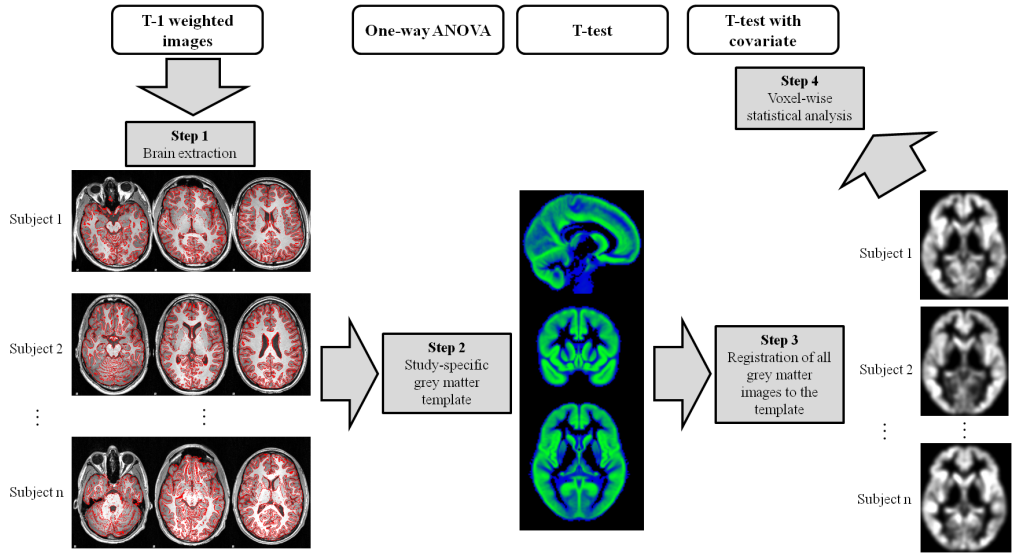

FIGURE 3.1: Graphical representation of the analysis pipeline. (Source: own creation)

3.2.3 Whole-brain analysis

The grey matter images were used for statistical analysis within the framework of GLM. A one-way ANOVA (referred as F-test in GLM) was used to test for inter-group differences when comparing G2/G2 (n = 12), G2/Non–G2 (n = 22) and Non–G2/Non–G2 (n = 29); a Monte Carlo permutation test was used, and hence, a random subset of 5000 permutations were performed. In the case of a significant F-test, individual t-tests (independent-samples) with a random subset of 5000 permutations were used to determine the direction of the effect. An independent-samples t-test with a random subset of 5000 permutations was also performed to test for differences between G2+ (n = 34) and G2– (n = 29). Additionally, a two-group difference test adjusted for covariate was performed to investigate possible differences between G2+ and G2–; here, the number of G2 alleles was included as a regressor to explain possible differences between the two groups and to investigate whether the number of G2 alleles in the individuals affects the grey matter volume in any area.

3.2.4 Region-of-interest analysis

Two masks corresponding to the left and right hippocampus were created from the MNI152 standard space according to the Harvard-Oxford Subcortical Structural Atlas (http://www.cma.mgh.harvard.edu/). The mean grey matter volumes were then extracted from the individual images generated by the VBM analysis and used for statistical analysis in SPSS software (Version 17.0, IBM SPSS Statistics).

A one-way ANOVA test was used to investigate inter-group differences in grey matter when comparing G2/G2, G2/Non–G2 and Non–G2/Non–G2 groups. A Tukey post-hoc test was performed to determine the direction of the effect. An independent-samples t-test was also performed to test for differences between G2+ and G2–.

3.3 Results

3.3.1 Whole-brain analysis

The VBM analysis protocol successfully generated a study-specific grey matter template, which included information from the 63 volunteers (Figure 3.2).

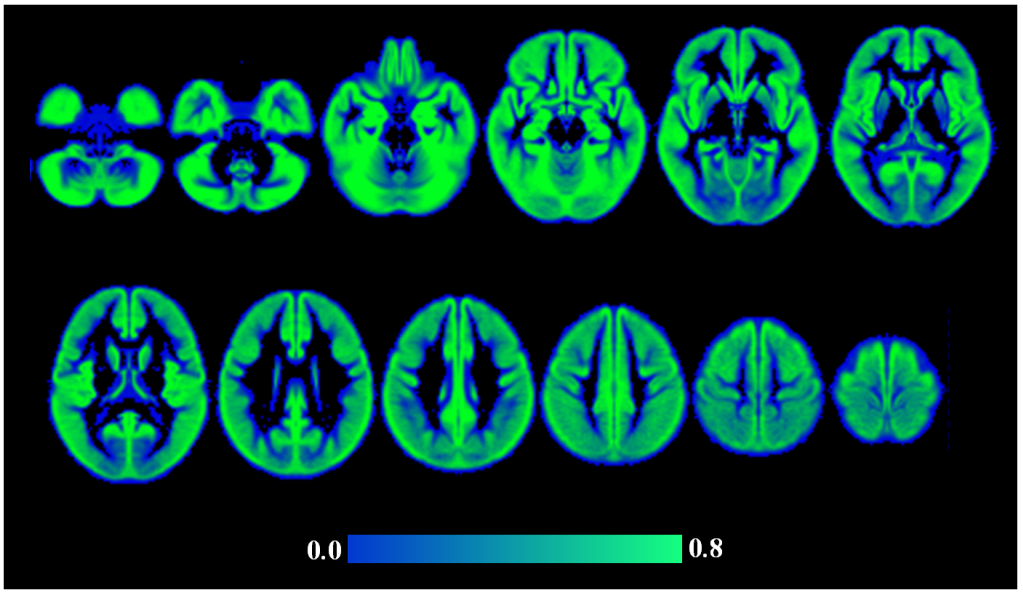

FIGURE 3.2: Study-specific grey matter template generated by the VBM analysis.

The voxel-wise statistical map generated by the one-way ANOVA exhibited voxels (corrected p values) where the F-test revealed differences among the groups (G2/G2, G2/Non–G2 and Non–G2/Non–G2). See Table 3.1. None of these voxels survived after thresholding for statistically significance (p <0.05).

Contrast	**Min. p**	**X, Y, Z of min. p**	**Structures of min. p**	**Hem.**
F-test	0.078	28, 0, -10	38% Right Cerebral White Matter, 17% Right Putamen	R

* $p \leq 0.05$

TABLE 3.1: Results of the F-test (one-way ANOVA) showing clusters of minimum p value (corrected), MNI coordinates, name of the structures and hemisphere. Only clusters with a minimum of 100 voxels are presented. Structures defined according to Harvard-Oxford cortical and subcortical structural atlases.

The voxel-wise statistical maps generated by the independent-samples t-test revealed voxels (corrected p values) where differences between the groups (G2+ and G2–) existed. See Table 3.2. None of these voxels survived after thresholding for statistically significance (at the level of $p \leq 0.025$, Bonferroni-corrected for the number of tests).

Contrast	**Min. *p***	**X, Y, Z of min. *p***	**Structures of min. *p***	**Hem.**
G2+ >G2–	0.821	14, -14, -28	6% Parahippocampal Gyrus, anterior division	R
	0.819	24, 2, -8	44% Right Putamen, 28% Right Cerebral White Matter	R
G2+ <G2–	0.455	26, -92, 14	39% Occipital Pole, 8% Lateral Occipital Cortex, superior division	R
	0.749	28, -56, -36	Cerebellum, 16% Right VI	R

* $p \leq 0.025$

TABLE 3.2: Results of the independent-samples t-test showing clusters of minimum p value (corrected), MNI coordinates, name of the structures and hemisphere. Only clusters with a minimum of 100 voxels are presented. Structures defined according to Harvard-Oxford cortical and subcortical structural atlases.

In the analysis of differences between G2+ and G2– adjusted for the number of G2 alleles none of the voxels survived after the thresholding for significance (at the level of $p \leq 0.0125$, Bonferroni-corrected for the number of tests). See Table 3.3. There were no clusters exhibiting any significant positive or negative effect with the number of G2 alleles. See Table 3.4.

3.3.2 Region-of-interest analysis

The one-way ANOVA showed that there were no differences in grey matter volume in left hippocampus among the groups based on the G2 allelic frequency (G2/G2, G2/Non–G2 and Non–G2/Non–G2); $F(2,60) = 0.439$, $p = 0.646$. That was also the case for the right hippocampus, where no statistically significant differences were found; $F(2,60) = 1.951$, $p = 0.151$. Box plots are presented in Figure 3.3.

The independent-samples t-test revealed that were no differences in grey matter volume in left hippocampus between the groups based on the G2 prevalence (G2+ and G2–); $t(61) = –0.851$, $p = 0.398$. That was also the case for the right hippocampus, where no statistically significant differences were found; $t(61) = –1.926$, $p = 0.059$. Box plots are presented in Figure 3.4.

Contrast	**Min. *p***	**X, Y, Z of min. *p***	**Structures of min. *p***	**Hem.**
G2+ >G2– adjusted	0.697	12, -2, -16	1% Parahippocampal Gyrus, anterior division	R
	0.778	-16, 6, -24	13% Frontal Orbital Cortex, 6% Temporal Pole	L
	0.447	46, 18, 52	27% Middle Frontal Gyrus	R
	0.385	-30, 0, 10	1% Insular Cortex	L
	0.116	36, -44, -22	79% Temporal Occipital Fusiform Cortex, 9% Temporal Fusiform Cortex, posterior division	R
G2+ <G2– adjusted	0.76	28, -36, 72	41% Postcentral Gyrus, 9% Superior Parietal Lobule	R
	0.828	-12, 66, 24	51% Frontal Pole	L
	0.432	26, -92, 16	41% Occipital Pole, 8% Lateral Occipital Cortex, superior division	R
	0.841	22, 50, -10	33% Frontal Pole	R
	0.79	-12, 66, -18	44% Frontal Pole	L
	0.863	48, 42, -8	78% Frontal Pole, 3% Frontal Orbital Cortex	R
	0.86	-38, -16, -46	3% Temporal Fusiform Cortex, posterior division	L

* $p \leq 0.0125$

TABLE 3.3: Results of the independent-samples t-test adjusted for the number of G2 alleles showing differences between groups G+ and G2–. Results show clusters of minimum p value (corrected), MNI coordinates, name of the structures and hemisphere. Only clusters with a minimum of 100 voxels are presented. Structures defined according to Harvard-Oxford cortical and subcortical structural atlases.

3.4 Discussion

In this chapter it was described how the T1-structural images from the sample of healthy male volunteers underwent VBM analysis. The analysis permitted the comparisons among subgroups on the basis of G2 allelic prevalence and G2 frequency.

The results showed that there were no statistically significant differences among the different subgroups on the basis of the G2 allelic prevalence or frequency. There was also no effect of the number of G2 alleles on the local volume of grey matter. The grey matter volume was not different in the different groups on the basis of G2 allelic frequency and prevalence. The results presented here suggest that the expression of the G2 allele do not affect the local grey matter volume in any macrostructure of the brain.

At his point, cautious interpretation of the results must be carried out. Firstly, the intrinsic limitations of the technique arise initially during the acquisition

Contrast	**Min. *p***	**X, Y, Z of min. *p***	**Structures of min. *p***	**Hem.**
	0.255	-60, -24, 20	24% Supramarginal Gyrus, anterior division, 23% Postcentral Gyrus	L
Positive effect of G2	0.272	36, -40, -24	48% Temporal Occipital Fusiform Cortex, 36% Temporal Fusiform Cortex, posterior division	R
	0.425	66, -6, 26	53% Postcentral Gyrus, 9% Precentral Gyrus	R
	0.379	-32, 0, 8	6% Insular Cortex	L
	0.691	38, -46, 54	51% Superior Parietal Lobule, 9% Angular Gyrus	R
	0.357	30, -2, 2	97% Right Putamen, 3% Right Cerebral White Matter	R
	0.882	26, 38, -10	43% Frontal Pole, 19% Frontal Orbital Cortex	R
Negative effect of G2	0.635	-14, 6, -22	14% Frontal Orbital Cortex, 1% Temporal Pole	L
	0.857	18, -8, -8	62% Right Cerebral White Matter, 30% Right Pallidum	R

* $p \leq 0.0125$

TABLE 3.4: Results of the independent-samples t-test adjusted for the number of G2 alleles showing the effect of the number of G2 alleles. Results show clusters of minimum p value (corrected), MNI coordinates, name of the structures and hemisphere. Only clusters with a minimum of 100 voxels are presented. Structures defined according to Harvard-Oxford cortical and subcortical structural atlases.

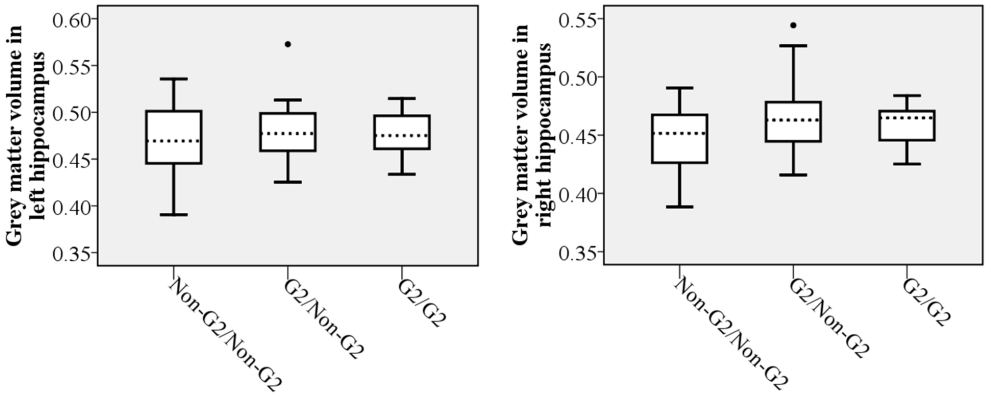

FIGURE 3.3: Box plots presenting the grey matter volumes in left and right hippocampi in the different groups on the basis of G2 allelic frequency.

of the structural data, where restrictions with respect to the resolution of the images exist. This limitation tried to be overcome by using 1 mm^3 isotropic voxels, although some brain structures actually range in the sub-millimetre-size. Therefore, the microstructure of the brain, particularly the local cortical-layer arrangement, remains mostly underestimated. Secondly, in this study statistical

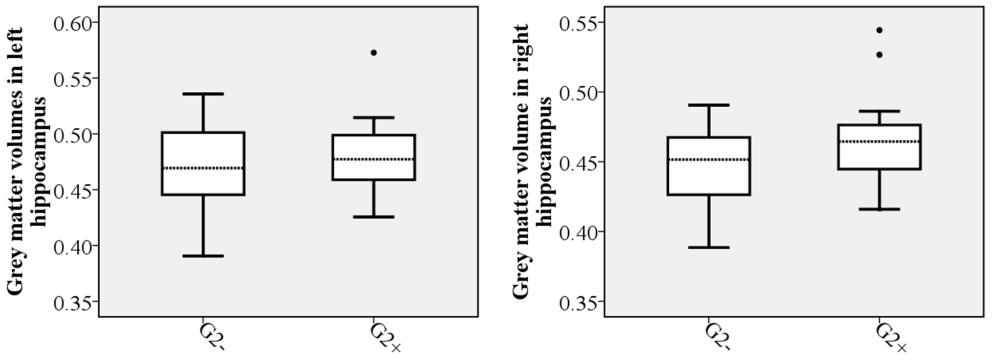

FIGURE 3.4: Box plots presenting the grey matter volumes in left and right hippocampi in the different groups on the basis of the G2 allelic prevalence.

comparisons were performed only on the basis of the most frequent CA allele of the GABRB3. Based on the allelic frequencies found for GABRB3 this approach makes sense, since non-carriers, homozygote carriers and heterozygote carriers should ideally be included in the analysis to properly examine the effect of the polymorphism on the population. This study was sufficiently powered with respect to G2 and included a sufficiently large sample in each subgroup; yet, no other subgroups could be formed on the basis of other allelic polymorphisms. For example, the second most frequent allele in this population, G4 (with a frequency of 0.19), was present in 20 individuals, although only 5 were homozygote carriers. Moreover, the process of investigating the effect of a candidate gene implies the use of much larger samples in order to be able to investigate the effect of all polymorphisms; the genetic investigation also implies the existence of representative samples where the results could be extended to the general population. The conclusions of this sub-study are therefore limited to the effect of G2 on the population.

In addition, VBM, as all other image analysis methods, has inherent limitations (Bookstein 2001). The most problematic point is the issue of inter-subject spatial normalisation. This difficulty arises from the fact that subjects have different gyral patterns, and there is little correspondence between them; smoothing can solve the problem, although bringing others of its own (Jones et al. 2005). However, when implemented rigorously and interpreted carefully, VBM can be a powerful technique (Ridgway et al. 2008).

VBM has been extensively used in neuroimaging genetic studies (Fujii et al. 2014; Forde et al. 2014), and the issue of false positives has been largely investigated (Meyer-Lindenberg et al. 2008). At this point the importance of reporting negative results in neuroimaging genetics studies should be highlighted, since they also provide understanding to the mechanisms of heredity. For example, it has been investigated whether carriers of APOE allele $\epsilon 4$ had any significant structural difference in brain compared to the carriers of other alleles (Matura et al. 2014); the $\epsilon 4$ allele of the APOE has been investigated for long time, particularly because carriers have increased risk of Alzheimer's disease (Saunders et al. 1993). Carriers of the $\epsilon 4$ allele have shown various differences in brain functional connectivity patterns (Filippini et al. 2009; Sheline et al. 2010; Yang et al. 2014), and therefore it was thought that local brain differences mirrored them. Matura et al. (2014) demonstrated that there are no differences in grey matter volume between healthy carriers and non-carriers of $\epsilon 4$. In this exemplary case the negative results provided useful results that explained how, in some cases, the genetic expression influences the functionality and leaves intact the macrostructural aspect.

Chapter 4

Investigation of the effect of GABRB3 polymorphisms on white matter using diffusion-weighted imaging

4.1 Background

Diffusion-weighted imaging (DWI), first applied for *in vivo* human brain research by Le Bihan et al. (1986), is a method that poses the capability of measuring the Brownian motion of spin-bearing particles by means of the nuclear magnetic resonance effect. DWI measures the net signal attenuation due to the spin dephasing arising from the incoherent displacement of particles along the axis of an applied magnetic field gradient. This field gradient encodes the position of the spin-bearing particles at two different time points (Jones et al. 2013). The portion of dephasing during the application of the gradient can be isolated by measuring the signal amplitude with and without the diffusion-encoding gradient applied (Le Bihan et al. 1986). The diffusion-weighted signal attenuation depends on the distribution of displacements during the diffusion time along the axis of the applied gradient, as well as on the strength and duration of the gradient. In the general case of an anisotropic diffusion, the assessment of the diffusion process in 3D can be achieved by measuring the diffusion-weighted signal attenuation

along multiple axes and strengths of diffusion weightings (b-values, Callaghan et al. 1988; Wedeen et al. 2005). Such attenuation reflects the general mobility of water molecules, which depends on the temperature, viscosity, presence of macromolecules, and other factors such as the arrangement of cell membranes, myelin sheaths and microtubules (Beaulieu 2002). These facts make the DWI a powerful technique for the detection of changes in the tissue microstructure as well as for the global organisation of anisotropic systems, such as the human brain white matter (Jones et al. 2013).

DWI serves to the assessment of the microstructural properties of tissues, and therefore, is nowadays widely used for the investigation of numerous experimental and clinical conditions, as well as for the investigation of the neuroanatomical correlates of different aspects of behaviour (Beaulieu 2002). The degree of mobility of water molecules displacement molecules is impeded by numerous factors such as fibre diameter, fibre density, membrane permeability, and myelination (Beaulieu 2002). Changes in these various tissue properties may be associated with disease, development, learning, and others. DWI has been used, for example, to investigate Alzheimer's disease (Avants et al. 2010; Damoiseaux et al. 2009), schizophrenia (Qiu et al. 2010), multiple sclerosis (Bodini et al. 2009; Roosendaal et al. 2009), Tourette's syndrome (Neuner et al. 2010), Parkinson's disease (Menke et al. 2009) and ageing (Kochunov et al. 2009).

The conventional approach to model DWI data, known as diffusion tensor imaging (DTI, Basser & Pierpaoli 1996), provides several rotationally-invariant scalar metrics, such as fractional anisotropy (FA), mean diffusivity (MD), radial and axial diffusivity (RD, AD), among others. Differences or changes in these measures are frequently interpreted as changes or differences in the integrity of the tissue microstructure. FA, one of most commonly derived metrics from conventional DTI data, is usually accepted as a measure of white matter integrity, although it has been suggested that it is also affected by intra-voxel orientational dispersion, myelination, packing density, membrane permeability and partial volume effects (Jones et al. 2013). Moreover, DTI provides information of the local direction of fibrous tissues, which can be used to investigate the global organisation of the brain white matter using a technique commonly designated as fibre tractography (Seunarine & Alexander 2014).

Recent improvements in the acquisition and analysis of DTI data permit nowadays to extract valuable information from the white matter cytoarchitecture (Smith et al. 2006). Among the novel tools, tract-based spatial statistics (TBSS, Smith et al. 2006) has gained special attention, since it aims at solving the issue of how to align FA images from multiple subjects in a way that valid conclusions could be drawn from the subsequent voxel-wise analysis. This method has been extensively and successfully used in a variety of clinical entities (Damoiseaux et al. 2009; Kochunov et al. 2009). Pre-processing of the data, prior to modelling, is an essential step particularly for correction of motion and eddy-current artefacts. Initially, TBSS applies nonlinear registration of the FA images into standard and mean FA images and skeletonise them. For group analyses it projects all FA data onto a mean FA skeleton and then feed it into a GLM modelling and thresholding in order to find voxels which correlate with a predefined model. Such manipulation of the images permits, for example, to find correlations or differences in DTI parameters among groups of subjects (Smith et al. 2006).

DTI and TBSS have been used in genetic studies in search for structural differences in the white matter that could be attributed to the expression of genetic variants (Forde et al. 2014). A study by Dietsche et al. (2014), for example, found that carriers of a polymorphism of a gene involved in the expression of calcium channels exhibited FA reduction in the hippocampal formation as well as differences in learning performance compared to control individuals. Similarly, Chiang et al. (2009) found that a common polymorphism in the BDNF gene (the brain-derived neurotrophic factor) influences the fibre integrity of the brain.

As it was discussed in Chapter 2, the GABRB3 is an important gene in neurodevelopment (Tanaka et al. 2012), and according to animal studies is of particular importance in the development of the thalamocortical circuits (DeLorey et al. 2011). Therefore, this sub-study aims at investigating whether differences in the diffusion parameters exist among the groups of healthy male volunteers on the basis of G2 allelic prevalence and G2 frequency.

4.2 Methods

4.2.1 Subjects and data acquisition

Data from 63 volunteers (mean age = 25.57, SD = 3.38) were included in this sub-study. Details about the samples are presented in Chapter 2. DW data were acquired with a standard double-refocused spin-echo EPI sequence with bipolar field gradient pulses (TR = 9100 ms, TE = 87 ms, b-values = 0 and 1000 s mm^{-2}, number of field gradient directions = 30, number of averages = 4, voxel-size = $1.9 \times 1.9 \times 1.9$ mm^3, matrix-size = $128 \times 128 \times 72$ with sagittal slices) in a 3 T Siemens Magnetom Trio scanner (Erlangen, Germany).

4.2.2 Data analysis

Pre-processing of the diffusion data was performed in FSL (Smith et al. 2004, http://fsl.fmrib.ox.ac.uk/fsl/fslwiki/). The diffusion data were initially corrected for eddy currents using FMRIB diffusion toolbox (FDT, Behrens et al. 2003, http://fsl.fmrib.ox.ac.uk/fsl/fslwiki/FDT) included in FSL. Gradient field directions were corrected using in-house Matlab scripts (Leemans & Jones 2009). FA maps were then created by fitting a tensor model to the raw diffusion data using FDT, and then brain-extracted using the brain extraction tool (BET, Smith 2002, http://fsl.fmrib.ox.ac.uk/fsl/fslwiki/BET) in FSL. Bias due to background noise was reduced using the power-images method (McGibney & Smith 1993; Miller & Joseph 1993), while the approach proposed by Aja-Fernamdez et al. (2009) was used to evaluate the standard deviation of the background noise. Voxel-wise statistical analysis of the FA data was carried out using TBSS (Smith et al. 2006, http://fsl.fmrib.ox.ac.uk/fsl/fslwiki/TBSS) part of FSL. FA data from all subjects were first aligned into a common space using non-linear registration (FNIRT, http://fsl.fmrib.ox.ac.uk/fsl/fslwiki/FNIRT), which uses a b-spline representation of the registration warp field (Rueckert et al. 1999). Next, a mean FA image was created and thinned to create a mean FA skeleton representing the centres of all tracts common to the group. FA images of each volunteer were then projected onto this skeleton. MD, AD, and RD skeletonised images were calculated using the 'non-FA' script part of TBSS, as well as the FA images as reference. The resulting data of FA, MD, AD and RD were fed into

voxel-wise statistical analyses in the framework of GLM, similarly as in Chapter 3. A graphical representation of the analysis steps is presented in Figure 4.1.

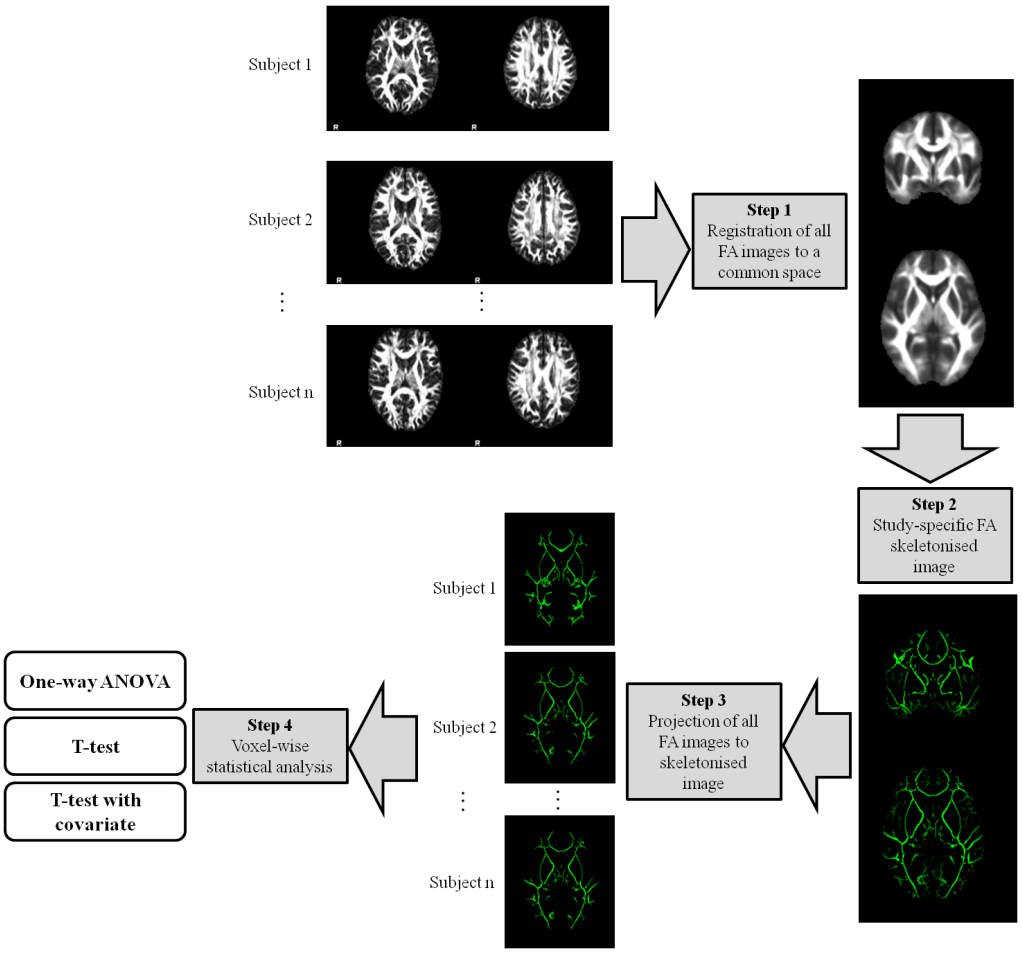

FIGURE 4.1: Graphical representation of the TBSS analysis pipeline. (Source: own creation)

For each diffusion parameter (FA, MD, AD, RD) the following statistical approach was performed: a one-way ANOVA was used to test for inter-group differences when comparing G2/G2, G2/Non–G2 and Non–G2/Non–G2 within the framework of GLM (referred as F-test) similarly as in Chapter 3; a Monte Carlo permutation test was used, and hence, a random subset of 5000 permutations were performed. In the case of a significant F-test, individual t-tests (independent-samples) with a random subset of 5000 permutations were used to determine the direction of the effect. An independent-samples t-test with a random subset of 5000 permutations was also performed to test for differences

between G2+ and G2–. Additionally, a two-group difference test adjusted for covariate was performed to investigate possible differences between G2+ and G2–; here, the number of G2 alleles was included as a regressor to explain possible differences between the two groups.

Additionally, symmetry analyses of the four diffusion parameters were carried out using the 'tbss_sym' script included in TBSS. Here, individual images were left-right flipped, and the latter subtracted from the former, resulting in an individual image of $Left{>}Right$ for each diffusion parameter. The same GLM statistical approach was performed to test whether the presence and/or frequency of G2 affect the symmetry of white matter.

4.3 Results

4.3.1 Fractional anisotropy

The voxel-wise statistical map generated by the one-way ANOVA exhibited voxels (corrected p values) where the F-test revealed differences in FA among the groups (G2/G2, G2/Non–G2 and Non–G2/Non–G2). See Appendix A.1. None of these voxels survived after thresholding for statistically significance ($p \leq 0.05$).

The voxel-wise statistical maps generated by the independent-samples t-test revealed voxels (corrected p values) where differences in FA existed between the groups (G2+ and G2–). See Appendix A.2. None of these voxels survived after thresholding for statistically significance (at the level of $p \leq 0.025$, Bonferroni-corrected for the number of tests).

In the analysis of differences between G2+ and G2– adjusted for the number of G2 alleles none of the voxels survived after the thresholding for significance (at the level of $p \leq 0.0125$, Bonferroni-corrected for the number of tests). See Appendix A.3. There were no clusters exhibiting any significant positive or negative effect with the number of G2 alleles. See Appendix A.4.

4.3.2 Mean diffusivity

The F-test revealed that differences in MD existed among the groups (G2/G2, G2/Non–G2 and Non–G2/Non–G2). See Table 4.1. The subsequent independent-samples t-tests did not reveal any statistically significant difference among the groups (at the level of $p \leq 0.025$, Bonferroni-corrected for the number of tests). See Table 4.2.

Contrast	**Min. *p***	**X, Y, Z of min. *p***	**Structures of min. *p***	**Hem.**
F–test	0.007*	-25, -21, 3	16% Corticospinal tract L, 3% Superior longitudinal fasciculus L	L

* $p \leq 0.05$

TABLE 4.1: Analysis of MD. Results of the F-test (one-way ANOVA) showing clusters of minimum p value (corrected), MNI coordinates, name of the structures and hemisphere. Only clusters with a minimum of 100 voxels are presented. Structures defined according to JHU White-Matter Tractography Atlas.

The independent-samples t-test for the G2+ and G2– samples did not show any significant difference (at the level of $p \leq 0.025$, Bonferroni-corrected for the number of tests). See Appendix A.5.

The analysis of differences between G2+ and G2– adjusted for the number of G2 alleles did not show any significant difference (at the level of $p \leq 0.0125$, Bonferroni-corrected for the number of tests). See Appendix A.6. There were no clusters exhibiting any significant positive or negative effect with the number of G2 alleles. See Appendix A.6.

4.3.3 Axial diffusivity

The F-test revealed that AD differences existed among the groups (G2/G2, G2/Non–G2 and Non–G2/Non–G2). See Table 4.3. The subsequent independent-samples t-tests revealed that a statistically significant difference (at the level of $p \leq 0.025$, Bonferroni-corrected for the number of tests) existed between G2/G2 and Non–G2/Non–G2 groups. See Table 4.4. The independent-samples t-test revealed that subjects in the Non–G2/Non–G2 group exhibited increased AD in the right superior longitudinal fasciculus compared to the subjects in the G2/G2 group (Figure 4.2). Areas of local minimum p value appeared also in the right

Contrast	**Min. *p***	**X, Y, Z of min. *p***	**Structures of min. *p***	**Hem.**
G2/G2 >Non–G2/Non–G2	0.695	5, -39, -35	26% Anterior thalamic radiation R, 5% Corticospinal tract R	R
	0.761	-13, -24, 29	†Body of corpus callosum	L
	0.755	9, 17, 20	†Body of corpus callosum	R
G2/G2 <Non–G2/Non–G2	0.031	29, -53, 37	3% Superior longitudinal fasciculus R	R
G2/Non–G2 >Non–G2/Non–G2	0.43	13, -46, -32	†Inferior cerebellar peduncle R	R
G2/Non–G2 <Non–G2/Non–G2	0.154	47, -13, 28	21% Superior longitudinal fasciculus R, 3% Superior longitudinal fasciculus (temporal part) R	R
G2/G2 >G2/Non–G2	0.277	8, 19, 20	3% Forceps minor	R
G2/G2 <G2/Non–G2	0.106	26, -53, 20	8% Forceps major, 3% Inferior fronto-occipital fasciculus R	R

* $p \leq 0.025$
† Areas defined according to JHU ICBM-DTI-81 White-Matter Labels

TABLE 4.2: Analysis of MD. Results of the independent-samples t-tests showing clusters of minimum p value (corrected), MNI coordinates, name of the structures and hemisphere. Only clusters with a minimum of 100 voxels are presented. Structures defined according to JHU White-Matter Tractography Atlas.

superior longitudinal fasciculus ($p = 0.018$), right corticospinal tract ($p = 0.025$) and body of the corpus callosum ($p = 0.02$). See Table 4.5

Contrast	**Min. *p***	**X, Y, Z of min. *p***	**Structures of min. *p***	**Hem.**
F–test	0.025*	-19, -7, 7	Posterior limb of internal capsule L	L
	0.547	20, -4, 11	Posterior limb of internal capsule R	R

* $p \leq 0.05$

TABLE 4.3: Analysis of AD. Results of the F-test (one-way ANOVA) showing clusters of minimum p value (corrected), MNI coordinates, name of the structures and hemisphere. Only clusters with a minimum of 100 voxels are presented. Structures defined according to JHU ICBM-DTI-81 White-Matter Labels.

The independent-samples t-test for the G2+ and G2– samples did not show

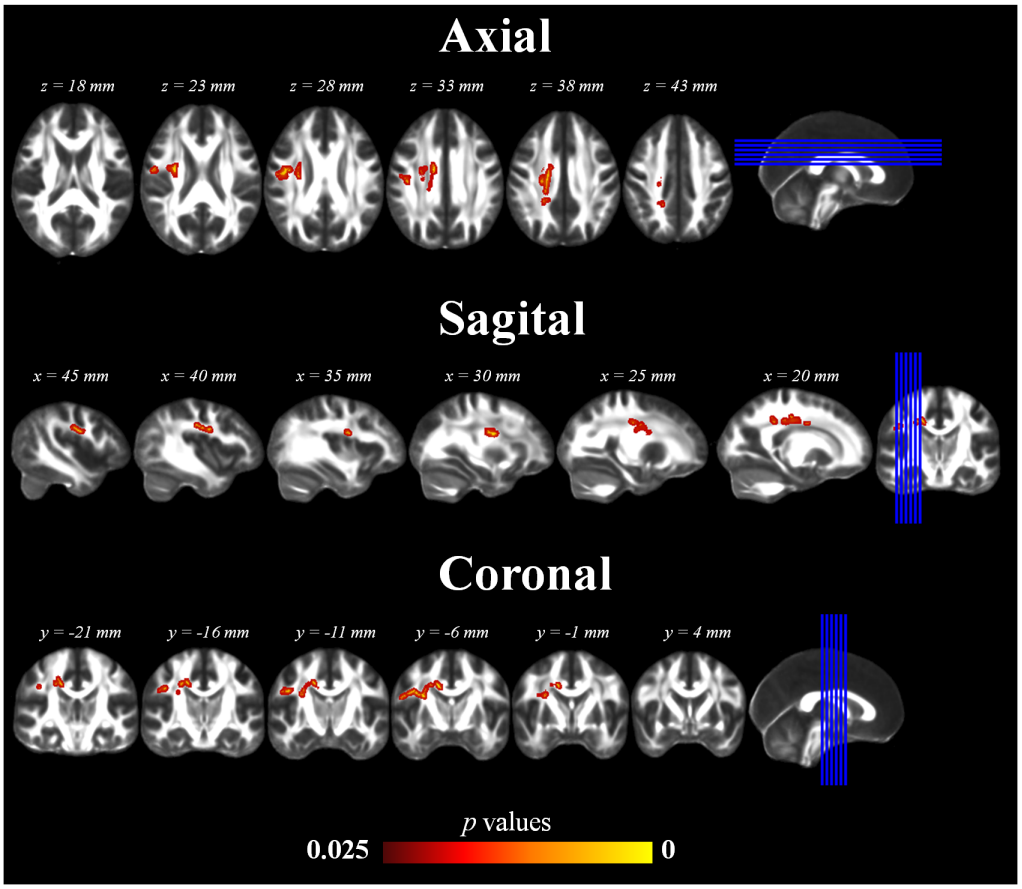

FIGURE 4.2: Results of the AD analysis. Areas of significant difference ($p \leq 0.025$) in the contrast G2/G2 < Non-G2/Non-G2.

any significant difference (at the level of $p \leq 0.025$, Bonferroni-corrected for the number of tests). See Appendix A.7.

The analysis of differences between G2+ and G2– adjusted for the number of G2 alleles did not show any significant difference (at the level of $p \leq 0.0125$, Bonferroni-corrected for the number of tests). See Appendix A.8. There were no clusters exhibiting any significant positive or negative effect with the number of G2 alleles. See Appendix A.8.

4.3.4 Radial diffusivity

The F-test revealed that no significant differences in RD existed among the groups (G2/G2, G2/Non–G2 and Non–G2/Non–G2). See Appendix A.9.

Contrast	**Min. *p***	**X, Y, Z of min. *p***	**Structures of min. *p***	**Hem.**
G2/G2	0.34	-15, -34, 27	†Splenium of corpus callosum	L
>Non–	0.65	25, -47, -36	3% Corticospinal tract R	R
G2/Non–G2	0.829	-22, -42, -39	3% Corticospinal tract L	L
G2/G2	0.018*	30, -7, 25	8% Superior longitudinal fasciculus R, 3% Superior longitudinal fasciculus (temporal part) R	R
<Non–				
G2/Non–G2	0.027	-17, -22, 35	†Body of corpus callosum	L
	0.727	11, -7, 5	53% Anterior thalamic radiation R	R
	0.861	-26, -20, 53	Unclassified	-
	0.78	3, -14, -6	32% Anterior thalamic radiation R	R
G2/Non–G2	0.725	10, -32, -28	18% Corticospinal tract R	R
>Non–	0.765	27, -65, -41	3% Corticospinal tract R	R
G2/Non–G2	0.748	20, -32, 9	†Fornix (cres) / Stria terminalis R	R
	0.847	11, -22, 11	16% Anterior thalamic radiation R	R
G2/Non–G2	0.118	17, -25, 53	3% Corticospinal tract R	R
<Non–				
G2/Non–G2	0.892	27, 27, 14	24% Inferior fronto-occipital fasciculus R	R
G2/G2	0.188	8, 17, 20	†Body of corpus callosum	R
>G2/Non–				
G2				
G2/G2	0.152	-22, -55, 30	8% Inferior longitudinal fasciculus L, 3% Inferior fronto-occipital fasciculus L	L
<G2/Non–				
G2				

* $p \leq 0.025$
† Areas defined according to JHU ICBM-DTI-81 White-Matter Labels

TABLE 4.4: Analysis of AD. Results of the independent-samples t-tests showing clusters of minimum p value (corrected), MNI coordinates, name of the structures and hemisphere. Only clusters with a minimum of 100 voxels are presented. Structures defined according to JHU White-Matter Tractography Atlas.

The independent-samples t-test for the G2+ and G2– samples did not show any significant difference (at the level of $p \leq 0.025$, Bonferroni-corrected for the number of tests). See Appendix A.10.

The analysis of differences between G2+ and G2– adjusted for the number of G2 alleles did not show any significant difference (at the level of $p \leq 0.0125$, Bonferroni-corrected for the number of tests). See Appendix A.11. There were no clusters exhibiting any significant positive or negative effect with the number of G2 alleles. See Appendix A.11.

Contrast	**Min. *p***	**X, Y, Z of min. *p***	**Structures of min. *p***	**Hem.**
G2/G2 <Non–G2/Non–G2	0.018*	30, -7, 25	8% Superior longitudinal fasciculus R, 3% Superior longitudinal fasciculus (temporal part) R	R
	0.02*	19, -24, 35	†Body of corpus callosum	R
	0.025*	26, -18, 34	34% Corticospinal tract R	R

* $p \leq 0.025$
† Areas defined according to JHU ICBM-DTI-81 White-Matter Labels

TABLE 4.5: Analysis of AD. Results of the independent-samples t-test of the contrast G2/G2 < Non–G2/Non–G2 showing clusters of minimum p value (corrected), MNI coordinates, name of the structures and hemisphere. Only clusters with a minimum of 100 voxels are presented. Structures defined according to JHU White-Matter Tractography Atlas.

4.3.5 Region-of-interest analysis

The individuals mean FA, MD, AD and RD were extracted from the regions exhibiting a significant difference of AD between the G2/G2 and Non–G2/Non–G2 groups (Figure 4.2). The mean values of the four parameters were used for statistical analysis in SPSS software (Version 17.0, IBM SPSS Statistics).

One-way ANOVA tests were used to investigate inter-group differences in the four parameters when comparing G2/G2, G2/Non–G2 and Non–G2/Non–G2 groups. Tukey post-hoc tests were performed to determine the direction of the effect. Independent-samples t-tests were also performed to test for differences between G2+ and G2–.

A one-way ANOVA showed that differences in FA existed among the groups based on the G2 allelic frequency (G2/G2, G2/Non–G2 and Non–G2/Non–G2); $F(2,60) = 4.094$, $p = 0.022$. A Tukey post-hoc test revealed that the FA in the G2/G2 group (0.515 ± 0.014) was statistically significantly lower than that in the Non–G2/Non–G2 group (0.533 ± 0.016), $p = 0.017$. Box plots and mean plots are presented in Figure 4.3. An independent-samples t-test revealed that were no differences in FA between the groups based on the G2 prevalence (G2+ and G2–); $t(61) = 1.820$, $p = 0.074$. Box plots are presented in Figure 4.4.

A one-way ANOVA showed that differences in MD existed among the groups based on the G2 allelic frequency (G2/G2, G2/Non–G2 and Non–G2/Non–G2); $F(2,60) = 6.839$, $p = 0.002$. A Tukey post-hoc test revealed that the MD in the G2/G2 group (0.000699 ± 0.000019) was statistically significantly lower than that

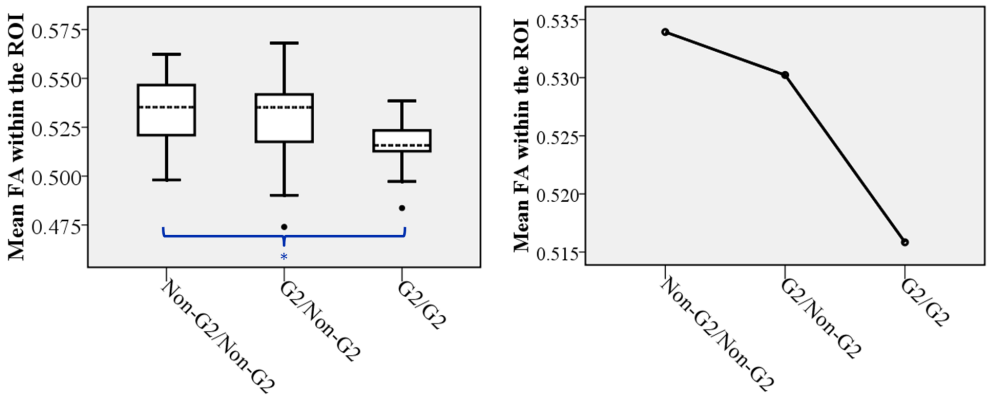

FIGURE 4.3: Box plots (left) and mean plot (right) of the mean FA within the ROI. Significant differences are shown in blue.

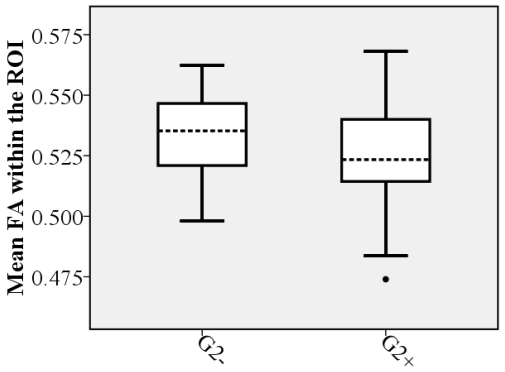

FIGURE 4.4: Box plots of the mean FA within the ROI.

in the Non–G2/Non–G2 group (0.000726 ± 0.000023), $p = 0.003$. Box plots and mean plots are presented in Figure 4.5. An independent-samples t-test revealed that MD in the G2+ was statistically significantly lower than that in the G2– group; $t(61) = 3.368$, $p = 0.001$. Box plots are presented in Figure 4.6.

A one-way ANOVA showed that differences in AD existed among the groups based on the G2 allelic frequency (G2/G2, G2/Non–G2 and Non–G2/Non–G2); $F(2,60) = 17.334$, $p < 0.001$. A Tukey post-hoc test revealed that the AD in the G2/G2 group (0.00112 ± 0.00002) was statistically significantly lower than that in the Non–G2/Non–G2 group (0.00119 ± 0.00003); $p < 0.001$. The Tukey post-hoc test also revealed that the AD in the G2/G2 group was statistically significantly lower than that in the G2/Non–G2 group (0.00116 ± 0.00004); $p =$

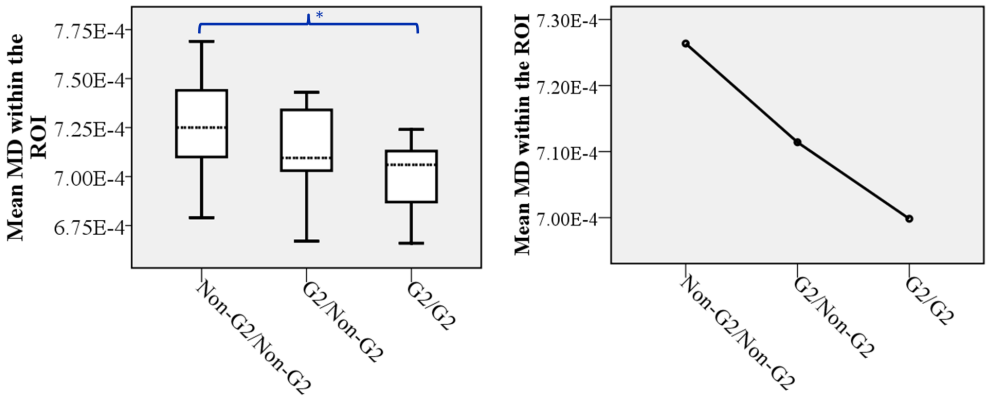

FIGURE 4.5: Box plots (left) and mean plot (right) of the mean MD within the ROI. Significant differences are shown in blue.

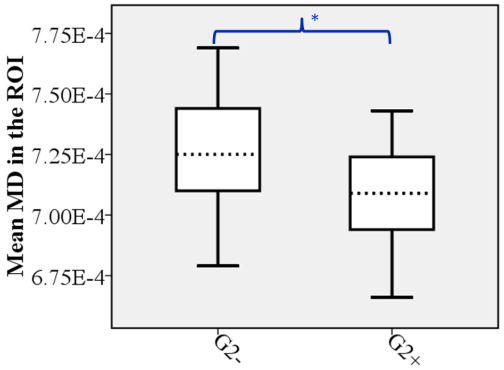

FIGURE 4.6: Box plots of the mean MD within the ROI. Significant differences are shown in blue.

0.007. The Tukey post-hoc test showed that the AD in the G2/Non–G2 group was statistically significantly lower than that in the Non–G2/Non–G2 group; $p = 0.011$. Box plots and mean plots are presented in Figure 4.7. An independent-samples t-test revealed that AD in the G2+ was statistically significantly lower than that in the G2– group; $t(61) = 4.624$, $p < 0.001$. Box plots are presented in Figure 4.8.

A one-way ANOVA showed that there were no differences in RD among the groups based on the G2 allelic frequency (G2/G2, G2/Non–G2 and Non–G2/Non–G2); $F(2,60) = 0.604$, $p = 0.550$. Box plots and mean plots are presented in Figure 4.9. An independent-samples t-test revealed that were no differences in

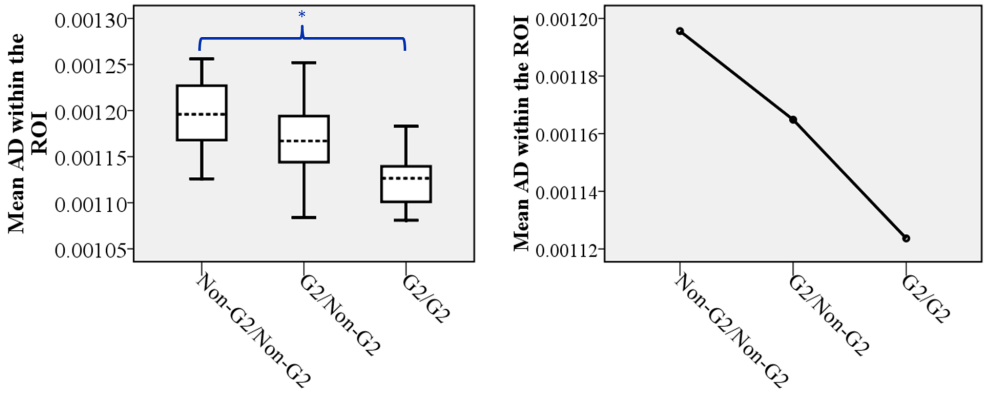

FIGURE 4.7: Box plots (left) and mean plot (right) of the mean AD within the ROI. Significant differences are shown in blue.

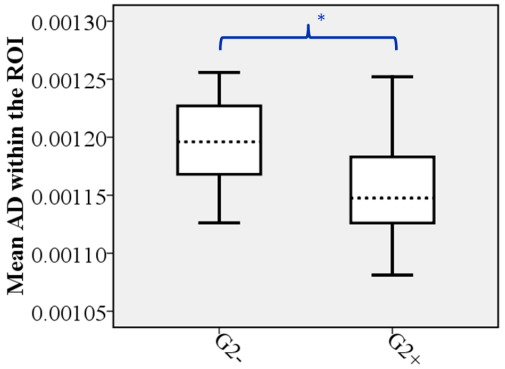

FIGURE 4.8: Box plots of the mean AD within the ROI. Significant differences are shown in blue.

RD between the groups based on the G2 prevalence (G2+ and G2–); $t(61) = 1.023$, $p = 0.310$. Box plots are presented in Figure 4.10.

4.3.6 Comparison of rigt and left hemispheres

The symmetry analysis did not reveal any significant difference in right-left FA in the groups based on the allelic prevalence or frequency of G2. See Appendix A.12.

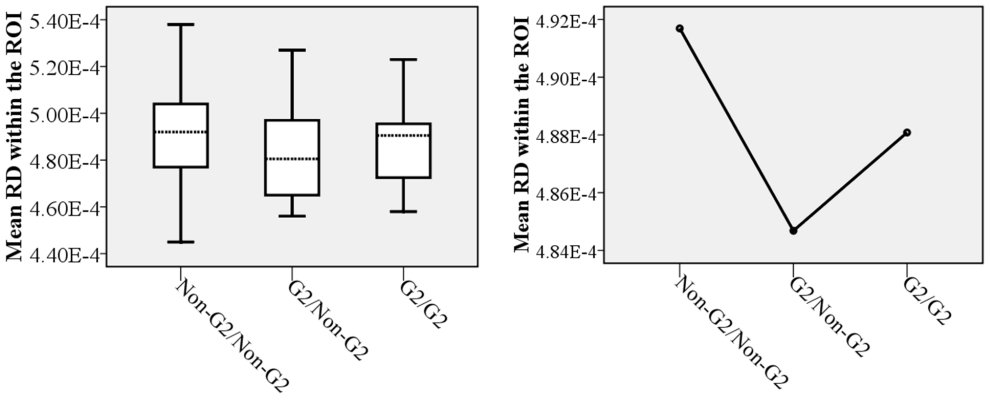

FIGURE 4.9: Box plots (left) and mean plot (right) of the mean RD within the ROI.

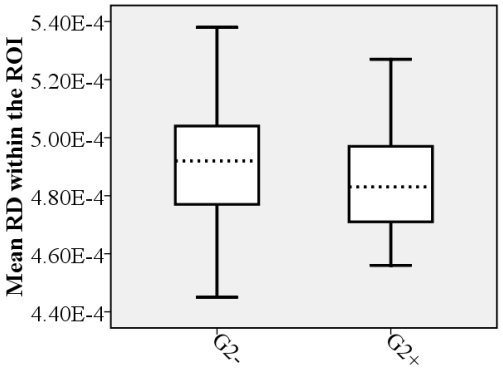

FIGURE 4.10: Box plots of the mean RD within the ROI.

The symmetry analysis did not reveal any significant difference in right-left MD in the groups based on the allelic prevalence or frequency of G2. See Appendix A.13.

The F-test revealed that differences in right-left AD existed among the groups (G2/G2, G2/Non–G2 and Non–G2/Non–G2). See Table 4.6. The subsequent independent-samples t-tests did not reveal any statistically significant difference among the groups (at the level of $p \leq 0.025$, Bonferroni-corrected for the number of tests). See Table 4.7.

The symmetry analysis did not reveal any significant difference in right-left RD in the groups based on the allelic prevalence or frequency of G2. See Appendix

A.14.

4.4 Discussion

In this chapter it was described how the DW images from the sample of healthy male volunteers underwent TBSS analysis. The analysis permitted comparisons among the subgroups on the basis of G2 allelic prevalence and frequency. The TBSS approach also permitted to investigate differences in symmetry on the basis of the prevalence or frequency of G2.

The results showed that there were significant differences in the diffusion parameters among the different subgroups depending on the presence and number of G2 alleles. In the analysis of tracts, non-carrier volunteers exhibited significantly increased AD in the right superior longitudinal fasciculus (SLF), right corticospinal tract (CST) and body of the corpus callosum in comparison to homozygote carriers of the G2 allele. Furthermore, when a ROI analysis of these tracts was performed additional differences in fractional anisotropy and mean diffusivity emerged. The morphologic interpretation of the results is challenging because the sample of volunteers measured were healthy individuals with no history of neurologic disease or head trauma, which means that the differences are not due to structural disruptions but to different fibre properties. In principle, anisotropic water diffusion in white matter is related to the ordered arrangement of the myelinated fibres (Beaulieu 2002), and it has been proposed that such diffusion process is perpendicularly limited by the myelin sheath around the axons, the axonal membrane itself and the neurofibrils (microtubules, neurofilaments) (Beaulieu 2002). Investigations about this issue suggest that axonal membranes play the primary role and that myelination modulates the degree of anisotropy (Beaulieu 2002).

The key for understanding the differences found could be in relation with brain development and maturation. It was proposed that changes in water apparent diffusion are likely related to changes in brain water content, and that changes in anisotropy are linked to changes in tissue microstructure (Neil et al. 2002). In principle, AD describes the water mobility along the axis of the fibre (Jones et al. 2013) and reflects a number of aspects related to the microstructure of white matter, although the exact features that contribute to the AD remain unknown.

Nevertheless, it has been widely accepted that AD is influenced by the integrity of the axons, as well as by the orientation spread of the fibres (Jones et al. 2013). Therefore, the differences reported in this sub-study could be attributed to differences in the arrangement and/or density of the fibres. Unfortunately, and despite years of investigation, there is still very little understanding of the actual mechanisms responsible for many of these phenomena.

It has been demonstrated that the presence of a difference in the diffusion-weighted signals between two or more groups of subjects is an useful outcome (Jones et al. 2013), although further developments and studies are needed for its understanding. In the case of this particular sub-study, the use of diffusion kurtosis imaging, multi-tensor imaging and ultra-high magnetic fields and gradients could uncover the microstructural correlates of the differences found.

The results presented here suggest that the expression of the G2 allele affects white matter microstructure as revealed by diffusion parameters. Interestingly, such differences are initially confined to particular tracts, such as the SLF, the right CST and the body of corpus callosum. This could mean that the expression of G2 alleles might be involved in the definition of white matter microstructure in those particular tracts.

The CST is a major tract of the human brain and originates from the frontoparietal cortices, including the primary motor cortex, secondary motor area and somatosensory cortex (Jang 2014). It is mainly involved in the movement of the limbs and trunk (York 1987; Davidoff 1990; Heffner & Masterton 1983). The SLF is a bundle of association fibres connecting the parietal, occipital and temporal lobes with the ipsilateral frontal cortices (Schmahmann et al. 2008; Kamali et al. 2014). The SLF facilitates the formation of a bidirectional neural network that is necessary for core processes such as attention, memory, emotions and language (Mesulam 1998; Petrides & Pandya 2002). In the animal study by Homanics et al. (1997) it was demonstrated that alterations in the expression of GABRB3 result in motor alterations, hyperactivity and lack of coordination. Therefore, the differences in diffusion parameters found in this study fit well with the notion that the expression of the GABRB3 gene is crucial for the configuration of the microstructure in motor and association tracts such as the CST and SLF.

With respect to the corpus callosum, it has already been suggested that the microstructure of this structure is under genetic control (Kanchibhotla et al. 2014). The results presented here support this notion, and highlight the role of GABRB3 in the definition of microstructural features of the corpus callosum.

Another interesting finding was that the differences found were only significant between the non-carriers and the homozygote carriers of G2. The heterozygote carriers of G2 exhibited intermediate values in FA, MD and AD, suggesting that the expression of both alleles is important, and therefore, co-dominance in the expression of GABRB3 could be hypothesised.

Interestingly, the differences found in diffusivity in this sub-study are limited to the non-dominant hemisphere, and the two tracts where differences were established are precisely tracts engaged in highly lateralised functions, such as motor functions of the hand and language. Crucially, leftward asymmetry of these two tracts has been previously described in a large sample of healthy individuals (Takao et al. 2011), mirroring the hemispheric lateralisation of their functions. The differences described here could imply differences in brain development that are compensated by the impact of hemispheric dominance, being only evident in the non-dominant hemisphere in the adult age. Some studies have shown that apparent diffusion coefficient and diffusion anisotropy measures change dramatically during development, reflecting underlying changes in tissue water content and cytoarchitecture (Neil et al. 2002). This fact will be described in greater detail in Chapter 8.

Contrast	Min. p	X, Y, Z of min. p	Structures of min. p	Hem.
F–test	0.045*	-25, -4, 33	5% Superior longitudinal fasciculus L	L
	0.449	-37, -13, 27	53% Superior longitudinal fasciculus L, 37% Superior longitudinal fasciculus (temporal part) L	L
	0.509	-23, 38, 9	37% Anterior thalamic radiation L, 5% Forceps minor	L
	0.744	-22, 46, -5	13% Anterior thalamic radiation L, 8% Uncinate fasciculus L	L
	0.515	-16, -23, -6	26% Corticospinal tract L	L
G2+ >G2–	0.291	-44, -8, 26	47% Superior longitudinal fasciculus L, 26% Superior longitudinal fasciculus (temporal part) L	L
	0.566	-20, -18, 50	11% Corticospinal tract L, 3% Anterior thalamic radiation L	L
	0.86	-18, -3, 41	†Superior corona radiata L	L
	0.842	-19, -1, 47	Unclassified	-
G2+ <G2–	0.444	-11, -25, -29	18% Corticospinal tract L	L
	0.588	-19, -13, -6	24% Corticospinal tract L	L
	0.747	-25, -81, 8	8% Inferior longitudinal fasciculus L, 8% Forceps major	L
	0.825	-30, -27, 7	†Retrolenticular part of internal capsule L	L
	0.838	-31, -53, 15	18% Inferior longitudinal fasciculus L, 11% Inferior fronto-occipital fasciculus L	L
G2+ >G2– adjusted	0.652	-44, -1, 25	8% Superior longitudinal fasciculus L, 5% Superior longitudinal fasciculus (temporal part) L	L
	0.765	-28, -47, 53	Unclassified	-
G2+ <G2– adjusted	0.539	-28, -17, 22	8% Corticospinal tract L, 3% Superior longitudinal fasciculus L	L
Positive effect of G2	0.531	-29, -11, 17	8% Superior longitudinal fasciculus L, 3% Superior longitudinal fasciculus (temporal part) L	L
	0.698	-9, -36, 21	†Splenium of corpus callosum	L
	0.637	-23, -52, 22	†Splenium of corpus callosum	L
	0.811	-21, -38, 31	3% Superior longitudinal fasciculus L, 3% Anterior thalamic radiation L	L
Negative effect of G2	0.664	-29, -72, 1	39% Inferior fronto-occipital fasciculus L, 18% Inferior longitudinal fasciculus L	L

* $p \leq 0.05$ ** $p \leq 0.025$ *** $p \leq 0.0125$

† Areas defined according to JHU ICBM-DTI-81 White-Matter Labels

TABLE 4.6: Analysis of AD symmetry. Results of the F-test (one-way ANOVA), independent-samples t-test, independent-samples t-test adjusted and the effect of the number of G2 alleles. Clusters of minimum p value (corrected), MNI coordinates, name of the structures and hemisphere. Only clusters with a minimum of 100 voxels are presented. Structures defined according to JHU White-Matter Tractography Atlas.

Contrast	**Min. *p***	**X, Y, Z of min. *p***	**Structures of min. *p***	**Hem.**
G2/G2 >Non–G2/Non–G2	0.774	-8, -29, 24	3% Anterior thalamic radiation L	L
	0.723	-44, -14, 27	55% Superior longitudinal fasciculus L, 18% Superior longitudinal fasciculus (temporal part) L	L
G2/G2 <Non–G2/Non–G2	0.619	-28, -62, 15	21% Forceps major, 8% Inferior longitudinal fasciculus L	L
	0.679	-26, -33, 26	3% Corticospinal tract L	L
G2/Non–G2 >Non–G2/Non–G2	0.297	-47, -10, 26	47% Superior longitudinal fasciculus L, 24% Superior longitudinal fasciculus (temporal part) L	L
	0.624	-37, -8, 46	Unclassified	L
G2/Non–G2 <Non–G2/Non–G2	0.57	-9, -22, -27	58% Corticospinal tract L	L
G2/G2 >G2/Non–G2	0.529	-29, -11, 17	8% Superior longitudinal fasciculus L, 3% Superior longitudinal fasciculus (temporal part) L	L
	0.625	-20, -51, 22	5% Forceps major	L
	0.731	-9, -36, 21	†Splenium of corpus callosum	L
	0.775	-21, -38, 31	3% Superior longitudinal fasciculus L, 3% Anterior thalamic radiation L	L
G2/G2 <G2/Non–G2	0.679	-29, -72, 1	39% Inferior fronto-occipital fasciculus L, 18% Inferior longitudinal fasciculus L	L
	0.799	-30, -66, 18	5% Inferior fronto-occipital fasciculus L, 5% Forceps major	L

* $p \leq 0.025$

† Areas defined according to JHU ICBM-DTI-81 White-Matter Labels

TABLE 4.7: Analysis of AD symmetry. Results of the independent-samples t-tests showing clusters of minimum p value (corrected), MNI coordinates, name of the structures and hemisphere. Only clusters with a minimum of 100 voxels are presented. Structures defined according to JHU White-Matter Tractography Atlas.

Chapter 5

Investigation of the effect of GABRB3 polymorphisms on resting state networks using functional magnetic resonance imaging

5.1 Background

The concept of resting state arose from positron emission tomography (PET) and functional magnetic resonance imaging (fMRI) studies in which the focus moved from the stimuli-related brain responses to the spontaneous fluctuations of activity when the brain is not engaged in any particular task (Biswal et al. 1995; Biswal et al. 1997; Raichle et al. 2001). It was thereby discovered that there exists a high correlation and temporal synchrony of the fMRI blood oxygen level-dependence (BOLD) series among relatively distant brain regions (Biswal et al. 1997). The analysis of resting state data is possible through independent component analysis (ICA, Beckmann et al. 2005), where the low-frequency patterns of the brain activity at rest are characterised and identified. ICA also permitted to differentiate the intrinsic brain activity at rest from the noise, and therefore, it has now been demonstrated that the functional connectivity has a neuronal

underpinning and cannot purely be the result of physiological noise (Birn 2012). The existence of such functional connectivity maps, namely resting state networks (RSN), has been confirmed through MRI and PET studies (Buckner et al. 2008), where the default-mode network (DMN) has gained particular interest due to its relationship with neurological and psychiatric conditions (Bluhm et al. 2007; Delaveau et al. 2010; Greicius et al. 2004; Leech & Sharp 2014; Quarantelli et al. 2013; Sorg et al. 2007; Werner et al. 2014; Whitfield-Gabrieli et al. 2009) as well as with normal ageing (Damoiseaux et al. 2008).

The canonical DMN comprises the precuneus, anterior cingulate cortex, posterior cingulate cortex (PCC), medial prefrontal cortex and lateral parietal inferior gyri (Fransson 2005; Greicius et al. 2004; Raichle et al. 2001). The DMN is thought to characterise the basal neural activity (Raichle & Snyder 2007; Snyder & Raichle 2012) and has been linked to self-referential thought, introspection and integration of cognitive and emotional processing (Greicius et al. 2003). The DMN shows strong activity during rest, as well as rapid deactivation during externally directed tasks (Fox et al. 2005). The DMN is also believed to represent an introspectively oriented mode of the mind, which provides readiness and alertness to changes in the external and internal environment (Fransson 2005). From all the regions that form the DMN, the posterior components, precuneus and PCC, seem to act as an intrinsic mediatory node of this network (Cavanna & Trimble 2006; Hagmann et al. 2008), a relevant fact that will be later discussed in Chapter 6.

The activity of the RSNs appears to be closely controlled by genetic factors (Glahn et al. 2010), where the main evidence emerged from the study of polymorphisms. In an fMRI study by Rao et al. (2007) the effect of a variant of the human serotonin transporter (5-HTT) gene was found to alter resting brain function in the amygdala and the ventromedial prefrontal cortex. The same gene showed in a different study to modulate the resting state cerebral blood flow in amygdala (El-Hage et al. 2013). Similarly, Clemens et al. (2014) found that carriers of a variant of the monoamine oxidase A gene exhibited increased activity within frontoparietal and temporal parts of the DMN and the cerebellum. Interestingly, a polymorphism of the KIBRA gene (rs17070145) was associated with differences in synchronisation within the DMN and executive control network (Wang et al. 2013). The gene that codifies for the apolipoprotein E (APOE) has been frequently investigated in fMRI studies and the effects of APOE on the

functional architecture of the resting brain appears to have an intrinsic effect on the differentiation of functional networks in the brain (Trachtenberg et al. 2012). Filippini et al. (2009), for example, found that carriers of the APOE4 allele exhibited different patterns of brain activity within the DMN. In a study by Yang et al. (2014), it was found that the allele APOE4 affects the complexity and functional connectivity of the resting brain.

As it was discussed in Chapter 2, the GABRB3 is an important gene in neurodevelopment (Tanaka et al. 2012), and according to animal studies it is of great importance in motor functions and coordination (Homanics et al. 1997). In Chapter 4, differences in structural connectivity were found, and therefore it would be of interest to test the functional connectivity at rest on the basis of the expression of the G2 allele. Therefore, this sub-study aims to investigate whether differences in the intrinsic activity of the RSNs exist among the groups of healthy male volunteers on the basis of G2 allelic prevalence and G2 frequency.

5.2 Methods

5.2.1 Subjects and data acquisition

Data from 63 volunteers (mean age = 25.57, SD = 3.38) were included in this sub-study. Details about the samples are presented in Chapter 2. FMRI images were acquired using a T2*-weighted EPI sequence (TR = 2.2 s, TE = 30 ms, voxel-size = $3.12 \times 3.12 \times 3.3$ mm^3 and matrix-size = $64 \times 64 \times 36$) in a 3 T Siemens Magnetom Trio scanner (Erlangen, Germany). The functional time series consisted of 165 volumes. Consistent instructions of eyes closed, do not think of anything in particular, and do not move or fall asleep, were given before the acquisition of the data.

5.2.2 Data analysis

Analysis of fMRI data was carried out using Probabilistic Independent Component Analysis (Beckmann & Smith 2004) as implemented in MELODIC (Multivariate Exploratory Linear Decomposition into Independent Components, Version 3.10, http://fsl.fmrib.ox.ac.uk/fsl/fslwiki/MELODIC), part of FSL (Smith

et al. 2004, http://fsl.fmrib.ox.ac.uk/fsl/fslwiki/). Individual pre-processing consisted of motion correction using MCFLIRT (Jenkinson et al. 2002, http://fsl.-fmrib.ox.ac.uk/fsl/fslwiki/MCFLIRT), brain extraction using BET (Smith 2002, http://fsl.fmrib.ox.ac.uk/fsl/fslwiki/BET), spatial smoothing using a Gaussian kernel of FWHM of 5 mm, and high-pass temporal filtering of 100 s (0.01 Hz). FMRI volumes were registered to the structural scan of each individual and standard space (MNI152) images using the nonlinear image registration tool (FNIRT, http://fsl.fmrib.ox.ac.uk/fsl/fslwiki/FNIRT) implemented in FSL. Group pre-processing consisted of voxel-wise de-meaning of the data and normalisation of the voxel-wise variance. Pre-processed data were whitened and projected into a 21-dimensional subspace using probabilistic principal component analysis where the number of dimensions was estimated using the Laplace approximation to the Bayesian evidence of the model order (Beckmann & Smith 2004). The whitened observations were decomposed into sets of vectors which described signal variation across the time-courses, the subject domain and across the spatial domain by optimising for non-Gaussian spatial source distributions using a fixed-point iteration technique (Hyvärinen 1999). Estimated component maps were divided by the standard deviation of the residual noise and thresholded by fitting a mixture model to the histogram of intensity values (Beckmann & Smith 2004). The resulting maps were compared with a set of well-described RSNs (Smith et al. 2009, http://fsl.fmrib.ox.ac.uk/fsl/fslwiki/BET) by calculating the correlation coefficient for each pair of maps. Any map with a correlation coefficient $r > 0.50$ was considered as a 'well described' RSN. The between-subject analysis of the resting data was carried out using a regression technique called 'dual regression' (Filippini et al. 2009, http://fsl.fmrib.ox.ac.uk/fsl/fslwiki/DualRegression) that allows for voxel-wise comparisons of activation patterns. The regression analysis generated spatial maps representing the individual contribution to the group resting state maps. Finally, a voxel-wise statistical analysis was applied using GLM and permutation-based testing, corrected for multiple comparisons across space, similarly as in Chapters 3 and 4. A graphical representation of the analysis steps is presented in Figure 5.1.

For each 'well described' RSN the following statistical approach was performed: a one-way ANOVA was used to test for inter-group differences when comparing G2/G2, G2/Non–G2 and Non–G2/Non–G2 within the framework of GLM (referred as F-test); a Monte Carlo permutation test was used, and hence, a random

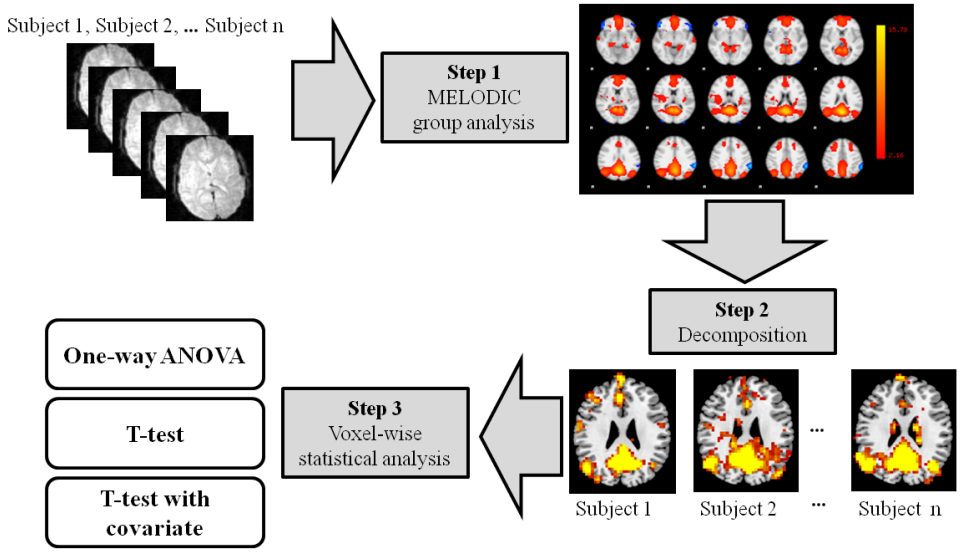

FIGURE 5.1: Pipeline of the resting state data analysis

subset of 5000 permutations were performed. In the case of a significant F-test, individual t-tests (independent-samples) with a random subset of 5000 permutations were used to determine the direction of the effect. An independent-samples t-test with a random subset of 5000 permutations was also performed to test for differences between G2+ and G2–. Additionally, a two-group difference test adjusted for covariate was performed to investigate possible differences between G2+ and G2–; here, the number of G2 alleles was included as a regressor to explain possible differences between the two groups.

5.3 Results

All the volunteers reported full compliance with the instructions given before the measurement. Twenty-one components were found after decomposition of the data by means of ICA, and eight were considered as 'well described' (i.e. those with a correlation coefficient r >0.50). In accordance with the study by Smith et al. (2009) the following eight RSNs were identified in the data: DMN, medial 'visual network' (MVN), lateral 'visual network' (LVN), 'sensorimotor' network (SMN), 'auditory' network (AN), 'executive control' network (ECN), right and left 'frontoparietal' networks (RFPN, LFPN), See Figure 5.2.

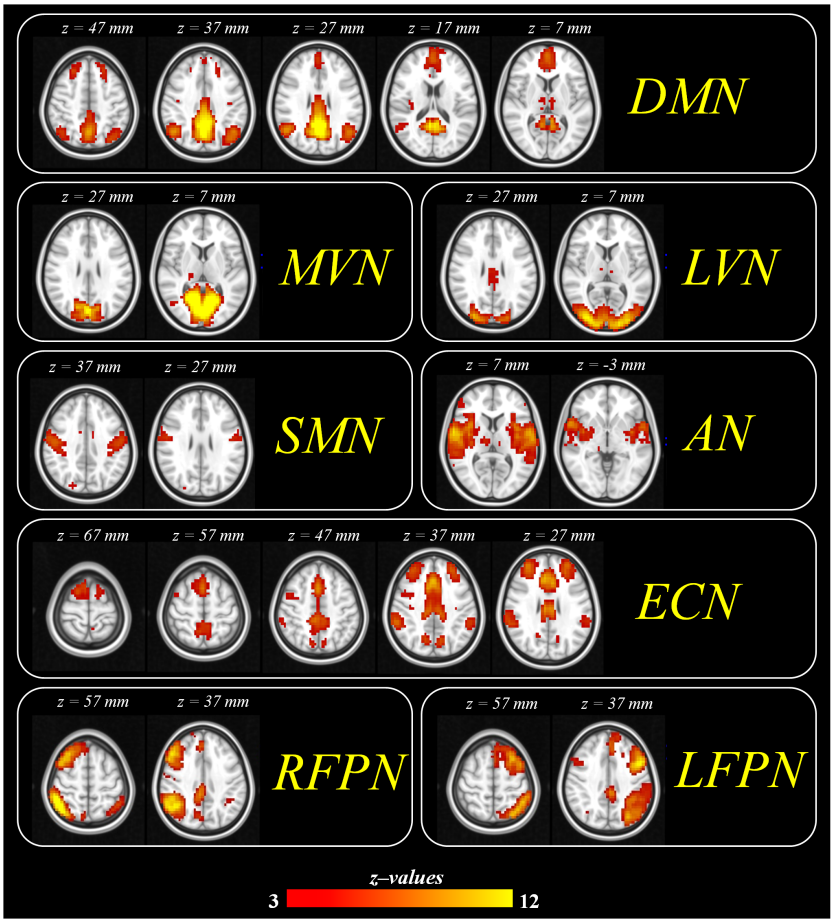

FIGURE 5.2: 'Well described' RSNs identified in the group analysis of the 63 subjects

The voxel-wise F-tests (one-way ANOVA) exhibited voxels where differences in activation pattern of the RSNs existed among the groups (G2/G2, G2/Non–G2 and Non–G2/Non–G2). After thresholding for statistically significance ($p \leq 0.05$), no differences were encountered for the DMN (Appendix B.1), MVN (Appendix B.2), LVN (Appendix B.3), SMN (Appendix B.4), AN (Appendix B.5), ECN (Appendix B.6), RFPN (Appendix B.7) or LFPN (Appendix B.8).

The voxel-wise independent-samples t-tests revealed voxels where differences in activation pattern of the RSNs existed between the groups (G2+ and G2–). After thresholding for statistically significance (at the level of $p \leq 0.025$, Bonferroni-corrected for the number of tests), no differences were encountered for the DMN (Appendix B.9), MVN (Appendix B.10), LVN (Appendix B.11), SMN (Appendix

B.12), AN (Appendix B.13), ECN (Appendix B.14), RFPN (Appendix B.15) or LFPN (Appendix B.16).

In the analysis of differences between G2+ and G2– adjusted for the number of G2 alleles none of the voxels survived after the thresholding for significance (at the level of $p \leq 0.0125$, Bonferroni-corrected for the number of tests) in the DMN (Appendix B.17), MVN (Appendix B.18), LVN (Appendix B.19), SMN (Appendix B.20), AN (Appendix B.21), ECN (Appendix B.22), RFPN (Appendix B.23) or LFPN (Appendix B.24). There were no clusters in any RSN exhibiting any significant positive or negative effect with the number of G2 alleles.

5.4 Discussion

In this chapter it was described how the resting state functional images from the sample of healthy male volunteers underwent group ICA and a regression analysis. The analyses permitted the comparisons of activation patterns of the RSNs among subgroups on the basis of G2 allelic prevalence and G2 frequency.

The results showed that there were no statistically significant differences in the patterns of the RSNs between the different subgroups on the basis of the G2 allelic prevalence or frequency. There was also no effect of the number of G2 alleles carried by the subjects. The results presented here suggest that the expression of the G2 allele do not affect the patterns of activation of the RSNs. Similarly as in Chapter 3, the importance of reporting negative results must be highlighted, since they also provide understanding of the mechanisms of heredity.

As it was discussed in the introduction of this sub-study, the genetic control over the activity of the RSNs has been already demonstrated (Glahn et al. 2010), and moreover, such genetic factors seem to influence neuroanatomy and functional connectivity distinctly, suggesting that unique genes influence the structure and function of the networks (Glahn et al. 2010). Nevertheless, the particular genes controlling the resting state activity still remain undiscovered. The identification of these genes will provide the basis in the understanding of the intrinsic architecture of the brain. Hence, although in this sub-study negative results were presented, it does not imply a lack of usefulness; on the contrary, one could

assert that these results add knowledge to the field of resting state. Interestingly, modulatory functions of GABA in the activity of the RSNs have been proved (Arrubla et al. 2014; Duncan, Wiebking & Northoff 2014; Northoff et al. 2007), and such functions do not seem to be controlled by the allelic forms of the GABRB3 expressed. This could imply that polymorphisms of such gene do not affect the binding area of GABA in the GABA-A receptor.

In this sub-study the statistical comparisons were performed on the basis of G2, the most frequent CA allele of the GABRB3. As it was discussed previously, this sub-study was sufficiently powered with respect to G2 and included a sufficiently large sample in each subgroup; yet, no other subgroups could be formed on the basis of other allelic polymorphisms. The process of investigating the effect of a candidate gene implies the use of much larger samples in order to be able to investigate the effect of all polymorphisms; the genetic investigation also implies the existence of representative samples where the results could be extended to the general population. Hence, the conclusions of this sub-study, similarly as in previous chapters, are limited to the effect of the G2 allele on the population. Studies including larger samples of volunteers and a complete genetic profile, such as the Human Connectome Project (Van Essen et al. 2012), have the potential to discover the particular genes controlling the patterns of resting state activity.

Chapter 6

Investigation of the effect of GABRB3 polymorphisms on GABA and glutamate in the posterior cingulate cortex using magnetic resonance spectroscopy

6.1 Background

Magnetic resonance spectroscopy (MRS) has been extensively used in neuroimaging studies in the last decade due to its potential in assessing the biochemistry of the brain noninvasively. A large amount of attention has been drawn to the concentration of glutamate and gamma-aminobutyric acid (GABA), the neurotransmitters responsible for the excitation-inhibition balance (Duncan, Wiebking, Muoz-Torres, et al. 2014). The role of these neurotransmitters has been investigated in several brain regions in relation to diseases (Hasler et al. 2007) as well as in relation to functional measures such as EEG and fMRI (Arrubla et al. 2014; Donahue et al. 2010; Enzi et al. 2012; Hahn et al. 2012; Kapogiannis et al. 2013; Muthukumaraswamy et al. 2009; Northoff et al. 2007). GABA is the

most important inhibitory neurotransmitter in the brain; therefore, it has been linked to several neurological and psychiatric disorders such as epilepsy, panic disorder and depression (Sanacora et al. 2004), and for example, abnormal levels of glutamate and GABA have been reported in patients suffering from major depressive disorder (Hasler et al. 2007). Measures of glutamate by means of MRS have gained particular attention due to studies in which changes in glutamate concentration have been observed during enhanced neuronal activity (Lin et al. 2012; Schaller et al. 2014). Glutamate is the major excitatory neurotransmitter in the human brain and is intimately related to its metabolism.

Recently, Napolitano et al. (2013) demonstrated that using a standard PRESS sequence with a set of optimised echo time parameters, they could reliably detect GABA and glutamate in the ACC and the precuneus region in a shorter measurement time and in a smaller voxel size than previous studies with MEGA-PRESS. Another often applied method to detect neurotransmitters is two-dimensional MRS (Ke et al. 2000) in which a series of spectra that differ by a single parameter, such as a delay duration or the timing of a refocusing pulse, are acquired. The second spectral dimension contains the coupling information which, in turn, allows overlapping multiplets to be resolved. However, these experiments usually require longer acquisition time due to the increased number of measurements. Because of the time constrain in this multi-modality investigation, the standard PRESS sequence with optimised echo time parameters is the preferred method to detect GABA and glutamate in a specific region.

As it was discussed in Chapter 5, precuneus and PCC act as an intrinsic mediatory node of the DMN (Cavanna & Trimble 2006; Hagmann et al. 2008), and interestingly, the PCC is one of the areas exhibiting significantly higher activity at rest, as it has been demonstrated by PET and arterial spin labelling studies (Zou et al. 2009). Connectivity studies also demonstrate that the PCC is one of the regions with the highest local functional connectivity in resting conditions (Tomasi & Volkow 2010). Although PCC has been widely investigated, there is no consensus regarding its function (Leech & Sharp 2014), and therefore, it is not surprising that most of the functional characterisation of the PCC has resulted from studies investigating its role within the DMN (Greicius et al. 2009). The PCC includes Brodmann areas 29, 30, 23, and 31; it has been extensively described as an 'evaluative' region, involved in spatial orientation and memory, and its connections to the parahippocampal cortices could contribute to these

processes (Vogt et al. 1992). The PCC is implicated in awareness (Vogt & Laureys 2005) and internally directed thoughts (Buckner et al. 2008), which is supported by an increased activity of this regions during internally directed thoughts or during retrieval of autobiographical memories.

As it was discussed in Chapter 2, several domains in the subunits of the GABAA-Rs are responsible for receptor assembly, receptor trafficking, binding to GABA, and channel gating (Kash et al. 2004). This evidence could imply that through complex modulatory relationships, the local concentration of GABA could depend on the presence of a certain subtype of GABAA-R. Moreover, the expression of a certain subunit could be directly related to the intrinsic processes of neurotransmitter synthesis. Since GABA and glutamate synthesis are tightly related, glutamate is also an interesting transmitter to be tested. Therefore, this sub-study aims to investigate whether differences in the amount of GABA and glutamate in the PCC exist among the groups of healthy male volunteers on the basis of G2 allelic prevalence and G2 frequency. The PRESS sequence with optimised echo time parameters (Napolitano et al. 2013) will be used to measure GABA in the PCC, as it was successfully demonstrated in the study by Arrubla et al. (2014).

6.2 Methods

6.2.1 Subjects and data acquisition

Data from 63 volunteers (mean age = 25.57, SD = 3.38) were included in this sub-study. Details about the samples are presented in Chapter 2. To reliably resolve GABA and glutamate resonance peaks at 1.9 ppm and 2.3 ppm, single voxel MR spectra were consecutively measured using standard point resolved spectroscopy (PRESS) with a set of optimised echo times reported by Napolitano et al. (2013) (TE1 = 14 ms, TE = 105 ms, TR = 2.5 s, NA = 128, voxel size = $25 \times 25 \times 25$ mm^3, RF pulse centred at 2.4 ppm, 16 step phase cycling) in a 3 T Siemens Magnetom Trio scanner (Erlangen, Germany). The duration of the measurement was 5 minutes and 30 seconds. One extra complete phase cycle was measured without the water suppression RF pulse to record a water peak reference for eddy current correction and absolute metabolite concentration

calibration. Before the spectroscopy measurements, the static magnetic field was homogenised by running FASTESTMAP (Gruetter & Tkác 2000) iteratively to ensure that the full-width at half maximum (FWHM) of the reference water peak was below 0.05 ppm. The spectroscopy voxel was placed at the PCC by a trained operator. See Figure 6.1. Part of this dataset was used in the publication of Arrubla et al. (2014), where the relationships between GABA and the DMN were further demonstrated, independently of the genetic aspect.

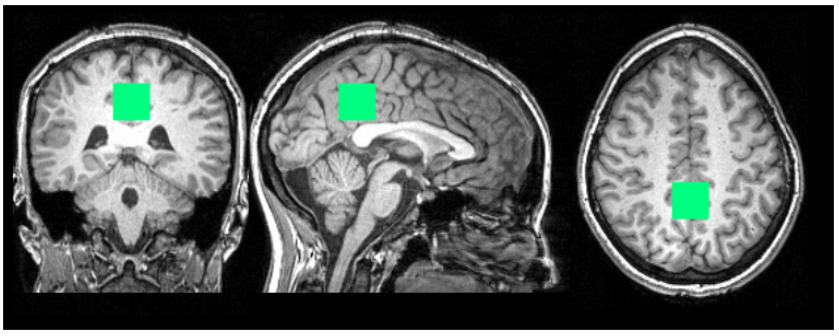

FIGURE 6.1: Depiction of voxel positioning for MRS on a background of a T1 individual structural image.

6.2.2 Data analysis

The MR spectra were analysed with LCModel version 6.3-0I (Provencher 2001) using a GAMMA simulated basis set (Smith et al. 1994). The simulation was 2D in the two directions where the slice selections were accomplished by 180-degree pulses (Maudsley et al. 2005). The numerical waveforms of the 180-degree pulses were obtained directly from the scanner. Individual GABA and glutamate ratios to total creatine (Cr+PCr) –hereafter referred to as the 'GABA and glutamate ratios'– were extracted and used for statistical analysis in SPSS software (Version 17.0, IBM SPSS Statistics).

One-way ANOVA tests were used to investigate inter-group differences in GABA and glutamate ratios when comparing G2/G2, G2/Non–G2 and Non–G2/Non–G2 groups. In the case of a significant F-test, individual t-tests were used to determine the direction of the effect. An independent-samples t-test was also performed to test for differences between G2+ and G2–.

6.3 Results

GABA and glutamate ratios were successfully measured in the PCC (Figure 6.2) using single voxel spectra. GABA ratio (mean = 0.179, SD = 0.029) exhibited a normal distribution according to a Shapiro-Wilk test (significance value = 0.404). See Figure 6.3. Glutamate ratio (mean = 2.810, SD = 0.212) also exhibited a normal distribution according to a Shapiro-Wilk test (significance value = 0.075). See Figure 6.4.

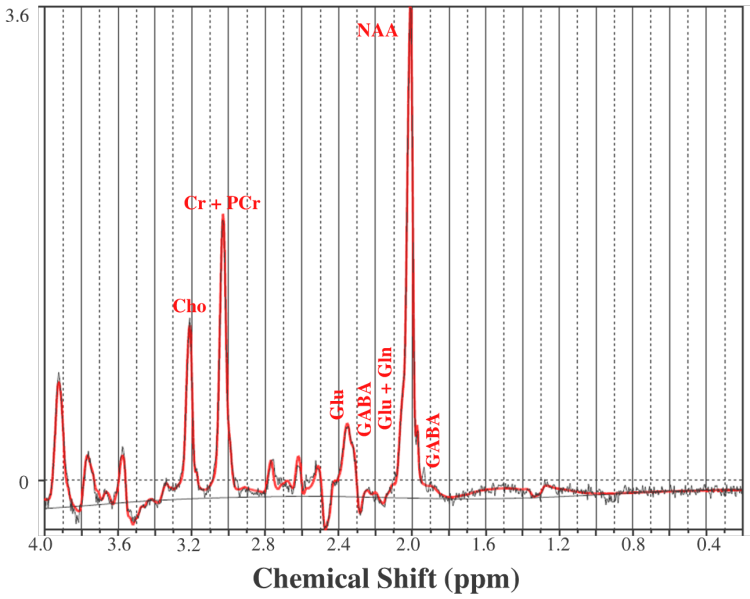

FIGURE 6.2: Spectra in an exemplary subject. The marked peaks correspond to N-acetylaspartate (NAA), creatine (Cr), phosphocreatine (Pcr), glutamate (Glu), glycine (Gln) and GABA.

A one-way ANOVA showed that there were no differences in GABA ratios among the groups based on the G2 allelic frequency (G2/G2, G2/Non–G2 and Non–G2/Non–G2); $F(2,60) = 0.145$, $p = 0.865$. A Levene's test did not reveal any statistically significant difference in the GABA ratio variances in the population ($p = 0.844$). Box plots are presented in Figure 6.5.

An independent-samples t-test revealed that there were no statistically significant differences in GABA ratios between the groups based on the G2 prevalence (G2+ and G2–); $t(61) = 0.131$, $p = 0.896$. A Levene's test did not reveal any statistically significant difference in the GABA ratio variances in the population ($p = 0.782$). Box plots are presented in Figure 6.6.

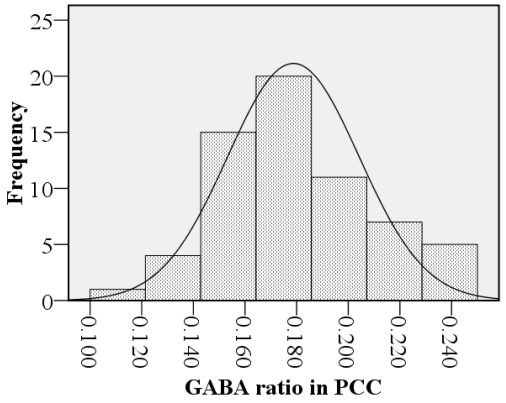

FIGURE 6.3: Distribution histogram of GABA ratio in the entire sample.

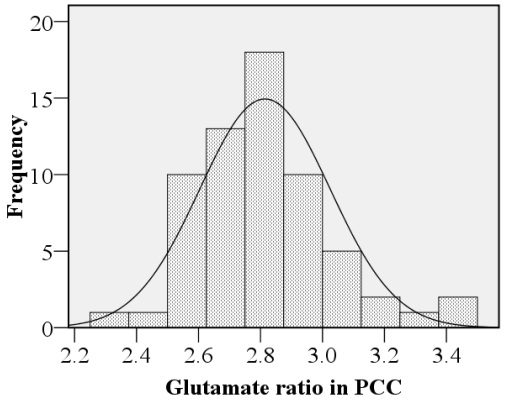

FIGURE 6.4: Distribution histogram of glutamate ratio in the entire sample.

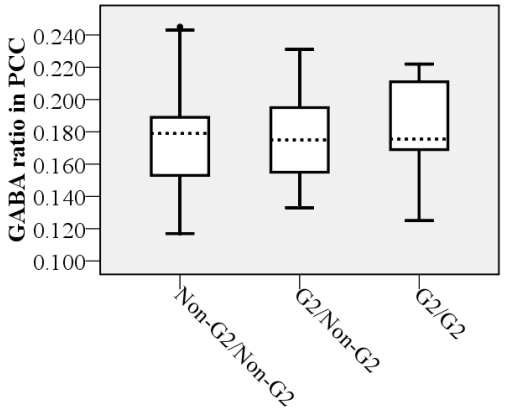

FIGURE 6.5: Box plot of the GABA ratio in the PCC in the different groups on the basis of the G2 allelic frequency.

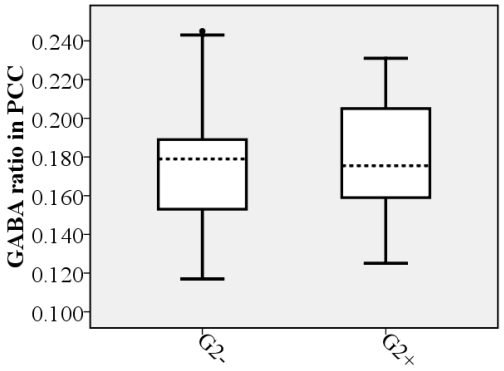

FIGURE 6.6: Box plot of the GABA ratio in the PCC in the different groups on the basis of the G2 allelic prevalence.

A one-way ANOVA showed that there were no differences in glutamate ratios among the groups based on the G2 allelic frequency (G2/G2, G2/Non–G2 and Non–G2/Non–G2); $F(2,60) = 0.651$, $p = 0.525$. A Levene's test did not reveal any statistically significant difference in the glutamate ratio variances in the population ($p = 0.275$). Box plots are presented in Figure 6.7.

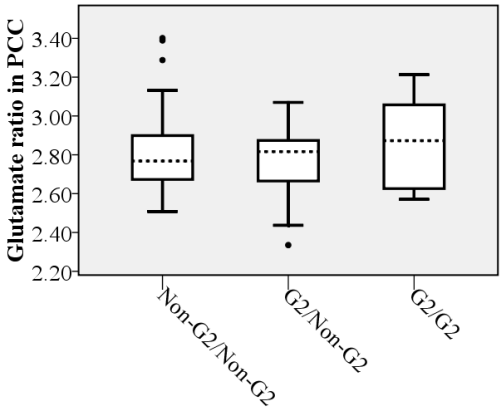

FIGURE 6.7: Box plot of the glutamate ratio in the PCC in the different groups on the basis of the G2 allelic frequency.

An independent-samples t-test revealed that there were no statistically significant differences in glutamate ratios between the groups based on the G2 prevalence (G2+ and G2–); $t(61) = 0.469$, $p = 0.64$. A Levene's test did not reveal any statistically significant difference in the glutamate ratio variances in the population ($p = 0.581$). Box plots are presented in Figure 6.8.

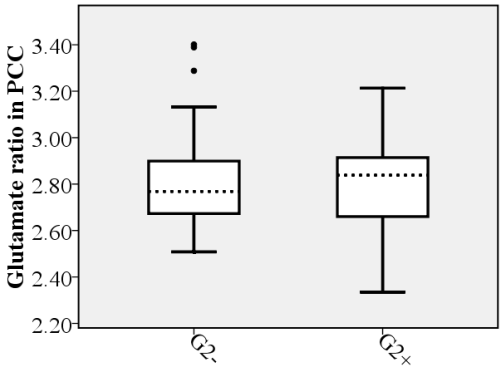

FIGURE 6.8: Box plot of the glutamate ratio in the PCC in the different groups on the basis of the G2 allelic prevalence.

6.4 Discussion

In this chapter it was described how GABA and glutamate ratios in the PCC were measured from the sample of healthy male volunteers using MR spectra. The ratios of both neurotransmitters were compared among subgroups on the basis of G2 allelic prevalence and frequency. This sub-study used PRESS with a set of optimised echo times reported by Napolitano et al. (2013), a sequence that was proved to be useful for measurements in the PCC in the study by Arrubla et al. (2014).

The results showed that there were no statistically significant differences in GABA or glutamate ratios depending on the expression of the G2 allele. The interpretation of these results must be carefully considered. Firstly, the statistical comparisons were performed only on the basis of the expression of G2, the most frequent CA allele of the GABRB3. As it was discussed in previous chapters, this study was sufficiently powered with respect to G2 and included a sufficiently large sample in each subgroup; yet, no other subgroups could be formed on the basis of other allelic polymorphisms. The conclusions of this sub-study are therefore limited to the effect of G2 on the population. Secondly, MRS, as all other image analysis methods, has inherent limitations that should be considered. The precise relationship between the concentrations of transmitters and their respective receptors at regional levels in humans (such as between GABA and GABA-A receptors, for example) still remains unclear. Thus, it is necessary to determine the

exact physiological mechanisms of any suggested neuro-biochemical relationship. In addition, the use of GABA and glutamate ratios in the present study instead of absolute concentration is in agreement with previous publications (Donahue et al. 2010; Muthukumaraswamy et al. 2009), in which metabolite levels are commonly reported as their ratio to creatine. Creatine has been shown to be a stable metabolite in healthy individuals (Soher et al. 1996) and thus is commonly used as an internal reference in brain spectroscopy. Furthermore, in a study by Bogner et al. (2010) GABA ratio exhibited the best reproducibility.

From a technical point of view, the separation and quantification of metabolites are often ambiguous and difficult due to several factors. First, since 80% of brain tissue is endogenous water, the water resonance peaks is several orders of magnitude higher than that of the metabolites, which can potentially distorts nearby metabolite resonance signals. Second, large subcutaneous lipids signals can potentially ruin metabolite signals. Third, the spectral resolution as well as the signal-to-noise ratio are often reduced by the anatomical induced magnetic field spatial inhomogeneity. Despite these difficulties were overcome in this study, the process of separating metabolite signals is still challenging because of the large number of overlapping metabolite resonance peaks confined in a narrow chemical shift range of 4 ppm.

Chapter 7

Investigation of the effect of GABRB3 polymorphisms on electroencephalography frequency bands

7.1 Background

The first recording of the electric activity of the human brain was performed by the German psychiatrist Hans Berger in 1924 in Jena, and was given the name of electroencephalogram (EEG, Berger 1929). The EEG reflects the mass action potentials of large neuronal groups, which are responsible for fast neural communication along the axons. Because the scalp electrodes for EEG recordings are at a distance of several centimetres from the neurons, the individual potentials are not measured, and thus, the EEG activity measurable at the scalp is the result of the mass action of neuronal populations with a high degree of synchronisation (Ullsperger & Debener 2010). The main sources of EEG are the slower local field potentials, which mainly reflect neuronal input from postsynaptic potentials and originate in grey matter; that is the reason why electro-physiological source models are constrained to grey matter structures (Ullsperger & Debener 2010).

Combining EEG and MRI is feasible nowadays, and permits the investigation of different aspects of the brain under the same physiological conditions. Simultaneously acquired EEG-fMRI has benefited cognitive neuroscience, pharmacological studies, sleep studies, resting state studies and evoked potential studies (for a review refer to Laufs, 2012). Combining the high spatial resolution of MR at high magnetic fields with electrophysiological data also has the potential to facilitate lesion detection in patients suffering from medication resistant epilepsy (Kim et al. 2011).

An important disadvantage of measuring EEG at high magnetic fields is the contamination of the signal as a consequence of the MR scanner operation, namely the gradient artefact, which is highly predictable and relatively straightforward to remove (Allen et al. 1998). The pulse artefact is considered to be the most challenging source of EEG data contamination in recordings performed at any magnetic field; it is produced by cardiac pulse related movement of the scalp electrodes inside the magnetic field (Debener et al. 2008; Mullinger et al. 2013), as well as the Hall effect of the blood movement, which results in a variation of the voltage at the scalp surface. Despite the disadvantages of the combination, such as the contaminated EEG signal, and the inhomogeneities in the fMRI images, the possibility of evaluating and integrating different measures acquired simultaneously appears desirable (Shah et al. 2013). Moreover, with all the advances made in the field until now it is possible to measure good quality EEG data in the MR environment.

In order to retrieve valuable information from EEG data recorded at high magnetic fields, reduction of the artefacts must be accomplished. Consequently, the reduction of pulse artefacts constitutes an essential step in studies where EEG was acquired simultaneously with MR data. A number of techniques have been proposed to suppress the pulse artefact; one of the most widely used is the optimal basis set (OBS) method (Niazy et al. 2005), which is based on the assumption that each pulse artefact occurs independently of any previous occurrence. OBS captures the occurrences of pulse artefacts in every EEG channel by applying a temporal principal component analysis (PCA). Typically, the first 3 principal components including the mean effect are subtracted from the EEG data to correct for pulse artefacts. The disadvantage of PCA is that an orthogonal transformation is used to decompose the data using second order statistics, meaning that the components can only be considered to be independent if the

joint distribution of the data is normally distributed. In contrast, independent component analysis (ICA) uses higher order statistics, where each component can be considered as statistically independent after decomposition. ICA was propounded as a tool with high potential for removing artefacts in the EEG recordings (Jung et al. 2000). It is widely used for separation of mixed data into its underlying informal components (Li et al. 2006; Makeig et al. 1997; Rasheed et al. 2009).

Removal of the pulse artefact in simultaneous EEG-fMRI studies performed at 1.5–3 T field strengths can be regarded as a solved problem using OBS prior to ICA, as suggested by Vanderperren et al. (2010). Improvements in the selection of ICA components have also been made, such as the method proposed by Maggioni et al. (2014), where the frequency information of the independent components is used in the selection of the artefactual ones.

As it was described in Chapter 5, some patterns of brain activity seem to be strictly controlled by genetic factors, and apparently, EEG activity is not an exception. EEG studies in twins have found that some patterns of EEG activity and connectivity are heritable (Smit et al. 2008; Schutte et al. 2013). For example, studies including candidate genes have shown a tendency towards more pronounced EEG slowing in patients suffering from Alzheimer's disease carrying the APOE4 allele (Lehtovirta et al. 1996). This finding was later confirmed in a study by Lee et al. (2012b), in which the APOE4 carriers exhibited different EEG features reflecting different levels of regional neural synchronisation and inter-regional neural interaction during rest. Similarly, alleles of the dopamine transporter gene (DAT1) appear to affect the cortical activity in children suffering from attention deficit with hyperactivity (Loo et al. 2003). Crucially, genetic variability in the cannabinoid receptor 1 is associated with resting state EEG power in the *theta* frequency band (Heitland et al. 2014). Another example was brought in a study by Wacker & Gatt (2010), where an association was found between *delta/theta* bands and a functional polymorphism of the enzyme catechol-O-methyltransferase (COMT VAL-158-MET) involved in dopamine catabolism. The list of similar examples is long, confirming that features of the EEG are indeed inherited, and that the search for genetic candidates is of tremendous importance in pathologies such as epilepsy, where the EEG activity is severely affected.

As it was discussed in Chapter 2, alterations in the expression of GABRB3 in humans are linked to epilepsy (Allen et al. 2013; DeLorey et al. 1998; Tanaka et al. 2012). Furthermore, animal studies found that alterations in the expression of GABRB3 lead to abnormalities in EEG and behaviour (DeLorey & Olsen 1999). Therefore, this sub-study aims to investigate whether differences in EEG activity patterns exist among the groups of healthy male volunteers on the basis of G2 allelic prevalence and G2 frequency. Additionally, and given the advantages of simultaneous EEG-MRI acquisitions under the same physiological conditions, this sub-study aims also at investigating possible relationships of EEG frequencies with GABA and glutamate ratios in the PCC, measured through MRS as it was described in Chapter 6.

7.2 Methods

7.2.1 Subjects and data acquisition

Data from 63 volunteers (mean age = 25.57, SD = 3.38) were included in this sub-study. Details about the samples are presented in Chapter 2. EEG data were recorded during rest condition using Brain Vision Recorder (Brain Products, Gilching, Germany) and a 32-channel MR compatible EEG system including an amplifier and a synchronisation box (Brain Products, Gilching, Germany). The EEG cap (BrainCap MR, EasyCap GmbH, Breitbrunn, Germany) consisted of 31 scalp electrodes distributed according to the 10–10 system and one additional electrode for recording the electrocardiogram (ECG). Data were recorded relative to an Fpz reference and a ground electrode that was located at AFz (10–5 electrode system, Oostenveld & Praamstra, 2001). Data were sampled at 5000 Hz, with a bandpass of 0.016–250 Hz. Impedances at all recording electrodes were kept below 10 kΩ.

7.2.2 Data analysis

The EEG data were processed using Brain Vision Analyzer (Version 2.0, Brain Products, Munich, Germany). Gradient artefact correction was performed using the method proposed by Allen et al. (2000) and included in Brain Vision Analyzer. Data were down-sampled to 250 Hz and re-referencing of the data was

carried out including all EEG channels as a new reference. Detection of the heartbeat event in the ECG signal was performed in Brain Vision Analyzer. Data were exported to EEGLAB (Delorme & Makeig 2004, http://sccn.ucsd.edu/eeglab/), where OBS was performed using the toolbox available in this software; the number of principal components to use was set to 3. The markers of heartbeat events were used for pulse artefact correction. The data were later exported back to Brain Vision Analyzer for further analysis.

The data were later segmented in 2.2 seconds epochs and those holding movement artefacts were excluded using manual selection. For further de-noising of the data, ICA was applied to the data using the extended Infomax algorithm (Lee et al. 1999). The entire-length EEG data were used for the calculation of the de-mixing matrix. The convergence bound was set to '10–7'. The selection of artefactual components was based on the spectral information provided by wavelet analysis of each independent component (IC) according to Maggioni et al. (2014), where the ICs having a peak time locked to the R–peak between the *delta* and *alpha* band were selected and removed. For the calculation of the wavelets the following parameters were used: morlet complex family of wavelets (minimal frequency = 0.5 Hz, maximal frequency = 30 Hz, frequency steps = 300, morlet parameter $c = 10$, linear steps). The de-noised data were later used for frequency analysis using Fast Fourier Transform (FFT) and for source analysis based on eLORETA.

For the investigation of the effect of G2 allele on EEG, the overall activity at each frequency was investigated. Firstly, the overall activity of all channels was calculated, where the average of all channels at each time-point was subtracted from the individual channels and then squared. These values were averaged and the root was calculated at each time-point. Secondly, the resulting global activities were transformed from the time domain to the frequency domain using FFT. The mean voltages of each frequency were extracted using FFT with the following parameters: full spectrum, maximum resolution, hanning window = 10% and window variance correction. The frequency bands were defined as follows: *delta* (0.5–3.5 Hz), *theta* (4–7 Hz), *alpha–1* (7.5–9.5 Hz), *alpha–2* (10–12 Hz), *beta–1* (13–23 Hz), and *beta–2* (24–34 Hz) according to the conventional International Federation of Clinical Neurophysiology guideline (Nuwer et al. 1999). Kruskal-Wallis H tests were performed to determine whether statistically significant differences in the global frequency voltages existed among the G2/G2,

G2/Non–G2 and Non–G2/Non–G2 groups. In the case of a significant difference, Mann-Whitney U tests were used to determine the direction of the effect. Mann-Whitney U tests were also performed to test for differences of global frequency voltages between G2+ and G2– groups. The Kruskal-Wallis H and Mann-Whitney U tests were chosen because the assumption of a Gaussian distribution could not be established for the EEG parameters in the recordings. Statistical tests were performed in SPSS software (Version 17.0, IBM SPSS Statistics). No correction for multiple comparisons was applied here because each test was considered independently and the Mann-Whitney U test was used only to find the direction of the effect.

Additionally to those analyses, and given the advantages of having measured EEG under the same physiological conditions, a multiple regression analysis was performed in SPSS. The aim of this analysis was to investigate whether G2 allelic frequency, GABA and glutamate ratios (see Chapter 6) predict the global frequency voltages of any of the frequency bands.

The de-noised data were also exported to LORETA-KEY software (Pascual-Marqui et al., 1994, http://www.uzh.ch/keyinst/loreta.htm), where cross-spectra were computed for the EEG of each subject and the 3D cortical distribution of the electrical neuronal generators were computed using eLORETA (Pascual-Marqui et al. 1994). Generators of eLORETA were computed for each subject and seven frequency bands. The frequency bands were *delta* (1.5–6 Hz), *theta* (6.5–8 Hz), *alpha–1* (8.5–10 Hz), *alpha–2* (10.5–12 Hz), *beta–1* (12.5–18 Hz), *beta–2* (18.5–21 Hz) and *beta–3* (21.5–30 Hz) according to the pre-defined frequencies in the LORETA-KEY software. For the calculation of the electrical generators, eLORETA uses a three-shell spherical head model for solving the forward problem, which is registered to a standardised stereotactic space available as digitised MRI data from the Brain Imaging Centre (Montreal Neurological Institute, MNI305. Collins et al. 1994; Evans et al. 1992; Lancaster et al. 2000). Finally, a voxel-wise statistical analysis was performed using the LORETA-KEY software, where the electrical generators of the different frequencies were tested for differences among the groups. A series of independent-samples t-tests with a random subset of 5000 permutations were performed to test for inter-group differences among G2/G2, G2/Non–G2 and Non–G2/Non–G2 groups. Independent-samples t-tests with a random subset of 5000 permutations were also performed to investigate possible differences between G2+ and G2– groups.

7.3 Results

7.3.1 Global frequency voltage

The Kruskal-Wallis H tests revealed no statically significant differences in the global voltages of *theta*, *alpha–1*, *alpha–2*, *beta–1*, and *beta–2* among subgroups G2/G2, G2/Non–G2 and Non–G2/Non–G2. A statistically significant difference in global *delta* voltage was found, $\chi^2(2) = 6.275$, $p = 0.043$, with a mean rank global voltage score of 41.75 for G2/G2 group, 25.45 for G2/Non–G2 group and 32.93 for Non–G2/Non–G2 group. Results are summarised in Table 7.1. A Mann-Whitney U test showed that the *delta* voltage was significantly higher in the G2/G2 group than the G2/Non–G2 group ($U = 59$, $p = 0.009$). Box plots are presented in Figure 7.1.

Parameter	**Group**	**N**	**Mean Rank**	χ^2	**df**	***p***
Delta voltage	Non-G2/Non-G2	29	32.93	6.275	2	0.043*
	G2/Non-G2	22	25.45			
	G2/G2	12	41.75			
Theta voltage	Non-G2/Non-G2	29	33.38	3.213	2	0.201
	G2/Non-G2	22	26.86			
	G2/G2	12	38.08			
Alpha–1 voltage	Non-G2/Non-G2	29	30.59	0.437	2	0.804
	G2/Non-G2	22	32.41			
	G2/G2	12	34.67			
Alpha–1-voltage	Non-G2/Non-G2	29	29.28	1.299	2	0.522
	G2/Non-G2	22	33.55			
	G2/G2	12	35.75			
Beta–1 voltage	Non-G2/Non-G2	29	31.10	0.799	2	0.671
	G2/Non-G2	22	30.86			
	G2/G2	12	36.25			
Beta–2 voltage	Non-G2/Non-G2	29	30.93	0.463	2	0.793
	G2/Non-G2	22	31.68			
	G2/G2	12	35.17			

* $p \leq 0.05$

TABLE 7.1: Results of the Kruskal-Wallis H tests for the different groups on the basis of the allelic frequency of G2.

Mann-Whitney U tests did not show any statistically significant difference in global voltages of *delta*, *theta*, *alpha–1*, *alpha–2*, *beta–1*, and *beta–2* between G2+ and G2– groups. Results are presented in Table 7.2. Box plots are presented in Figure 7.2.

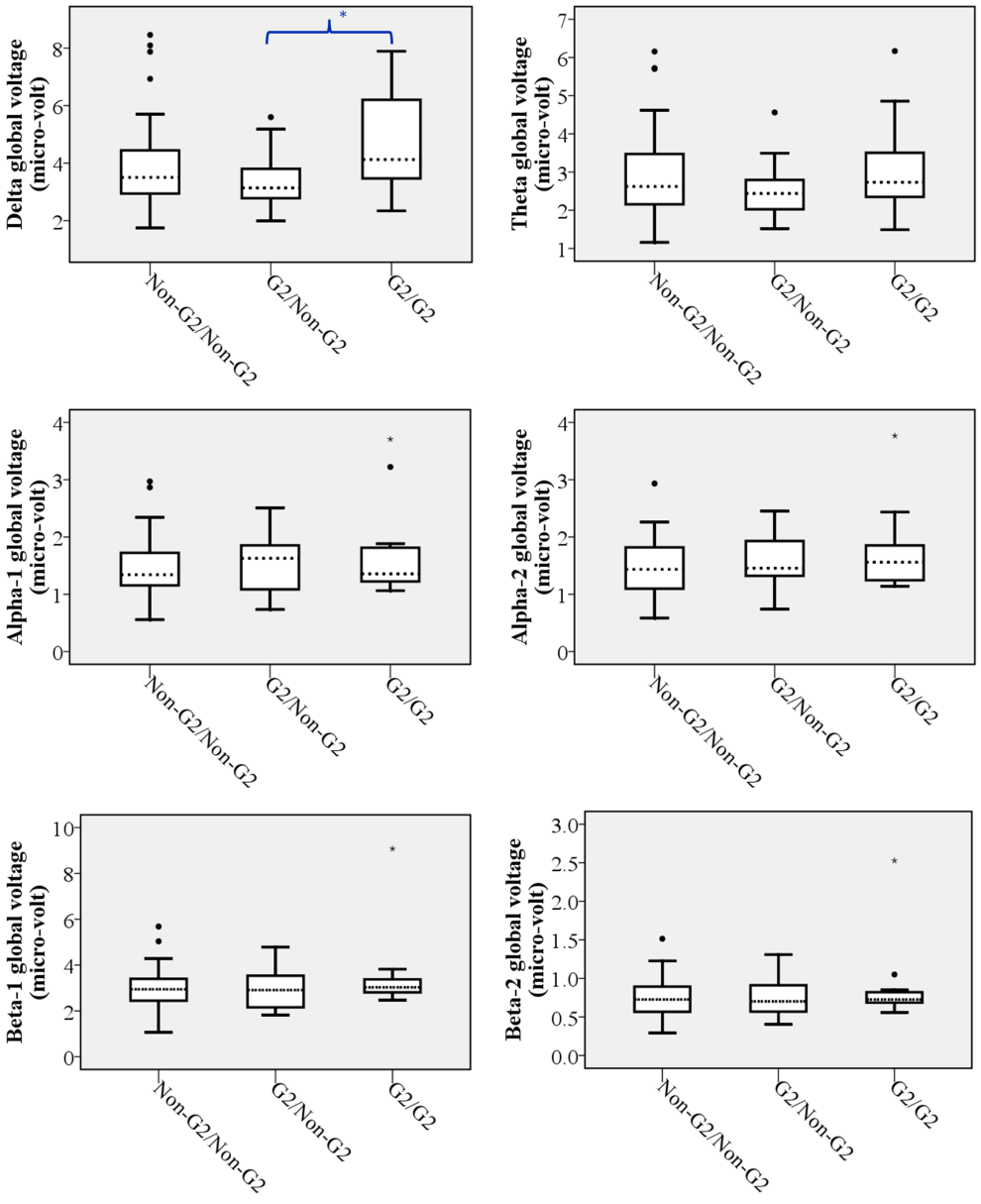

FIGURE 7.1: Box plots showing global voltages of the EEG bands on the basis of the G2 allelic frequency. Significant differences are shown in blue.

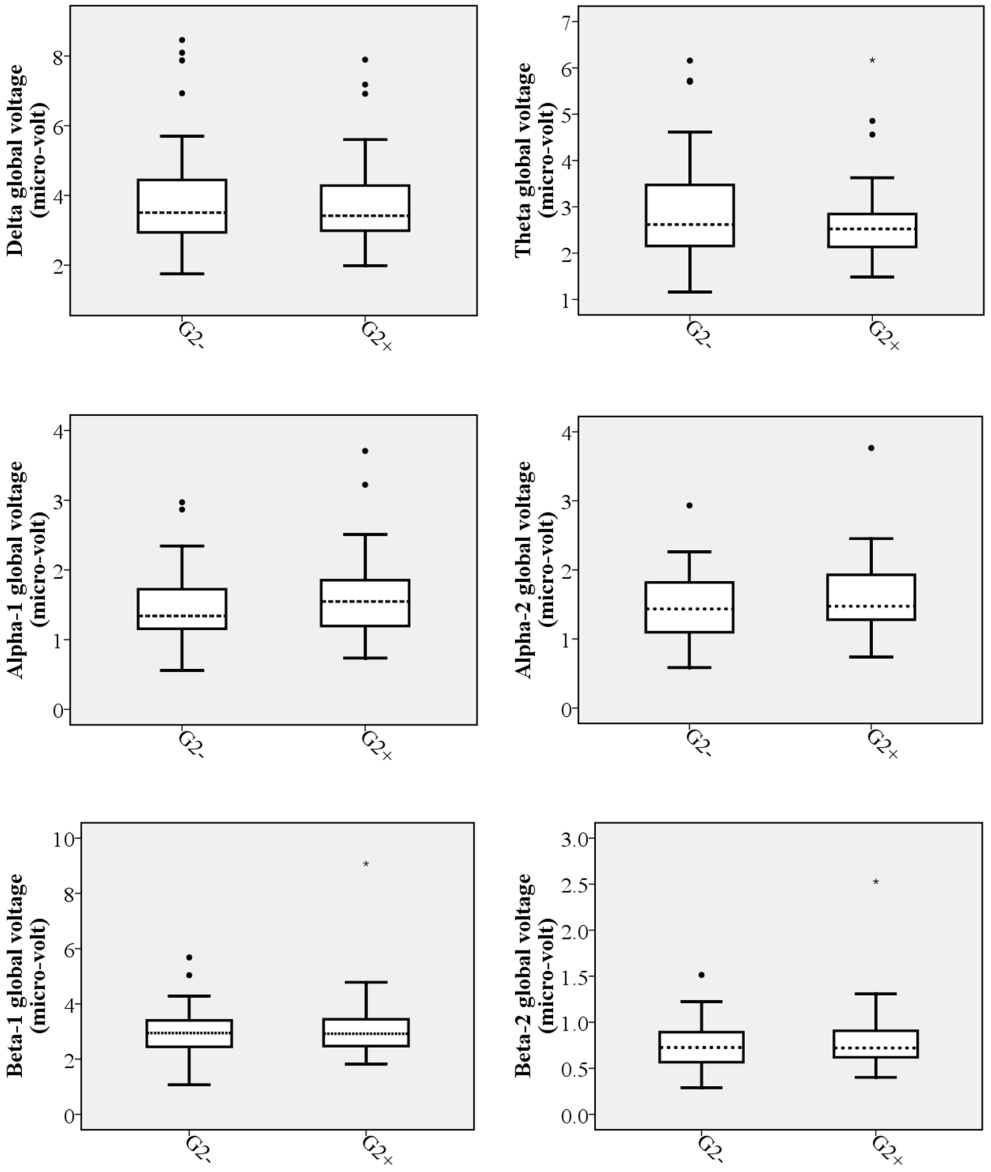

FIGURE 7.2: Box plots showing global voltages of the EEG bands on the basis of the G2 allelic prevalence.

Parameter	Group	N	Mean Rank	Mann-Whitney U	*p*
Delta voltage	G2– G2+	29 34	32.93 31.21	466.000	0.710
Theta voltage	G2– G2+	29 34	33.38 30.82	453.000	0.581
Alpha–1 voltage	G2– G2+	29 34	30.59 33.21	452.000	0.572
Alpha–1-voltage	G2– G2+	29 34	29.28 34.32	414.000	0.276
Beta–1 voltage	G2– G2+	29 34	31.10 32.76	467.000	0.720
Beta–2 voltage	G2– G2+	29 34	30.93 32.91	462.000	0.669

* $p \leq 0.05$

TABLE 7.2: Results of the Mann-Whitney U tests for the different groups on the basis of the allelic prevalence of G2.

7.3.2 Multiple regression analysis

A multiple regression analysis was performed to predict the global voltage of the different frequencies from G2 allelic frequency, GABA and glutamate ratios in PCC. These variables did not significantly predict the global voltages of *delta* ($F(3, 59) = 1.231$, $p = 0.306$, $R^2 = 0.059$) *theta* ($F(3, 59) = 1.3$, $p = 0.283$, $R^2 = 0.062$), *alpha–1* ($F(3, 59) = 0.444$, $p = 0.723$, $R^2 = 0.022$), *alpha–2* ($F(3, 59) = 0.960$, $p = 0.418$, $R^2 = 0.047$), *beta–1* ($F(3, 59) = 0.846$, $p = 0.474$, $R^2 = 0.041$), or *beta–2* ($F(3, 59) = 0.869$, $p = 0.462$, $R^2 = 0.042$). None of the variables added statistically significantly to the prediction, although in the case of *theta* frequency, glutamate ratio exhibited a tendency for prediction ($t = -1.961$, $p = 0.055$). This tendency for negative correlation was also visible in a scatter plot (Figure 7.3).

7.3.3 Low resolution brain electromagnetic tomography – LORETA

There were no statistically significant independent-samples t-tests ($p \leq 0.05$) revealing differences in the electrical generators of any EEG band on the basis of G2 allelic frequency or prevalence. Results are summarised in Tables 7.3, 7.4 and 7.5.

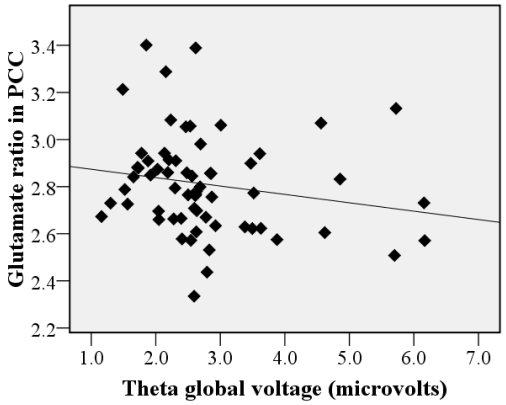

FIGURE 7.3: Scatter plot of *theta* global voltage vs. Glutamate ratio in the PCC.

7.4 Discussion

In this chapter it was described how EEG data were acquired from the sample of healthy male volunteers using MR-compatible devices. The global voltages of different frequency bands were compared among subgroups on the basis of G2 allelic prevalence and frequency. Additionally, electrical generators of EEG frequencies were calculated and compared on the basis of G2 expression. A regression analysis was performed to investigate whether the number of G2 alleles, GABA and glutamate ratios in the PCC predict the EEG activity in any frequency.

The results showed that homozygote carriers of G2 exhibit increased *delta* voltage compared to heterozygote carriers. Previous studies confirmed the importance of the GABRB3 expression in the resulting EEG activity patterns (DeLorey & Olsen 1999). Mutations of the GABRB3 gene in humans have been associated with epilepsy (Allen et al. 2013; DeLorey et al. 1998; Tanaka et al. 2012), particularly with childhood absence epilepsy, in which punctual mutations alter receptor expression and channel gating (Gurba et al. 2012; Lachance-Touchette et al. 2010; Feucht et al. 1999). The results presented here confirm once more that differences in the expression of GABRB3 lead to different patterns of EEG. Since in the sample only healthy male volunteers with no history of seizures or epilepsy were included, one can hypothesise that the expression of the G2 allele does not imply alterations in the function, although results in different patterns

Contrast	**Frequency**	**Max. t value**	**Threshold of t for significance ($p \leq 0.05$)**
G2/G2 >Non–G2/Non–G2	Delta	0.654	1.316
	Theta	0.747	
	Alpha–1	0.757	
	Alpha–2	1.072	
	Beta–1	0.532	
	Beta–2	0.844	
	Beta–3	0.871	
G2/G2 <Non–G2/Non–G2	Delta	0.654	-1.476
	Theta	0.747	
	Alpha–1	0.757	
	Alpha–2	1.072	
	Beta–1	0.532	
	Beta–2	0.844	
	Beta–3	0.871	
G2/Non-G2 >Non–G2/Non–G2	Delta	-0.672	1.549
	Theta	0.452	
	Alpha–1	0.692	
	Alpha–2	0.647	
	Beta–1	-0.604	
	Beta–2	-0.656	
	Beta–3	1.419	

TABLE 7.3: Analysis of the electrical generators of the EEG frequencies. Results of the independent-samples t-tests for the different groups on the basis of G2 allelic frequency. Part 1.

of measurable brain activity, particularly in the slow fluctuations. As it was discussed in Chapter 2, the expression of polymorphic forms of the genes could lead to changes in a wide range of functional aspects. Conformational changes, for example, might lead to changes in sensitivity profiles to neurotransmitters, drugs or even in the coupling with other molecules or proteins. The results presented here could be due to different patterns of local receptor density or even reflect different profiles in channel gating, given the importance of GABRB3 in the morphology of GABAA-Rs. Crucially, differences could not be found in the electrical generators of *delta* or in any other frequency, which could be due to the inherent limitations of the source analysis used or by an increased level of noise introduced by the MR environment that could not be completely removed.

Several methods have been developed for solving the EEG inverse problem keeping in mind low localisation error, low computational complexity and validation of the achieved results. One of the most popular methods is the one used here, eLORETA, which performs well in terms of less localisation error and visibility

Contrast	**Frequency**	**Max. *t* value**	**Threshold of *t* for significance ($p \leq 0.05$)**
G2/Non-G2 <Non-G2/Non-G2	Delta	-0.672	-1.407
	Theta	0.452	
	Alpha–1	0.692	
	Alpha–2	0.647	
	Beta–1	-0.604	
	Beta–2	-0.656	
	Beta–3	1.419	
G2/G2 >G2/Non-G2	Delta	1.017	1.975
	Theta	0.711	
	Alpha–1	1.299	
	Alpha–2	0.692	
	Beta–1	-0.747	
	Beta–2	0.860	
	Beta–3	-1.247	
G2/G2 <G2/Non-G2	Delta	1.017	-1.704
	Theta	0.711	
	Alpha–1	1.299	
	Alpha–2	0.692	
	Beta–1	-0.747	
	Beta–2	0.860	
	Beta–3	-1.247	

TABLE 7.4: Analysis of the electrical generators of the EEG frequencies. Results of the independent-samples t-tests for the different groups on the basis of G2 allelic frequency. Part 2.

as compared to other low resolution techniques (Jatoi et al. 2014). However, eLORETA possess as an intrinsic limitation the use of a single normalised head template to calculate the sources of electrophysiological activity, and therefore, inter-individual variations in brain and skull morphology remain largely ignored.

Interestingly, when looking at the multiple regression analysis, glutamate ratio in the PCC exhibited the highest level of predictability of *theta* voltage ($p = 0.055$). This relationship, although not significant, showed a trend for negative correlation between these two variables. The activity of *theta*-band has been linked to working memory, emotional arousal and fear conditioning (Knyazev 2007). The PCC has been described as an 'evaluative' region with high activity at rest, particularly engaged in spatial orientation and memory retrieval (Vogt et al. 1992). As a result, one could hypothesise that *theta* in the PCC could be strongly linked to memory functions, and that the level of glutamate in the area plays an important role in the modulation of *theta* amplitude, and therefore, in memory.

Contrast	**Frequency**	**Max. t value**	**Threshold of t for significance ($p \leq 0.05$)**
G2+ >G2–	Delta	-0.442	1.27
	Theta	0.546	
	Alpha–1	0.685	
	Alpha–2	0.784	
	Beta–1	-0.371	
	Beta–2	0.440	
	Beta–3	1.140	
G2+ <G2–	Delta	-0.442	-1.328
	Theta	0.546	
	Alpha–1	0.685	
	Alpha–2	0.784	
	Beta–1	-0.371	
	Beta–2	0.440	
	Beta–3	1.140	

TABLE 7.5: Analysis of the electrical generators of the EEG frequencies. Results of the independent-samples t-tests for the different groups on the basis of G2 allelic prevalence.

The results presented here confirm the notion of heritability of EEG activity patterns (Smit et al. 2008; Schutte et al. 2013), and point to the GABRB3 as an interesting gene that could explain such differences. It is expected that the study of this gene in larger samples will provide more insight into the physiopathology of diseases such as epilepsy. Again, the results of this study can only be conclusive for the expression of the G2 allele, since no other subgroups could be formed.

Chapter 8

An integrative view of the effect of GABRB3 polymorphisms on the function and structure of the brain

The investigation of genetics by the means of imaging techniques extends our knowledge of brain function, structure and development by identifying the intrinsic roles of the different genes and their expression. In this sense defining candidate genes, such as the one chosen for this study, is useful for the investigation of neurogenetics. The GABRB3 gene is of great interest due to its role in neurodevelopment (Al-Jaberi et al. 2013) and its relationship with pathologies such as epilepsy (Allen et al. 2013), Angelman syndrome (DeLorey et al. 1998; DeLorey & Olsen 1999; Tanaka et al. 2012), autism (Buxbaum et al. 2002; Fatemi et al. 2009; Pizzarelli & Cherubini 2011; Schroer et al. 1998) and cleft lip and palate (Filézio et al. 2013).

In order to investigate the possible effects of GABRB3 on brain structure and function, a sample of 63 healthy young male volunteers was measured using multimodal imaging techniques, including structural imaging, diffusion-weighted imaging, resting state fMRI, magnetic resonance spectroscopy and electroencephalography. Inter-group differences in brain function and structure were

tested on the basis of frequency and prevalence of G2, the most frequent allele in the population. The differences found were expected to represent the structural and functional aspects where the expression of the GABRB3 variants was critical.

No differences in the local grey matter volume were found to depend on the expression of the G2 allele. This was also the case for the patterns of activity of the resting state networks. The measures of magnetic resonance spectroscopy revealed that GABA and glutamate ratios in the posterior cingulate cortex had no connection with the frequency or prevalence of the G2 allele.

The analysis of diffusion-weighted data revealed that differences existed between homozygote carriers of G2 and non-carriers. Differences in fractional anisotropy, axial and mean diffusivity were confined to the right superior longitudinal fasciculus, right corticospinal tract and body of the corpus callosum. The microstructure of the brain has been demonstrated to be controlled by genetic factors (Chiang et al. 2011; Dietsche et al. 2014; Forde et al. 2014; Kochunov et al. 2010a), and in the case of this study, the expression of GABRB3 variants seems to affect the white matter microstructure. However, the interpretation of these results is challenging and requires information from Angelman syndrome studies, where alterations in the expression of GABRB3 occur (Schroer et al. 1998). DTI studies in patients suffering from Angelman syndrome suggest the presence of decreased myelination, decreased axonal density and aberrant axonal organisation in the brain (Peters et al. 2011; Tiwari et al. 2012). In a study by Tiwari et al. (2012), children with Angleman syndrome exhibited significantly lower anisotropy values in various areas of the brain, such as the corpus callosum and the corticospinal tract. Importantly, the results presented here show that the expression of G2 alleles is crucial in defining the microstructure of the corticospinal tract and corpus callosum, along with the superior longitudinal fasciculus.

The particular case of the corticospinal tract might offer an interesting perspective of how the expression of the GABRB3 gene affects the white matter. The corticospinal tract is a major neural tract in the human brain and is mainly involved in the movement of the limbs and trunk (York 1987). The corticospinal tract originates from the frontoparietal cortices, including the primary motor

cortex, supplementary motor area and somatosensory cortex. Anatomical differences in the fibres of the corticospinal tract have been found according to their cerebral origin. For example, the extent and density of fibres originated in the primary motor cortex were found to be greater than those originated in the supplementary motor cortex (Dum & Strick 1996; Maier et al. 2002). Importantly, the expression of the GABRB3 gene is essential for neuronal migration (Culiat et al. 1995; Dellovade et al. 2001), and the expression of polymorphic variants might result in different patterns of neuronal migration, and consequently microstructural differences could occur. Furthermore, such differences could imply the existence of variations in brain development that are compensated by the impact of hemispheric dominance, being only evident in the non-dominant hemisphere in the adult age. Some studies have shown that apparent diffusion coefficient and diffusion anisotropy measures change dramatically during development, reflecting underlying changes in tissue water content and cytoarchitecture (Neil et al. 2002). Neurodevelopment studies are conclusive in finding a decrease in water diffusivity with brain maturation, likely related to changes in brain water content. Increased anisotropy has also been described to occur during maturation, apparently due to changes in tissue microstructure, such as 'premyelination' changes and myelination itself (Neil et al. 2002).

The decreased axial and mean diffusivity found in the homozygote carriers of G2 is not likely due to an 'abnormality' in maturation, since the volunteers did not exhibit any motor or sensory deficit and were neurologically normal. Such decreased diffusion parameters might be rather due to variability in the amount of fibres with different brain origin. This change in microstructure might affect anisotropy along with diffusivity. Therefore, the previous evidence and the results of this study strengthen the hypothesis that specific white matter tracts of the homozygote carriers of G2 exhibit decreased diffusivity and anisotropy due to intrinsic differences in the microstructure of the axon bundles.

The discussion about alterations in Angelman syndrome applies also for the findings of this study with respect to the superior longitudinal fasciculus, a bundle of association fibres connecting the parietal, occipital and temporal lobes with the frontal cortices (Schmahmann et al. 2008; Kamali et al. 2014). The superior longitudinal fasciculus is an important structure for language (Mesulam 1998; Petrides & Pandya 2002), and interestingly, patients with Angelman syndrome have global impairment of white matter integrity in association tracts along with

severe language impairments (Wilson et al. 2011). The results presented here suggest that the expression of GABRB3 is crucial for defining the features of the white matter in several tracts, and in this particular case of the superior longitudinal fasciculus.

With respect to the corpus callosum, it has already been suggested that the microstructure of this structure is under strict genetic control (Kanchibhotla et al. 2014). In the study by Peters et al. (2011), decreased anisotrpy was found in some tracts including the corpus callosum in patients suffering from Angelman syndrome compared to healthy controls. The results presented here support this notion, and highlight the role of GABRB3 in the definition of microstructural features of the corpus callosum.

The results in white matter found in this study confirm once more that the features of brain structure are genetically determined. The existence of different alleles of a gene leads in most of the cases to normal variants of the same feature. Nevertheless, the results presented here suggest that mutations of this gene might lead to structural abnormalities in particular tracts and might be responsible for many neurologic diseases.

This study also showed that homozygote carriers of G2 exhibit increased global *delta* voltage compared to heterozygote carriers. This difference suggests that differences in the expression of GABRB3 lead to different patterns of EEG activity, as it was revealed by studies in animals (DeLorey & Olsen 1999). Alterations in the expression of GABRB3 have also been described as a crucial etiologic factor of epilepsy in humans (Allen et al. 2013; DeLorey et al. 1998; Tanaka et al. 2012). As discussed in Chapters 2 and 7, polymorphic variants of genes might lead conformational or signalling changes, resulting in different patterns in a variety of features, such as receptor density or channel gating. The existence of such differences could explain inter-individual variations in the EEG signal, and in the case of G2, of *delta* amplitude.

The mechanisms through which the allelic variants of GABRB3 ultimately define the features of white matter and EEG signalling should also be studied. One could hypothesise that variations in the linear sequence of the genetic code might trigger different signalling mechanisms, and be definitive during development and/or maturation. Moreover, a change in a single enzyme or protein could

disrupt a single biochemical phenomenon, although result in more than one effect on the phenotype, a circumstance known as *pleiotropy*.

This study is a good example of imaging genetics, where a candidate gene was chosen and investigated individually, exploiting the advantages of multimodal imaging. Since no method is exempt of drawbacks, the inherent limitations of each technique were also taken into account for the interpretation of the results, being the biggest limitation of this study the relatively small sample that only permitted to yield conclusions about the G2 allele. Nevertheless, it is worthy to mention that for an imaging study the sample sizes investigated are considered as sufficient.

In order to perform objective analyses, all volunteers fulfilling the criteria were included, and only those who did not complete the study were excluded. Thus, the conclusions of this study should be considered unbiased.

Of particular importance is to mention that all statistical comparisons were performed after all data were acquired, and the allelic status of the subjects was only revealed to perform such comparisons. In other words, neither subject nor investigator knew the group to which each volunteer would be assigned.

Studies including complete individual genomic information appear to be the next step for the investigation of imaging genetics. The use of novel imaging techniques combined with complete genomic information in large samples of volunteers will definitively increase the knowledge of the mechanisms of heredity in the particular case of the brain, which resist to be fully understood.

Until now, this is the first time that the GABRB3 gene has been tested in any imaging genetics study. The results of this study confirmed the importance of the GABRB3 gene in defining features of brain structure and functioning, and put the basis for future studies including the same gene. Studies including mutations of this gene would also be of great interest for the complete understanding of the effect of GABRB3 expression.

Appendix A

Supplementary information Chapter 4

Contrast	Min. p	X, Y, Z of min. p	Structures of min. p	Hem.
F–test	0.28	-7, 31, 4	74% Forceps minor	L
	0.186	11, -32, 24	3% Anterior thalamic radiation L	L

* $p \leq 0.05$

TABLE A.1: Analysis of FA. Results of the F-test (one-way ANOVA) showing clusters of minimum p value (corrected), MNI coordinates, name of the structures and hemisphere. Only clusters with a minimum of 100 voxels are presented. Structures defined according to JHU White-Matter Tractography Atlas.

Contrast	**Min. *p***	**X, Y, Z of min. *p***	**Structures of min. *p***	**Hem.**
G2+ >G2–	0.7	34, -12, 37	39% Superior longitudinal fasciculus R, 10% Superior longitudinal fasciculus (temporal part) R	R
	0.704	31, -33, 16	5% Inferior fronto-occipital fasciculus R, 3% Inferior longitudinal fasciculus R	R
	0.721	27, 19, 4	32% Inferior fronto-occipital fasciculus R, 3% Uncinate fasciculus R	R
	0.768	33, -6, 9	8% Superior longitudinal fasciculus R	R
	0.74	35, -61, 31	Unclassified	-
	0.795	-30, -1, 14	5% Superior longitudinal fasciculus L	L
G2+ <G2–	0.732	16, -30, 55	11% Corticospinal tract R	R
	0.753	-17, -18, 36	†Body of corpus callosum	L
	0.739	14, -3, 33	†Body of corpus callosum	R

* $p \leq 0.025$

† Areas defined according to JHU ICBM-DTI-81 White-Matter Labels

TABLE A.2: Analysis of FA. Results of the independent-samples t-test showing clusters of minimum p value (corrected), MNI coordinates, name of the structures and hemisphere. Only clusters with a minimum of 100 voxels are presented. Structures defined according to JHU White-Matter Tractography Atlas.

Contrast	Min. *p*	X, Y, Z of min. *p*	Structures of min. *p*	Hem.
G2+ >G2– adjusted	0.684	11, -6, 8	50% Anterior thalamic radiation R	R
	0.622	-20, 11, 32	†Superior corona radiata L	L
	0.813	-44, -6, 24	45% Superior longitudinal fasciculus L, 21% Superior longitudinal fasciculus (temporal part) L	L
	0.76	35, -14, 35	61% Superior longitudinal fasciculus R, 19% Superior longitudinal fasciculus (temporal part) R	R
	0.733	-13, -24, 29	†Body of corpus callosum	L
	0.773	-26, -70, 14	37% Forceps major, 5% Inferior longitudinal fasciculus L	L
	0.829	18, 28, 25	8% Forceps minor	R
	0.717	26, -25, 26	29% Corticospinal tract R	R
	0.852	16, -32, 11	5% Anterior thalamic radiation R	R
G2+ <G2– adjusted	0.441	-16, -46, 22	†Splenium of corpus callosum	L
	0.746	-14, -11, 57	Unclassified	-
	0.841	-37, -58, -36	Unclassified	-
	0.81	21, -38, -34	3% Corticospinal tract R	R
	0.856	6, -45, -25	8% Anterior thalamic radiation R	R
	0.882	-7, -24, -33	42% Corticospinal tract L	L

* $p \leq 0.0125$
† Areas defined according to JHU ICBM-DTI-81 White-Matter Labels

TABLE A.3: Analysis of FA. Results of the independent-samples t-test adjusted for the number of G2 alleles. Results show clusters of minimum p value (corrected), MNI coordinates, name of the structures and hemisphere. Only clusters with a minimum of 100 voxels are presented. Structures defined according to JHU White-Matter Tractography Atlas.

Contrast	Min. *p*	X, Y, Z of min. *p*	Structures of min. *p*	Hem.
Positive effect of G2	0.209	-17, -46, 23	†Splenium of corpus callosum	L
	0.65	-17, -62, 41	3% Inferior longitudinal fasciculus L	L
	0.807	-36, -58, 34	8% Superior longitudinal fasciculus L	L
	0.759	18, -52, 48	Unclassified	-
Negative effect of G2	0.4	-20, 11, 32	†Superior corona radiata L	L
	0.81	11, -6, 7	61% Anterior thalamic radiation R	R
	0.844	31, 33, 9	32% Inferior fronto-occipital fasciculus R	R
	0.778	-28, -67, 15	16% Forceps major, 5% Inferior fronto-occipital fasciculus L	L

* $p \leq 0.0125$
† Areas defined according to JHU ICBM-DTI-81 White-Matter Labels

TABLE A.4: Analysis of FA. Results of the effect of the number of G2 alleles. Results show clusters of minimum p value (corrected), MNI coordinates, name of the structures and hemisphere. Only clusters with a minimum of 100 voxels are presented. Structures defined according to JHU White-Matter Tractography Atlas.

Contrast	**Min. *p***	**X, Y, Z of min. *p***	**Structures of min. *p***	**Hem.**
G2+ >G2–	0.487	12, -46, -32	†Inferior cerebellar peduncle R	R
	0.791	14, -14, -13	16% Corticospinal tract R	R
G2+ <G2–	0.05	21, -39, 39	†Posterior corona radiata R	R

* $p \leq 0.025$
† Areas defined according to JHU ICBM-DTI-81 White-Matter Labels

TABLE A.5: Analysis of MD. Results of the independent-samples t-test showing clusters of minimum p value (corrected), MNI coordinates, name of the structures and hemisphere. Only clusters with a minimum of 100 voxels are presented. Structures defined according to JHU White-Matter Tractography Atlas.

Contrast	**Min. *p***	**X, Y, Z of min. *p***	**Structures of min. *p***	**Hem.**
G2+ >G2– adjusted	0.484	-26, -57, 15	26% Forceps major	L
	0.676	26, -53, 20	8% Forceps major, 3% Inferior fronto-occipital fasciculus R	R
	0.868	23, -89, 0	13% Inferior fronto-occipital fasciculus R, 8% Forceps major	R
	0.875	13, -57, 30	3% Cingulum (cingulate gyrus) R	R
G2+ <G2– adjusted	0.317	9, 17, 20	†Body of corpus callosum	R
	0.86	49, -19, 26	8% Superior longitudinal fasciculus R	R
Positive effect of G2	0.3	9, 17, 20	†Body of corpus callosum	R
Negative effect of G2	0.11	26, -53, 20	8% Forceps major, 3% Inferior fronto-occipital fasciculus R	R

* $p \leq 0.0125$
† Areas defined according to JHU ICBM-DTI-81 White-Matter Labels

TABLE A.6: Analysis of MD. Results of the independent-samples t-test and the effect of the number of G2 alleles. Results show clusters of minimum p value (corrected), MNI coordinates, name of the structures and hemisphere. Only clusters with a minimum of 100 voxels are presented. Structures defined according to JHU White-Matter Tractography Atlas.

Contrast	**Min. *p***	**X, Y, Z of min. *p***	**Structures of min. *p***	**Hem.**
G2+ >G2–	0.575	12, -43, -35	†Inferior cerebellar peduncle R	R
	0.772	13, -32, 26	†Splenium of corpus callosum	R
	0.769	-15, -38, 25	†Splenium of corpus callosum	L
	0.729	-17, -46, 11	53% Forceps major	L
	0.84	22, -71, -31	Unclassified	-
G2+ <G2–	0.087	17, -12, 52	3% Corticospinal tract R	R

* $p \leq 0.025$
† Areas defined according to JHU ICBM-DTI-81 White-Matter Labels

TABLE A.7: Analysis of FA. Results of the independent-samples t-test showing clusters of minimum p value (corrected), MNI coordinates, name of the structures and hemisphere. Only clusters with a minimum of 100 voxels are presented. Structures defined according to JHU White-Matter Tractography Atlas.

Contrast	**Min. *p***	**X, Y, Z of min. *p***	**Structures of min. *p***	**Hem.**
G2+ >G2– adjusted	0.568	-22, -55, 30	8% Inferior longitudinal fasciculus L, 3% Inferior fronto-occipital fasciculus L	L
	0.63	27, -27, 21	8% Corticospinal tract R	R
	0.718	10, -23, 9	11% Anterior thalamic radiation R	R
	0.736	24, -57, -35	5% Corticospinal tract R	R
	0.882	20, 28, 25	5% Forceps minor	R
	0.794	22, -52, 22	5% Forceps major	R
	0.842	-22, -59, -35	†Middle cerebellar peduncle	L
	0.844	35, -48, 8	13% Inferior fronto-occipital fasciculus R, 3% Inferior longitudinal fasciculus R	R
	0.852	37, -18, 34	53% Superior longitudinal fasciculus R, 23% Superior longitudinal fasciculus (temporal part) R	R
	0.832	-6, -58, -27	Unclassified	-
G2+ <G2– adjusted	0.352	5, 17, 19	†Body of corpus callosum	R
	0.776	-15, -13, 55	Unclassified	-
	0.758	18, -26, 53	16% Corticospinal tract R	R
Positive effect of G2	0.248	5, 19, 17	3% Forceps minor	R
Negative effect of G2	0.132	-22, -55, 30	8% Inferior longitudinal fasciculus L, 3% Inferior fronto-occipital fasciculus L	L

* $p \leq 0.0125$
† Areas defined according to JHU ICBM-DTI-81 White-Matter Labels

TABLE A.8: Analysis of AD. Results of the independent-samples t-test adjusted and the effect of the number of G2 alleles. Results show clusters of minimum p value (corrected), MNI coordinates, name of the structures and hemisphere. Only clusters with a minimum of 100 voxels are presented. Structures defined according to JHU White-Matter Tractography Atlas.

Contrast	**Min. *p***	**X, Y, Z of min. *p***	**Structures of min. *p***	**Hem.**
F–test	0.387	-25, -4, 33	5% Superior longitudinal fasciculus L	L
	0.874	-18, 20, -5	13% Anterior thalamic radiation L, 11% Inferior fronto-occipital fasciculus L, 8% Uncinate fasciculus L	L
	0.886	-33, -3, 20	18% Superior longitudinal fasciculus L, 5% Superior longitudinal fasciculus (temporal part) L	L
	0.888	-21, 8, -14	Unclassified	-
	0.893	-41, -26, 3	5% Inferior longitudinal fasciculus L	L

* $p \leq 0.05$

TABLE A.9: Analysis of RD. Results of the F-test (one-way ANOVA) showing clusters of minimum p value (corrected), MNI coordinates, name of the structures and hemisphere. Only clusters with a minimum of 100 voxels are presented. Structures defined according to JHU White-Matter Tractography Atlas.

Contrast	**Min. *p***	**X, Y, Z of min. *p***	**Structures of min. *p***	**Hem.**
G2+ >G2–	-	-	-	-
G2+ <G2–	0.157	36, -32, 27	58% Superior longitudinal fasciculus R, 23% Superior longitudinal fasciculus (temporal part) R	R
	0.775	24, -42, -2	22% Cingulum (hippocampus) R	R

* $p \leq 0.025$

TABLE A.10: Analysis of RD. Results of the independent-samples t-test showing clusters of minimum p value (corrected), MNI coordinates, name of the structures and hemisphere. Only clusters with a minimum of 100 voxels are presented. Structures defined according to JHU White-Matter Tractography Atlas.

Contrast	**Min. *p***	**X, Y, Z of min. *p***	**Structures of min. *p***	**Hem.**
G2+ >G2– adjusted	0.351	-14, -45, 20	†Splenium of corpus callosum	L
	0.829	-4, 28, 1	29% Forceps minor	L
	0.825	-36, -4, -33	Unclassified	-
	0.817	-25, -16, 48	Unclassified	-
	0.871	15, 35, -5	37% Forceps minor, 9% Uncinate fasciculus R, 5% Inferior fronto-occipital fasciculus R	R
	0.86	-40, 6, 18	11% Superior longitudinal fasciculus L, 8% Superior longitudinal fasciculus (temporal part) L	L
	0.847	-29, 35, 19	3% Anterior thalamic radiation L	L
	0.857	-37, 32, 8	29% Inferior fronto-occipital fasciculus L, 16% Anterior thalamic radiation L	L
G2+ <G2– adjusted	0.712	10, 15, 22	†Body of corpus callosum	R
	0.579	-13, -24, 29	†Body of corpus callosum	L
	0.748	-16, 20, 27	3% Cingulum (cingulate gyrus) L	L
	0.811	41, -15, 29	58% Superior longitudinal fasciculus R, 16% Superior longitudinal fasciculus (temporal part) R	R
	0.857	27, -24, 22	21% Corticospinal tract R	R
Positive effect of G2	0.518	-13, -24, 29	†Body of corpus callosum	L
	0.86	-16, 17, 30	†Anterior corona radiata L	L
Negative effect of G2	0.109	-18, -46, 24	†Splenium of corpus callosum	L

* $p \leq 0.0125$

† Areas defined according to JHU ICBM-DTI-81 White-Matter Labels

TABLE A.11: Analysis of RD. Results of the independent-samples t-test adjusted and the effect of the number of G2 alleles. Results show clusters of minimum p value (corrected), MNI coordinates, name of the structures and hemisphere. Only clusters with a minimum of 100 voxels are presented. Structures defined according to JHU White-Matter Tractography Atlas.

Contrast	**Min. *p***	**X, Y, Z of min. *p***	**Structures of min. *p***	**Hem.**
F–test	0.299	-14, -15, 17	Unclassified	-
G2+ >G2–	0.53	-15, -24, 60	16% Corticospinal tract L	L
G2+ <G2–	0.9072	-35, -12, 37	21% Superior longitudinal fasciculus L, 8% Superior longitudinal fasciculus (temporal part) L	L
G2+ >G2– adjusted	-	-	-	-
G2+ <G2– adjusted	0.794	-18, -26, 15	3% Anterior thalamic radiation L	L
Positive effect of G2	-	-	-	-
Negative effect of	0.431	-29, -65, 13	26% Forceps major, 11% Inferior fronto-occipital fasciculus L	L
G2	0.361	-25, -35, 27	8% Anterior thalamic radiation L	L

* $p \leq 0.05$ ** $p \leq 0.025$ *** $p \leq 0.0125$

TABLE A.12: Analysis of FA symmetry. Results of the F-test (one-way ANOVA), independent-samples t-test, independent-samples t-test adjusted and the effect of the number of G2 alleles. Clusters of minimum p value (corrected), MNI coordinates, name of the structures and hemisphere. Only clusters with a minimum of 100 voxels are presented. Structures defined according to JHU White-Matter Tractography Atlas.

Contrast	Min. *p*	X, Y, Z of min. *p*	Structures of min. *p*	Hem.
F–test	0.798	-28, -2, 22	3% Superior longitudinal fasciculus L	L
	0.809	-37, -15, 26	61% Superior longitudinal fasciculus L, 26% Superior longitudinal fasciculus (temporal part) L	L
G2+ >G2–	0.285	-36, -32, 28	84% Superior longitudinal fasciculus L, 53% Superior longitudinal fasciculus (temporal part) L	L
	0.301	-31, -17, 41	11% Superior longitudinal fasciculus L	L
	0.455	-52, -10, 23	18% Superior longitudinal fasciculus L, 5% Superior longitudinal fasciculus (temporal part) L	L
	0.419	-20, -18, 49	11% Corticospinal tract L	L
	0.722	-22, -51, 37	5% Anterior thalamic radiation L	L
	0.602	-10, -62, 29	3% Cingulum (cingulate gyrus) L	L
	0.759	-41, -51, 35	5% Superior longitudinal fasciculus L	L
G2+ <G2–	0.383	-13, -46, -32	3% Anterior thalamic radiation L	L
	0.774	-23, -6, 16	†Posterior limb of internal capsule L	L
	0.733	-24, -75, -30	Unclassified	-
	0.719	-25, -49, -38	3% Corticospinal tract L	L
	0.807	-19, -11, 0	11% Corticospinal tract L, 3% Superior longitudinal fasciculus L	L
	0.852	-26, -65, -35	Unclassified	-
G2+ >G2– adjusted	-	-	-	-
G2+ <G2– adjusted	-	-	-	-
Positive effect of G2	-	-	-	-
Negative effect of G2	0.634	-10, 16, 23	5% Cingulum (cingulate gyrus) L	L

* $p \leq 0.05$ ** $p \leq 0.025$ *** $p \leq 0.0125$

† Areas defined according to JHU ICBM-DTI-81 White-Matter Labels

TABLE A.13: Analysis of MD symmetry. Results of the F-test (one-way ANOVA), independent-samples t-test, independent-samples t-test adjusted and the effect of the number of G2 alleles. Clusters of minimum p value (corrected), MNI coordinates, name of the structures and hemisphere. Only clusters with a minimum of 100 voxels are presented. Structures defined according to JHU White-Matter Tractography Atlas.

Contrast	**Min. *p***	**X, Y, Z of min. *p***	**Structures of min. *p***	**Hem.**
F–test	-	-	-	-
G2+ >G2–	0.452 0.36	-20, -62, 36 -31, -17, 43	5% Inferior longitudinal fasciculus L 8% Superior longitudinal fasciculus L	L L
G2+ <G2–	-	-	-	-
G2+ >G2– adjusted	-	-	-	-
G2+ <G2– adjusted	-	-	-	-
Positive effect of G2	0.635	-28, -67, 13	29% Forceps major, 8% Inferior longitudinal fasciculus L	L
Negative effect of G2	-	-	-	-

* $p \leq 0.05$ ** $p \leq 0.025$ *** $p \leq 0.0125$

TABLE A.14: Analysis of RD symmetry. Results of the F-test (one-way ANOVA), independent-samples t-test, independent-samples t-test adjusted and the effect of the number of G2 alleles. Clusters of minimum p value (corrected), MNI coordinates, name of the structures and hemisphere. Only clusters with a minimum of 100 voxels are presented. Structures defined according to JHU White-Matter Tractography Atlas.

Appendix B

Supplementary information Chapter 5

Contrast	**Min. *p***	**X, Y, Z of min. *p***	**Structures of min. *p***	**Hem.**
F–test	0.114	-4, -32, 30	60% Cingulate Gyrus, posterior division	L

* $p \leq 0.05$

TABLE B.1: Analysis of the default-mode network. Results of the F-test (one-way ANOVA) showing clusters of minimum p value (corrected), MNI coordinates, name of the structures and hemisphere. Only clusters with a minimum of 100 voxels are presented. Structures defined according to Harvard-Oxford Cortical and Subcortical Structural Atlases.

Contrast	**Min. *p***	**X, Y, Z of min. *p***	**Structures of min. *p***	**Hem.**
F–test	-	-	-	-

* $p \leq 0.05$

TABLE B.2: Analysis of the medial visual network. Results of the F-test (one-way ANOVA) showing clusters of minimum p value (corrected), MNI coordinates, name of the structures and hemisphere. Only clusters with a minimum of 100 voxels are presented. Structures defined according to Harvard-Oxford Cortical and Subcortical Structural Atlases.

Contrast	**Min. *p***	**X, Y, Z of min. *p***	**Structures of min. *p***	**Hem.**
F–test	-	-	-	-

* $p \leq 0.05$

TABLE B.3: Analysis of the lateral visual network. Results of the F-test (one-way ANOVA) showing clusters of minimum p value (corrected), MNI coordinates, name of the structures and hemisphere. Only clusters with a minimum of 100 voxels are presented. Structures defined according to Harvard-Oxford Cortical and Subcortical Structural Atlases.

Contrast	**Min. *p***	**X, Y, Z of min. *p***	**Structures of min. *p***	**Hem.**
F–test	0.41	32, -36, 54	39% Postcentral Gyrus, 24% Superior Parietal Lobule	R
	0.612	44, -20, 38	36% Postcentral Gyrus, 3% Supramarginal Gyrus, anterior division	R

* $p \leq 0.05$

TABLE B.4: Analysis of the sensorimotor network. Results of the F-test (one-way ANOVA) showing clusters of minimum p value (corrected), MNI coordinates, name of the structures and hemisphere. Only clusters with a minimum of 100 voxels are presented. Structures defined according to Harvard-Oxford Cortical and Subcortical Structural Atlases.

Contrast	**Min. *p***	**X, Y, Z of min. *p***	**Structures of min. *p***	**Hem.**
F–test	-	-	-	-

* $p \leq 0.05$

TABLE B.5: Analysis of the auditory network. Results of the F-test (one-way ANOVA) showing clusters of minimum p value (corrected), MNI coordinates, name of the structures and hemisphere. Only clusters with a minimum of 100 voxels are presented. Structures defined according to Harvard-Oxford Cortical and Subcortical Structural Atlases.

Contrast	**Min. *p***	**X, Y, Z of min. *p***	**Structures of min. *p***	**Hem.**
F–test	-	-	-	-

* $p \leq 0.05$

TABLE B.6: Analysis of the executive control network. Results of the F-test (one-way ANOVA) showing clusters of minimum p value (corrected), MNI coordinates, name of the structures and hemisphere. Only clusters with a minimum of 100 voxels are presented. Structures defined according to Harvard-Oxford Cortical and Subcortical Structural Atlases.

Contrast	**Min. *p***	**X, Y, Z of min. *p***	**Structures of min. *p***	**Hem.**
F–test	-	-	-	-

* $p \leq 0.05$

TABLE B.7: Analysis of the right frontoparietal network. Results of the F-test (one-way ANOVA) showing clusters of minimum p value (corrected), MNI coordinates, name of the structures and hemisphere. Only clusters with a minimum of 100 voxels are presented. Structures defined according to Harvard-Oxford Cortical and Subcortical Structural Atlases.

Contrast	**Min. *p***	**X, Y, Z of min. *p***	**Structures of min. *p***	**Hem.**
F–test	-	-	-	-

* $p \leq 0.05$

TABLE B.8: Analysis of the left frontoparietal network. Results of the F-test (one-way ANOVA) showing clusters of minimum p value (corrected), MNI coordinates, name of the structures and hemisphere. Only clusters with a minimum of 100 voxels are presented. Structures defined according to Harvard-Oxford Cortical and Subcortical Structural Atlases.

Contrast	**Min. *p***	**X, Y, Z of min. *p***	**Structures of min. *p***	**Hem.**
G2+ >G2–	0.739	-56, -34, 4	53% Superior Temporal Gyrus, posterior division, 3% Middle Temporal Gyrus, posterior division	L
G2+ <G2–	0.492	50, -60, 18	35% Lateral Occipital Cortex, superior division, 25% Angular Gyrus	R
	0.408	2, 64, -8	79% Frontal Pole	R

* $p \leq 0.025$

TABLE B.9: Analysis of the default-mode network. Results of the independent-samples t-test showing clusters of minimum p value (corrected), MNI coordinates, name of the structures and hemisphere. Only clusters with a minimum of 100 voxels are presented. Structures defined according to Harvard-Oxford Cortical and Subcortical Structural Atlases.

Contrast	**Min. *p***	**X, Y, Z of min. *p***	**Structures of min. *p***	**Hem.**
G2+ >G2–	0.574	22, -50, 48	11% Superior Parietal Lobule	R
	0.467	-16, -56, 72	31% Superior Parietal Lobule, 19% Lateral Occipital Cortex, superior division	L
	0.661	-14, -50, 50	21% Precuneous Cortex, 3% Superior Parietal Lobule	L
G2+ <G2–	0.739	34, 70, 12	Unclassified	-

* $p \leq 0.025$

TABLE B.10: Analysis of the medial visual network. Results of the independent-samples t-test showing clusters of minimum p value (corrected), MNI coordinates, name of the structures and hemisphere. Only clusters with a minimum of 100 voxels are presented. Structures defined according to Harvard-Oxford Cortical and Subcortical Structural Atlases.

Contrast	**Min. *p***	**X, Y, Z of min. *p***	**Structures of min. *p***	**Hem.**
G2+ >G2–	0.313	10, 18, 0	80% Right Caudate, 12% Right Accumbens	R
	0.906	42, -66, 12	39% Lateral Occipital Cortex, inferior division, 12% Lateral Occipital Cortex, superior division	R
	0.917	56, -76, -26	Unclassified	-
G2+ <G2–	-	-	-	-

* $p \leq 0.025$

TABLE B.11: Analysis of the lateral visual network. Results of the independent-samples t-test showing clusters of minimum p value (corrected), MNI coordinates, name of the structures and hemisphere. Only clusters with a minimum of 100 voxels are presented. Structures defined according to Harvard-Oxford Cortical and Subcortical Structural Atlases.

Contrast	**Min. *p***	**X, Y, Z of min. *p***	**Structures of min. *p***	**Hem.**
G2+ >G2–	-	-	-	-
G2+ <G2–	0.224	-22, -16, 28	100% Left Cerebral White Matter	L

* $p \leq 0.025$

TABLE B.12: Analysis of the sensorimotor network. Results of the independent-samples t-test showing clusters of minimum p value (corrected), MNI coordinates, name of the structures and hemisphere. Only clusters with a minimum of 100 voxels are presented. Structures defined according to Harvard-Oxford Cortical and Subcortical Structural Atlases.

Contrast	**Min. *p***	**X, Y, Z of min. *p***	**Structures of min. *p***	**Hem.**
G2+ >G2–	0.559	-40, -36, 0	99% Left Cerebral White Matter, 1% Left Cerebral Cortex	L
	0.818	-42, -30, 58	50% Postcentral Gyrus, 2% Superior Parietal Lobule, 2% Precentral Gyrus	L
G2+ <G2–	0.356	-46, -80, 34	32% Lateral Occipital Cortex, superior division	L
	0.83	28, -94, 26	33% Occipital Pole, 5% Lateral Occipital Cortex, superior division	R
	0.806	-42, -76, 54	Unclassified	-

* $p \leq 0.025$

TABLE B.13: Analysis of the auditory network. Results of the independent-samples t-test showing clusters of minimum p value (corrected), MNI coordinates, name of the structures and hemisphere. Only clusters with a minimum of 100 voxels are presented. Structures defined according to Harvard-Oxford Cortical and Subcortical Structural Atlases.

Contrast	**Min. *p***	**X, Y, Z of min. *p***	**Structures of min. *p***	**Hem.**
G2+ >G2–	-	-	-	-
G2+ <G2–	0.617	-54, -32, -34	2% Inferior Temporal Gyrus, posterior division	L
	0.535	10, 4, 68	35% Superior Frontal Gyrus, 8% Juxtapositional Lobule Cortex	R
	0.829	42, -48, 14	11% Angular Gyrus, 9% Middle Temporal Gyrus, temporooccipital part	R
	0.608	20, -36, -4	6% Cingulate Gyrus, posterior division, 3% Parahippocampal Gyrus, posterior division	R
	0.558	-36, 8, 24	11% Inferior Frontal Gyrus, pars opercularis, 9% Precentral Gyrus	L
	0.831	-68, -48, -2	42% Middle Temporal Gyrus, temporooccipital part, 4% Middle Temporal Gyrus, posterior division	L
	0.772	44, -46, -14	41% Temporal Occipital Fusiform Cortex, 23% Inferior Temporal Gyrus, temporooccipital part	R

* $p \leq 0.025$

TABLE B.14: Analysis of the executive control network. Results of the independent-samples t-test showing clusters of minimum p value (corrected), MNI coordinates, name of the structures and hemisphere. Only clusters with a minimum of 100 voxels are presented. Structures defined according to Harvard-Oxford Cortical and Subcortical Structural Atlases.

Contrast	**Min. *p***	**X, Y, Z of min. *p***	**Structures of min. *p***	**Hem.**
G2+ >G2–	0.248	52, -78, -14	11% Lateral Occipital Cortex, inferior division	R
	0.89	18, 58, 48	Unclassified	-
	0.814	-18, 30, 48	42% Superior Frontal Gyrus, 3% Middle Frontal Gyrus	L
	0.861	-18, -26, 60	34% Precentral Gyrus, 5% Postcentral Gyrus	L
G2+ <G2–	-	-	-	-

* $p \leq 0.025$

TABLE B.15: Analysis of the right frontoparietal network. Results of the independent-samples t-test showing clusters of minimum p value (corrected), MNI coordinates, name of the structures and hemisphere. Only clusters with a minimum of 100 voxels are presented. Structures defined according to Harvard-Oxford Cortical and Subcortical Structural Atlases.

Contrast	**Min. *p***	**X, Y, Z of min. *p***	**Structures of min. *p***	**Hem.**
G2+ >G2–	0.275	-16, -52, 50	7% Precuneous Cortex, 6% Superior Parietal Lobule	L
G2+ <G2–	0.53	16, -30, 28	95% Right Cerebral White Matter, 5% Right Lateral Ventricle	R

* $p \leq 0.025$

TABLE B.16: Analysis of the left frontoparietal network. Results of the independent-samples t-test showing clusters of minimum p value (corrected), MNI coordinates, name of the structures and hemisphere. Only clusters with a minimum of 100 voxels are presented. Structures defined according to Harvard-Oxford Cortical and Subcortical Structural Atlases.

Contrast	**Min. *p***	**X, Y, Z of min. *p***	**Structures of min. *p***	**Hem.**
G2+ >G2– adjusted	-	-	-	-
	0.125	12, -54, 6	46% Precuneous Cortex, 21% Lingual Gyrus	R
	0.247	28, -34, 68	43% Postcentral Gyrus, 7% Precentral Gyrus	R
	0.442	50, -60, 20	34% Lateral Occipital Cortex, superior division, 28% Angular Gyrus	R
G2+ <G2– adjusted	0.434	-12, 0, 16	89% Left Caudate, 5% Left Lateral Ventrical	L
	0.523	20, 56, 32	79% Frontal Pole	R
	0.739	-32, -24, 20	18% Insular Cortex, 10% Parietal Operculum Cortex	L
	0.567	46, 50, 6	83% Frontal Pole	R
	0.356	-10, 48, 38	45% Frontal Pole, 2% Superior Frontal Gyrus	L
	0.691	-44, 52, 8	68% Frontal Pole	L
	0.717	-36, 62, 24	Unclassified	-
Positive effect of G2	0.204	-4, -32, 32	61% Cingulate Gyrus, posterior division	L
	0.528	-66, -30, -26	28% Inferior Temporal Gyrus, posterior division, 5% Middle Temporal Gyrus, posterior division	L
	0.737	-28, -36, -12	34% Parahippocampal Gyrus, posterior division, 8% Lingual Gyrus	L
	0.731	-10, -100, -16	31% Occipital Pole, 3% Lateral Occipital Cortex, inferior division	L
Negative effect of G2	-	-	-	-

* $p \leq 0.0125$

TABLE B.17: Analysis of the default-mode network. Results of the independent-samples t-test and the effect of the number of G2 alleles. Results show clusters of minimum p value (corrected), MNI coordinates, name of the structures and hemisphere. Only clusters with a minimum of 100 voxels are presented. Structures defined according to Harvard-Oxford Cortical and Subcortical Structural Atlases.

Contrast	**Min. *p***	**X, Y, Z of min. *p***	**Structures of min. *p***	**Hem.**
G2+ >G2– adjusted	0.462	58, -20, 46	47% Postcentral Gyrus, 24% Supramarginal Gyrus, anterior division	R
	0.559	-2, -74, 30	54% Precuneous Cortex, 30% Cuneal Cortex	L
G2+ <G2– adjusted	0.442	8, -10, 52	43% Juxtapositional Lobule Cortex (formerly Supplementary Motor Cortex), 12% Precentral Gyrus	R
	0.227	-38, 0, 56	43% Middle Frontal Gyrus, 21% Precentral Gyrus	L
	0.619	34, 20, 58	51% Middle Frontal Gyrus, 11% Superior Frontal Gyrus	R
	0.488	16, 6, -14	7% Frontal Orbital Cortex	R
Positive effect of G2	0.277	16, 6, -14	7% Frontal Orbital Cortex	R
	0.63	-6, 4, 50	60% Juxtapositional Lobule Cortex (formerly Supplementary Motor Cortex), 8% Cingulate Gyrus, anterior division	L
	0.639	-38, -2, 66	15% Middle Frontal Gyrus, 5% Precentral Gyrus	L
Negative effect of G2	0.623	-56, -30, 48	50% Supramarginal Gyrus, anterior division, 22% Postcentral Gyrus	L

* $p \leq 0.0125$

TABLE B.18: Analysis of the medial visual network. Results of the independent-samples t-test and the effect of the number of G2 alleles. Results show clusters of minimum p value (corrected), MNI coordinates, name of the structures and hemisphere. Only clusters with a minimum of 100 voxels are presented. Structures defined according to Harvard-Oxford Cortical and Subcortical Structural Atlases.

Contrast	**Min. *p***	**X, Y, Z of min. *p***	**Structures of min. *p***	**Hem.**
G2+ >G2– adjusted	0.123	48, -32, 16	47% Planum Temporale, 17% Parietal Operculum Cortex	R
	0.448	12, -100, 28	5% Occipital Pole	R
	0.546	-28, 52, -16	72% Frontal Pole	L
	0.397	38, 18, 56	56% Middle Frontal Gyrus, 2% Superior Frontal Gyrus	R
	0.523	2, -34, -28	100% Brain-Stem	R
	0.57	44, 50, -18	30% Frontal Pole	R
	0.815	42, -22, -24	54% Temporal Fusiform Cortex, posterior division, 29% Inferior Temporal Gyrus, posterior division	R
	0.769	-48, 34, 36	4% Middle Frontal Gyrus, 2% Frontal Pole	L
	0.799	52, -38, 56	52% Supramarginal Gyrus, posterior division, 6% Angular Gyrus	R
G2+ <G2– adjusted	-	-	-	-
Positive effect of G2	-	-	-	-
Negative effect of G2	0.184	48, -32, 18	38% Parietal Operculum Cortex, 31% Planum Temporale	R
	0.736	2, -34, -28	100% Brain-Stem	R
	0.703	38, 18, 56	56% Middle Frontal Gyrus, 2% Superior Frontal Gyrus	R
	0.846	44, 50, -18	30% Frontal Pole	R
	0.977	-48, -82, -4	71% Lateral Occipital Cortex, inferior division	L

* $p \leq 0.0125$

TABLE B.19: Analysis of the lateral visual network. Results of the independent-samples t-test and the effect of the number of G2 alleles. Results show clusters of minimum p value (corrected), MNI coordinates, name of the structures and hemisphere. Only clusters with a minimum of 100 voxels are presented. Structures defined according to Harvard-Oxford Cortical and Subcortical Structural Atlases.

Contrast	**Min. *p***	**X, Y, Z of min. *p***	**Structures of min. *p***	**Hem.**
G2+ >G2– adjusted	-	-	-	-
G2+ <G2– adjusted	0.1	42, -54, 54	34% Angular Gyrus, 17% Superior Parietal Lobule	R
	0.63	-12, 58, 32	79% Frontal Pole	L
Positive effect of G2	0.305	42, -54, 52	31% Angular Gyrus, 17% Superior Parietal Lobule	R
	0.913	64, -70, -2	Unclassified	R
Negative effect of G2	-	-	-	-

* $p \leq 0.0125$

TABLE B.20: Analysis of the sensorimotor network. Results of the independent-samples t-test and the effect of the number of G2 alleles. Results show clusters of minimum p value (corrected), MNI coordinates, name of the structures and hemisphere. Only clusters with a minimum of 100 voxels are presented. Structures defined according to Harvard-Oxford Cortical and Subcortical Structural Atlases.

Contrast	**Min. *p***	**X, Y, Z of min. *p***	**Structures of min. *p***	**Hem.**
G2+ >G2– adjusted	0.594	-28, -74, -8	57% Occipital Fusiform Gyrus, 3% Lateral Occipital Cortex, inferior division	L
	0.397	58, -42, 50	47% Supramarginal Gyrus, posterior division, 17% Angular Gyrus	R
	0.725	-70, -22, 16	1% Supramarginal Gyrus, anterior division	L
	0.751	-44, -52, -16	44% Inferior Temporal Gyrus, temporooccipital part, 31% Temporal Occipital Fusiform Cortex	L
	0.536	-48, -26, 0	13% Superior Temporal Gyrus, posterior division, 8% Planum Temporale	L
	0.738	-38, -12, 52	49% Precentral Gyrus, 2% Middle Frontal Gyrus	L
	0.76	4, -50, 24	67% Cingulate Gyrus, posterior division, 18% Precuneous Cortex	R
	0.704	-64, -2, -16	35% Middle Temporal Gyrus, anterior division, 6% Middle Temporal Gyrus, posterior division	L
	0.773	12, -44, 40	28% Precuneous Cortex, 22% Cingulate Gyrus, posterior division	R
G2+ <G2– adjusted	0.675	52, -58, 16	38% Angular Gyrus, 18% Lateral Occipital Cortex, superior division	R
	0.441	-22, -68, 56	68% Lateral Occipital Cortex, superior division, 1% Precuneous Cortex	L
Positive effect of G2	0.796	46, -54, 14	24% Angular Gyrus, 20% Middle Temporal Gyrus, temporooccipital part	R
	0.622	-22, -68, 56	68% Lateral Occipital Cortex, superior division, 1% Precuneous Cortex	L
Negative effect of G2	0.492	-18, -74, 4	26% Intracalcarine Cortex, 10% Lingual Gyrus	L
	0.623	26, 34, 56	6% Superior Frontal Gyrus, 5% Frontal Pole	R
	0.571	56, -34, 54	28% Supramarginal Gyrus, posterior division, 27% Supramarginal Gyrus, anterior division	R
	0.933	-2, 24, -16	93% Subcallosal Cortex, 1% Frontal Medial Cortex	L
	0.68	-2, -18, 18	89% Left Caudate, 5% Left Lateral Ventrical	L
	0.866	-36, -12, 54	37% Precentral Gyrus, 2% Middle Frontal Gyrus	L
	0.969	42, -74, 38	82% Lateral Occipital Cortex, superior division	R

* $p \leq 0.0125$

TABLE B.21: Analysis of the auditory network. Results of the independent-samples t-test and the effect of the number of G2 alleles. Results show clusters of minimum p value (corrected), MNI coordinates, name of the structures and hemisphere. Only clusters with a minimum of 100 voxels are presented. Structures defined according to Harvard-Oxford Cortical and Subcortical Structural Atlases.

Contrast	**Min. *p***	**X, Y, Z of min. *p***	**Structures of min. *p***	**Hem.**
G2+ >G2– adjusted	0.569	32, -52, 58	49% Superior Parietal Lobule, 3% Lateral Occipital Cortex, superior division	R
G2+ <G2– adjusted	0.422	-4, 44, 42	64% Superior Frontal Gyrus, 2% Frontal Pole	L
	0.514	-12, 48, 20	19% Paracingulate Gyrus, 6% Superior Frontal Gyrus	L
	0.726	16, -80, 50	60% Lateral Occipital Cortex, superior division, 1% Precuneous Cortex	R
	0.763	46, -2, 32	18% Precentral Gyrus	R
	0.778	16, -40, -12	58% Lingual Gyrus, 13% Parahippocampal Gyrus, posterior division	R
Positive effect of G2	-	-	-	-
Negative effect of G2	0.323	32, -52, 58	49% Superior Parietal Lobule, 3% Lateral Occipital Cortex, superior division	R
	0.712	-10, -42, 10	7% Cingulate Gyrus, posterior division, 1% Parahippocampal Gyrus, posterior division	L
	0.783	56, -48, 20	57% Angular Gyrus, 13% Supramarginal Gyrus, posterior division	R

* $p \leq 0.0125$

TABLE B.22: Analysis of the executive control network. Results of the independent-samples t-test and the effect of the number of G2 alleles. Results show clusters of minimum p value (corrected), MNI coordinates, name of the structures and hemisphere. Only clusters with a minimum of 100 voxels are presented. Structures defined according to Harvard-Oxford Cortical and Subcortical Structural Atlases.

Contrast	**Min. *p***	**X, Y, Z of min. *p***	**Structures of min. *p***	**Hem.**
G2+ >G2– adjusted	0.433	60, 2, -24	5% Temporal Pole, 4% Superior Temporal Gyrus, anterior division	R
	0.703	-24, 62, 2	78% Frontal Pole	L
	0.833	20, -82, 52	32% Lateral Occipital Cortex, superior division	R
G2+ <G2– adjusted	0.707	22, -22, 52	4% Precentral Gyrus, 1% Postcentral Gyrus	R
Positive effect of G2	0.3	32, -26, 56	36% Precentral Gyrus, 28% Postcentral Gyrus	R
Negative effect of G2	0.345	32, 4, 14	14% Insular Cortex, 7% Central Opercular Cortex	R
	0.9	-48, -82, 4	76% Lateral Occipital Cortex, inferior division, 2% Lateral Occipital Cortex, superior division	L
	0.975	-32, -84, -18	39% Occipital Fusiform Gyrus, 32% Lateral Occipital Cortex, inferior division	L
	0.79	-70, -40, -14	9% Middle Temporal Gyrus, posterior division, 1% Inferior Temporal Gyrus, posterior division	L
	0.958	-32, -82, 28	69% Lateral Occipital Cortex, superior division	L

* $p \leq 0.0125$

TABLE B.23: Analysis of the right frontoparietal network. Results of the independent-samples t-test and the effect of the number of G2 alleles. Results show clusters of minimum p value (corrected), MNI coordinates, name of the structures and hemisphere. Only clusters with a minimum of 100 voxels are presented. Structures defined according to Harvard-Oxford Cortical and Subcortical Structural Atlases.

Contrast	**Min. *p***	**X, Y, Z of min. *p***	**Structures of min. *p***	**Hem.**
G2+ >G2– adjusted	0.693	-38, 50, -18	36% Frontal Pole	L
	0.562	10, -40, 54	36% Precuneous Cortex, 34% Postcentral Gyrus	R
	0.65	8, -26, 38	38% Cingulate Gyrus, posterior division, 2% Cingulate Gyrus, anterior division	R
	0.578	28, -32, 66	47% Postcentral Gyrus, 16% Precentral Gyrus	R
G2+ <G2– adjusted	-	-	-	-
Positive effect of G2	0.766	-44, -12, 52	55% Precentral Gyrus, 14% Postcentral Gyrus	L
	0.623	0, 52, -22	53% Frontal Medial Cortex, 17% Frontal Pole	-
Negative effect of G2	0.352	46, -68, 14	37% Lateral Occipital Cortex, inferior division, 33% Lateral Occipital Cortex, superior division	R
	0.49	58, -24, 6	17% Planum Temporale, 15% Superior Temporal Gyrus, posterior division	R
	0.403	32, -44, 16	99% Right Cerebral White Matter, 1% Right Lateral Ventricle	R
	0.695	12, -26, 38	48% Cingulate Gyrus, posterior division, 2% Precentral Gyrus	R
	0.706	32, -94, 20	38% Occipital Pole, 4% Lateral Occipital Cortex, superior division	R
	0.787	42, -96, 6	1% Occipital Pole, 1% Lateral Occipital Cortex, inferior division	R
	0.747	-32, 20, -14	77% Frontal Orbital Cortex, 3% Insular Cortex	L
	0.693	28, -32, 64	47% Postcentral Gyrus, 14% Precentral Gyrus	R

* $p \leq 0.0125$

TABLE B.24: Analysis of the left frontoparietal network. Results of the independent-samples t-test and the effect of the number of G2 alleles. Results show clusters of minimum p value (corrected), MNI coordinates, name of the structures and hemisphere. Only clusters with a minimum of 100 voxels are presented. Structures defined according to Harvard-Oxford Cortical and Subcortical Structural Atlases.

Appendix C

Addendum of valorisation

C.1 Relevance of the study

The study presented here must be judged in the context of the neuroimaging genetic studies, an emerging field with a great potential.

The study of heredity has brought numerous and great advances in the understanding and treatment of several pathological entities. This is valid not just for diseases that result from mutations, but also for diseases where the genetic predisposition plays an important role, such as the metabolic, neurological and psychiatric diseases. Interestingly, even the immunological responses during infectious diseases are known to be strongly determined by genetic factors. Nowadays, it is clear that heredity is involved in the development and course of a large number of entities affecting the human being. This dissertation is, therefore, a piece of scientific work focused on elucidating the mechanisms through which heredity influences the function and structure of the brain.

The brain is the most complex of all organs. Their individual cells are quite different from each other in their transcriptomes, proteomes, phenotypes and also in the thousands of connections and interactions. The neurogenetic studies have greatly contributed to the understanding of how the nervous system of individuals differ despite belonging to the same species, and how the structural differences influence traits in personality and define predisposition to diseases. Several of the inter-individual differences are not easily observable, and are difficult to measure and quantify. This is precisely the role of neuroimaging tools

in imaging genetic studies: to provide quantifiable and measureable features to make inferences about the variances observed.

Unquestionably, variations in the linear sequence of the genetic code play a key role in explaining inter-individual differences in structure and function of the brain, as well as give insight into susceptibility and resistance in a wide range of diseases. There is strong evidence that a number of psychiatric illnesses such as schizophrenia, bipolar disorder, autism, and alcoholism have a genetic basis. A number of neurologic diseases such as dementias, epilepsies, dystonias, Parkinsons disease, ataxias, polyneuropathies, dystrophies and phakomatoses have also been associated with genetic factors. This dissertation focused on the beta-3 subunit of the GABA type A receptors (GABRB3), which has associations with epileptic encephalopathies in humans, Angelman syndrome and autism. The case of epilepsy, for example, is particularly interesting, for the reason that it implies the failures of several regulatory systems. Alterations in the expression of the GABRB3 gene might affect the expression of the GABA type A receptors by altering receptor function and/or by impairing receptor biogenesis. Alterations in the expression of the beta-3 subunits might lead to several alterations: inhibition of receptor trafficking, reduction in the subunit mRNA transcription or stability, impairing subunit folding, stability, or oligomerization. Although the actual mechanisms must be elucidated, the results presented strongly suggest the existence of changes in the activity of both gene and receptor. This dissertation is, in this sense, putting the grounds for further studies.

This dissertation is an example of a neuroimaging genetic study, where a candidate gene is chosen and comparisons are performed on the basis of the most prevalent genetic variant in a population. The most prevalent genetic variant found in this study was the same one found in all populations studied thus far. Therefore, the results presented in this study have a great deal of importance for the general population. The results presented in the dissertation found, for the first time, the actual features where the expression of the GABRB3 gene influences brain structure. Therefore, this study is pioneer in using the GABRB3 gene as candidate gene in a neuroimaging genetics study. Interestingly, the results of the dissertation confirm the alterations found in Angelman syndrome. This was an un-expected outcome and opens the possibilities to assess progresses in an eventual genetic therapeutic approach targeting this rare disease. Moreover, the differences in slow-frequency EEG oscillations might also be of utility in the

follow-up of patients suffering from epilepsy caused by alterations in GABRB3 expression. For the causal diagnosis of epilepsy, the results found here would be of help in case of altered global delta voltage. Although more studies are needed, quantitative EEG might be used in the future as diagnostic tool, and might play an important role in the future of epilepsy treatment.

C.2 Target groups

The diagnosis and treatment of epilepsy are a great deal in everyday medicine practice. About 2% of adults have a seizure at some time during their life. In most of the cases the cause remains unknown. The results presented in this dissertation might establish the basis for future studies investigating the cause of idiopathic seizures. In particular, the neuroanatomical areas described in the results might represent structures closely related with the physiopathology of seizures. Moreover, the lateralised areas described in the results might explain how hemisphere dominance affects brain microstructure and give hints of improvement for future rehabilitation therapy.

These results put the basis for future investigations of the GABRB3 gene, which was shown once more to be important for neurodevelopment and for the definition of brain features. This dissertation is, therefore, of interest for people in the world with mutations or rare variants of this gene and also for their offspring.

With respect to Angelman syndrome, a hypothetical prospect benefit will be to assess the success of gene therapy directed to the GABRB3 gene via imaging techniques targeted to the areas described in the results.

For all these reasons, these results are not only interesting for the neuroscientists, but also for the patients with epilepsy and Angelmans syndrome, and of course, for their families. Although this dissertation does not provide concrete solutions for their trouble, it certainly gives reasons to believe that future treatments and even prevention are possible.

C.3 Commercial activities

Many of the pharmacological interventions for epilepsy are directed to the GABA receptors. A deeper knowledge of the structure of the GABA receptors and its influence in the brain activity and structure will definitively help in the development of drugs targeting alterations in its signalling. It is known, for example, that carriers of some polymorphisms have different pharmacodynamic and pharmacokinetic drug profiles. Here the pharmaceutical companies are expending a lot of effort and resources in this field of research. A better understanding of genetics will definitively result in better and more focused treatments. Drugs with better affinity for certain proteins and causing fewer side effects are the future prospect where the field is moving to.

The pharmaceutical industry produces millions of new compounds every year, although only a few actually reach the market. One of the reasons is that the effects in humans are completely unpredictable. In this sense, the MRI and other computational techniques can be maximised to improve drugs development. MRI, for example, has reached an important degree of technical maturity, along with enormous developmental prospects; it poses the advantages of a having a large clinical availability and being a non-invasive technique. The effects of drugs with mechanisms of action involving the brain might be tested using imaging techniques, similarly as it was done in this dissertation. Multimodal imaging, referring to the combination of techniques, fits well in the development of brain-targeted drugs due to the desirability of measuring different aspects of the brain under the same physiological conditions.

This dissertation could be used as an exemplary study for drug research. In fact, investigating a candidate gene is a similar source of controlled variance system as the use of a pharmacological manipulation.

C.4 Schedule and implementation

The field of genetics has grown in complexity dramatically since its origins and promises to keep growing and showing paths for curative treatments in the future. Gene therapy is a concept that illustrates the progresses in the field; it refers to a therapeutic approach where nucleic acid polymers are provided to the cells of

a patient, similarly as a drug, to treat a disease. Individualised drugs designed according to the genome of an individual are the next step in the treatment of many other diseases. The field is moving really fast, and now is possible to sequence the entire genome of a person within hours, something that the first geneticist of the 20th century never dreamed of.

The benefits of the work presented in the thesis might probably not be seen immediately, although along with the advances in genome sequencing they will definitively be of importance in the next decade when the genetic diagnosis expands and becomes routine. A few years ago, for example, the only tool available for avoiding hereditary diseases was the preconception counselling of people affected by those diseases; now the complete genome sequencing is becoming available for the general population, allowing for an accurate preconception diagnosis even in healthy people.

After having found the importance of the GABRB3 gene in the definition of microstructure in the white matter, future genetic methods should be able to detect early mutations of this gene and correct them in order to avoid alterations of the neurodevelopment. The coming advances in the genetic techniques, along with the knowledge provided by this and other studies, can impact the diagnosis and treatment of epilepsy and Angelman syndrome in the following decade.

C.5 Final thought

Apart from the therapeutic benefits that the understanding of genetics will bring, the knowledge is a goal itself. The question about the purpose of science has also something to do with the inherent curiosity of the human beings, and their wish to understand their world, which also applies to the interior sphere: the body. Among the many questions that have not been answered, the one about the brain occupies an important place. The Cartesian notion of a mind controlling the body has now been found to be absurd, and the notion of a unique entity mind-body emerged, with the evident consequence: the human being is, but not only, brain. As a consequence, the understanding of the human being is a process where the exploration of the brain and its functioning is crucial. The vast complexity of this organ overwhelms (but does not discourage) the researchers, and is here where it becomes evident that the creation of knowledge is a slow

process, where every bit represents a big step towards the understanding of the system as a whole.

The construction of knowledge should be the aim of all scientists, and should have as consequence the search for well-being of all human beings. This process needs to be determined by the conviction that our species will only be able to survive as a group and not as individuals. The science should not be restricted to accumulation of data and knowledge; it should also be translated into facts, with impact on our future as species and on our environment.

Since the evolution gave us the ability to alter the planet, the responsibility of transforming it in a positive way should also be one of the aims of science. The process of transformation cannot take place in isolation; respect should be paid to other species that also won the race of evolution. However, we are not in the final phases of human sciences, we are merely at a stage previous to a more advanced and refined knowledge.

References

Abbott, A., 2008. Psychiatric genetics: The brains of the family. *Nature*, 454(7201), pp.154–157.

Abell, F. et al., 1999. The neuroanatomy of autism: a voxel-based whole brain analysis of structural scans. *Neuroreport*, 10(8), pp.1647–1651.

Aja-Fernández, S., Tristán-Vega, A. & Alberola-López, C., 2009. Noise estimation in single- and multiple-coil magnetic resonance data based on statistical models. *Magnetic Resonance Imaging*, 27(10), pp.1397–1409.

Al-Jaberi, N. et al., 2015. The Early Fetal Development of Human Neocortical GABAergic Interneurons. *Cerebral Cortex*, 25(3), pp.631–645.

Allen, A.S. et al., 2013. De novo mutations in epileptic encephalopathies. *Nature*, 501(7466), pp.217–221.

Allen, P.J. et al., 1998. Identification of EEG events in the MR scanner: the problem of pulse artifact and a method for its subtraction. *NeuroImage*, 8(3), pp.229–239.

Allen, P.J., Josephs, O. & Turner, R., 2000. A method for removing imaging artifact from continuous EEG recorded during functional MRI. *NeuroImage*, 12(2), pp.230–239.

Arrubla, J. et al., 2014. GABA Concentration in Posterior Cingulate Cortex Predicts Putamen Response during Resting State fMRI. *PloS One*, 9(9), p.e106609.

Ashburner, J. & Friston, K.J., 2000. Voxel-based morphometry–the methods. *NeuroImage*, 11(6 Pt 1), pp.805–821.

Avants, B.B. et al., 2010. Dementia induces correlated reductions in white matter integrity and cortical thickness: a multivariate neuroimaging study with sparse canonical correlation analysis. *NeuroImage*, 50(3), pp.1004–1016.

Baaré, W.F. et al., 2001. Volumes of brain structures in twins discordant for schizophrenia. *Archives of General Psychiatry*, 58(1), pp.33–40.

Barnard, E.A. et al., 1998. International Union of Pharmacology. XV. Subtypes of gamma-aminobutyric acidA receptors: classification on the basis of subunit structure and receptor function. *Pharmacological Reviews*, 50(2), pp.291–313.

Baron, J.C. et al., 2001. In vivo mapping of gray matter loss with voxel-based morphometry in mild Alzheimer's disease. *NeuroImage*, 14(2), pp.298–309.

Barros, S.P. & Offenbacher, S., 2009. Epigenetics: connecting environment and genotype to phenotype and disease. *Journal of Dental Research*, 88(5), pp.400–408.

Bartley, A.J., Jones, D.W. & Weinberger, D.R., 1997. Genetic variability of human brain size and cortical gyral patterns. *Brain*, 120(Pt 2), pp.257–269.

Basser, P.J. & Pierpaoli, C., 1996. Microstructural and physiological features of tissues elucidated by quantitative-diffusion-tensor MRI. *Journal of Magnetic Resonance. Series B*, 111(3), pp.209–219.

Beaulieu, C., 2002. The basis of anisotropic water diffusion in the nervous system - a technical review. *NMR in Biomedicine*, 15(7-8), pp.435–455.

Beckmann, C.F. et al., 2005. Investigations into resting-state connectivity using independent component analysis. *Philosophical transactions of the Royal Society of London. Series B, Biological sciences*, 360(1457), pp.1001–1013.

Beckmann, C.F. & Smith, S.M., 2004. Probabilistic independent component analysis for functional magnetic resonance imaging. *IEEE Transactions on Medical Imaging*, 23(2), pp.137–152.

Behrens, T.E.J. et al., 2003. Characterization and propagation of uncertainty in diffusion-weighted MR imaging. *Magnetic Resonance in Medicine*, 50(5), pp.1077–1088.

Benarroch, E.E., 2007. GABAA receptor heterogeneity, function, and implications for epilepsy. *Neurology*, 68(8), pp.612–614.

Berger, H., 1929. Über das Elektrenkephalogramm des Menschen. *Archiv für Psychiatrie und Nervenkrankheiten*, 87(1), pp.527–570.

Le Bihan, D. et al., 1986. MR imaging of intravoxel incoherent motions: application to diffusion and perfusion in neurologic disorders. *Radiology*, 161(2), pp.401–407.

Birn, R.M., 2012. The role of physiological noise in resting-state functional connectivity. *NeuroImage*, 62(2), pp.864–870.

Biswal, B. et al., 1995. Functional connectivity in the motor cortex of resting human brain using echo-planar MRI. *Magnetic Resonance in Medicine*, 34(4), pp.537–541.

Biswal, B.B., Van Kylen, J. & Hyde, J.S., 1997. Simultaneous assessment of flow and BOLD signals in resting-state functional connectivity maps. *NMR in Biomedicine*, 10(4-5), pp.165–170.

Blokland, G.A.M. et al., 2014. Genetic effects on the cerebellar role in working memory: same brain, different genes? *NeuroImage*, 86, pp.392–403.

Blokland, G.A.M. et al., 2008. Quantifying the heritability of task-related brain activation and performance during the N-back working memory task: a twin fMRI study. *Biological Psychology*, 79(1), pp.70–79.

Bluhm, R.L. et al., 2007. Spontaneous low-frequency fluctuations in the BOLD signal in schizophrenic patients: anomalies in the default network. *Schizophrenia Bulletin*, 33(4), pp.1004–1012.

Bodini, B. et al., 2009. Exploring the relationship between white matter and gray matter damage in early primary progressive multiple sclerosis: an in vivo study with TBSS and VBM. *Human Brain Mapping*, 30(9), pp.2852–2861.

Bogner, W. et al., 2010. In vivo quantification of intracerebral GABA by single-voxel (1)H-MRS-How reproducible are the results? *European Journal of Radiology*, 73(3), pp.526–531.

Bookstein, F.L., 2001. "Voxel-based morphometry" should not be used with imperfectly registered images. *NeuroImage*, 14(6), pp.1454–1462.

Bryant, D.M. et al., 2011. Neuroanatomical phenotype of Klinefelter syndrome in childhood: a voxel-based morphometry study. *The Journal of Neuroscience*, 31(18), pp.6654–6660.

Buckner, R.L., Andrews-Hanna, J.R. & Schacter, D.L., 2008. The brain's default network: anatomy, function, and relevance to disease. *Annals of the New York Academy of Sciences*, 1124, pp.1–38.

Buxbaum, J.D. et al., 2002. Association between a GABRB3 polymorphism and autism. *Molecular Psychiatry*, 7(3), pp.311–316.

Callaghan, P.T., Eccles, C.D. & Xia, Y., 1988. NMR microscopy of dynamic displacements: k-space and q-space imaging. *Journal of Physics E: Scientific Instruments*, 21(8), pp.820–822.

Callicott, J.H. & Weinberger, D.R., 2003. Brain imaging as an approach to phenotype characterization for genetic studies of schizophrenia. *Methods in Molecular Medicine*, 77, pp.227–247.

Callicott, J.H. & Weinberger, D.R., 1999. Neuropsychiatric dynamics: the study of mental illness using functional magnetic resonance imaging. *European Journal of Radiology*, 30(2), pp.95–104.

Cannon, T.D. et al., 2002. Cortex mapping reveals regionally specific patterns of genetic and disease-specific gray-matter deficits in twins discordant for schizophrenia. *Proceedings of the National Academy of Sciences of the United States of America*, 99(5), pp.3228–3233.

Cannon, T.D. et al., 2006. Mapping heritability and molecular genetic associations with cortical features using probabilistic brain atlases. *Neuroinformatics*, 4(1), pp.5–19.

Cavanna, A.E. & Trimble, M.R., 2006. The precuneus: a review of its functional anatomy and behavioural correlates. *Brain*, 129(Pt 3), pp.564–583.

Chakrabarti, B. et al., 2009. Genes related to sex steroids, neural growth, and social-emotional behavior are associated with autistic traits, empathy, and Asperger syndrome. *Autism Research*, 2(3), pp.157–177.

Chen, R., Jiao, Y. & Herskovits, E.H., 2011. Structural MRI in autism spectrum disorder. *Pediatric Research*, 69(5 Pt 2), p.63R–8R.

Chiang, M.-C. et al., 2009. Extending genetic linkage analysis to diffusion tensor images to map single gene effects on brain fiber architecture. *Medical Image Computing and Computer-assisted Intervention*, 12(Pt 2), pp.506–513.

Chiang, M.-C. et al., 2011. Genetics of white matter development: a DTI study of 705 twins and their siblings aged 12 to 29. *NeuroImage*, 54(3), pp.2308–2317.

Clemens, B. et al., 2014. Effect of MAOA Genotype on Resting-State Networks in Healthy Participants. *Cerebral Cortex*, In press.

Collins, D.L. et al., 1994. Automatic 3D intersubject registration of MR volumetric data in standardized Talairach space. *Journal of Computer Assisted Tomography*, 18(2), pp.192–205.

Cooper, D. et al., 2014. Multimodal voxel-based meta-analysis of structural and functional magnetic resonance imaging studies in those at elevated genetic risk of developing schizophrenia. *Psychiatry Research*, 221(1), pp.69–77.

Cooper, D.N. et al., 2013. Where genotype is not predictive of phenotype: towards an understanding of the molecular basis of reduced penetrance in human inherited disease. *Human Genetics*, 132(10), pp.1077–1130.

Coulter, D.A., 2001. Epilepsy-associated plasticity in gamma-aminobutyric acid receptor expression, function, and inhibitory synaptic properties. *International Review of Neurobiology*, 45, pp.237–252.

Cowan, W.M., Kopnisky, K.L. & Hyman, S.E., 2002. The human genome project and its impact on psychiatry. *Annual Review of Neuroscience*, 25, pp.1–50.

Culiat, C.T. et al., 1995. Deficiency of the beta 3 subunit of the type A gamma-aminobutyric acid receptor causes cleft palate in mice. *Nature Genetics*, 11(3), pp.344–346.

Damoiseaux, J.S. et al., 2008. Reduced resting-state brain activity in the "default network" in normal aging. *Cerebral Cortex*, 18(8), pp.1856–1864.

Damoiseaux, J.S. et al., 2009. White matter tract integrity in aging and Alzheimer's disease. *Human Brain Mapping*, 30(4), pp.1051–1059.

Danglot, L., Triller, A. & Bessis, A., 2003. Association of gephyrin with synaptic and extrasynaptic GABAA receptors varies during development in cultured hippocampal neurons. *Molecular and Cellular Neurosciences*, 23(2), pp.264–278.

Davidoff, R.A., 1990. The pyramidal tract. *Neurology*, 40(2), pp.332–339.

Debener, S. et al., 2008. Properties of the ballistocardiogram artefact as revealed by EEG recordings at 1.5, 3 and 7 T static magnetic field strength. *International Journal of Psychophysiology*, 67(3), pp.189–199.

Delahanty, R.J. et al., 2011. Maternal transmission of a rare GABRB3 signal peptide variant is associated with autism. *Molecular Psychiatry*, 16(1), pp.86–96.

Delaveau, P. et al., 2010. Dopaminergic modulation of the default mode network in Parkinson's disease. *European Neuropsychopharmacology*, 20(11), pp.784–792.

Dellovade, T.L. et al., 2001. GABA influences the development of the ventromedial nucleus of the hypothalamus. *Journal of Neurobiology*, 49(4), pp.264–276.

DeLorey, T.M. et al., 2008. Gabrb3 gene deficient mice exhibit impaired social and exploratory behaviors, deficits in non-selective attention and hypoplasia of cerebellar vermal lobules: a potential model of autism spectrum disorder. *Behavioural Brain Research*, 187(2), pp.207–220.

DeLorey, T.M., 2005. GABRB3 gene deficient mice: a potential model of autism spectrum disorder. *International Review of Neurobiology*, 71, pp.359–382.

DeLorey, T.M. et al., 1998. Mice lacking the beta3 subunit of the GABAA receptor have the epilepsy phenotype and many of the behavioral characteristics of Angelman syndrome. *The Journal of Neuroscience*, 18(20), pp.8505–8514.

DeLorey, T.M. et al., 2011. Somatosensory and sensorimotor consequences associated with the heterozygous disruption of the autism candidate gene, Gabrb3. *Behavioural Brain Research*, 216(1), pp.36–45.

DeLorey, T.M. & Olsen, R.W., 1999. GABA and epileptogenesis: comparing gabrb3 gene-deficient mice with Angelman syndrome in man. *Epilepsy Research*, 36(2-3), pp.123–132.

Delorme, A. & Makeig, S., 2004. EEGLAB: an open source toolbox for analysis of single-trial EEG dynamics including independent component analysis. *Journal of Neuroscience Methods*, 134(1), pp.9–21.

Dietsche, B. et al., 2014. The impact of a CACNA1C gene polymorphism on learning and hippocampal formation in healthy individuals. *NeuroImage*, 89, pp.256–261.

Diwadkar, V.A. & Keshavan, M.S., 2002. Newer techniques in magnetic resonance imaging and their potential for neuropsychiatric research. *Journal of Psychosomatic Research*, 53(2), pp.677–685.

Donahue, M.J. et al., 2010. Baseline GABA concentration and fMRI response. *NeuroImage*, 53(2), pp.392–398.

Douaud, G. et al., 2007. Anatomically related grey and white matter abnormalities in adolescent-onset schizophrenia. *Brain*, 130(Pt 9), pp.2375–2386.

Dum, R.P. & Strick, P.L., 1996. Spinal cord terminations of the medial wall motor areas in macaque monkeys. *The Journal of Neuroscience*, 16(20), pp.6513–6525.

Duncan, N.W., Wiebking, C., Muoz-Torres, Z., et al., 2014. How to investigate neuro-biochemical relationships on a regional level in humans? Methodological considerations for combining functional with biochemical imaging. *Journal of Neuroscience Methods*, 221, pp.183–188.

Duncan, N.W., Wiebking, C. & Northoff, G., 2014. Associations of regional GABA and glutamate with intrinsic and extrinsic neural activity in humans A review of multimodal imaging studies. *Neuroscience and Biobehavioral Reviews*, 47C, pp.36–52.

El-Hage, W. et al., 2013. Resting-state cerebral blood flow in amygdala is modulated by sex and serotonin transporter genotype. *NeuroImage*, 76, pp.90–97.

Enzi, B. et al., 2012. Glutamate modulates resting state activity in the perigenual anterior cingulate cortex - a combined fMRI-MRS study. *Neuroscience*, 227, pp.102–109.

Van Essen, D.C. et al., 2012. The Human Connectome Project: A data acquisition perspective. *NeuroImage*, 62(4), pp.1–10.

Esslinger, C. et al., 2009. Neural mechanisms of a genome-wide supported psychosis variant. *Science*, 324(5927), p.605.

Evans, A.C. et al., 1992. Anatomical mapping of functional activation in stereotactic coordinate space. *NeuroImage*, 1(1), pp.43–53.

Fatemi, S.H. et al., 2009. GABA(A) receptor downregulation in brains of subjects with autism. *Journal of Autism and Developmental Disorders*, 39(2), pp.223–230.

Ferguson, C. et al., 2007. New insight into the role of the beta3 subunit of the GABAA-R in development, behavior, body weight regulation, and anesthesia revealed by conditional gene knockout. *BMC Neuroscience*, 8, p.85.

Feucht, M. et al., 1999. Possible association between childhood absence epilepsy and the gene encoding GABRB3. *Biological Psychiatry*, 46(7), pp.997–1002.

Filézio, M.R. et al., 2013. Polymorphisms in GABRB3 and oral clefting in the Brazilian population. *DNA and Cell Biology*, 32(3), pp.125–129.

Filippini, N. et al., 2009. Distinct patterns of brain activity in young carriers of the APOE-epsilon4 allele. *Proceedings of the National Academy of Sciences of the United States of America*, 106(17), pp.7209–7214.

Flint, J. & Munafò, M.R., 2007. The endophenotype concept in psychiatric genetics. *Psychological Medicine*, 37(2), pp.163–180.

Forde, N.J. et al., 2014. Structural neuroimaging correlates of allelic variation of the BDNF val66met polymorphism. *NeuroImage*, 90, pp.280–289.

Fox, M.D. et al., 2005. The human brain is intrinsically organized into dynamic, anticorrelated functional networks. *Proceedings of the National Academy of Sciences of the United States of America*, 102(27), pp.9673–9678.

Fox, N.C., Warrington, E.K. & Rossor, M.N., 1999. Serial magnetic resonance imaging of cerebral atrophy in preclinical Alzheimer's disease. *Lancet*, 353(9170), p.2125.

Fransson, P., 2005. Spontaneous low-frequency BOLD signal fluctuations: an fMRI investigation of the resting-state default mode of brain function hypothesis. *Human Brain Mapping*, 26(1), pp.15–29.

Friston, K.J. et al., 1996. Detecting activations in PET and fMRI: levels of inference and power. *NeuroImage*, 4(3 Pt 1), pp.223–235.

Friston, K.J. et al., 1994. Statistical parametric maps in functional imaging: A general linear approach. *Human Brain Mapping*, 2(4), pp.189–210.

Fujii, T. et al., 2014. Association between the common functional FKBP5 variant (rs1360780) and brain structure in a non-clinical population. *Journal of Psychiatric Research*, 58, pp.96–101.

Furman, D.J., Chen, M.C. & Gotlib, I.H., 2011. Variant in oxytocin receptor gene is associated with amygdala volume. *Psychoneuroendocrinology*, 36(6), pp.891–897.

Glahn, D.C. et al., 2010. Genetic control over the resting brain. *Proceedings of the National Academy of Sciences of the United States of America*, 107(3), pp.1223–1228.

Glahn, D.C., Thompson, P.M. & Blangero, J., 2007. Neuroimaging endophenotypes: strategies for finding genes influencing brain structure and function. *Human Brain Mapping*, 28(6), pp.488–501.

Glatt, K., Glatt, H. & Lalande, M., 1997. Structure and organization of GABRB3 and GABRA5. *Genomics*, 41(1), pp.63–69.

Goldman, A.L. et al., 2008. Heritability of brain morphology related to schizophrenia: a large-scale automated magnetic resonance imaging segmentation study. *Biological Psychiatry*, 63(5), pp.475–483.

Goldman, A.L. et al., 2009. Widespread reductions of cortical thickness in schizophrenia and spectrum disorders and evidence of heritability. *Archives of General Psychiatry*, 66(5), pp.467–477.

Good, C.D. et al., 2001. A voxel-based morphometric study of ageing in 465 normal adult human brains. *NeuroImage*, 14(1 Pt 1), pp.21–36.

Gottesman, I.I. & Gould, T.D., 2003. The endophenotype concept in psychiatry: etymology and strategic intentions. *The American Journal of Psychiatry*, 160(4), pp.636–645.

Gottesman, I.I. & Shields, J., 1967. A polygenic theory of schizophrenia. *Proceedings of the National Academy of Sciences of the United States of America*, 58(1), pp.199–205.

Greicius, M.D. et al., 2004. Default-mode network activity distinguishes Alzheimer's disease from healthy aging: evidence from functional MRI. *Proceedings of the National Academy of Sciences of the United States of America*, 101(13), pp.4637–4642.

Greicius, M.D. et al., 2003. Functional connectivity in the resting brain: a network analysis of the default mode hypothesis. *Proceedings of the National Academy of Sciences of the United States of America*, 100(1), pp.253–258.

Greicius, M.D. et al., 2009. Resting-state functional connectivity reflects structural connectivity in the default mode network. *Cerebral Cortex*, 19(1), pp.72–78.

Gruetter, R. & Tkác, I., 2000. Field mapping without reference scan using asymmetric echo-planar techniques. *Magnetic Resonance in Medicine*, 43(2), pp.319–323.

Gurba, K.N. et al., 2012. GABRB3 mutation, G32R, associated with childhood absence epilepsy alters $\alpha 1\beta 3\gamma 2$L γ-aminobutyric acid type A (GABAA) receptor expression and channel gating. *The Journal of Biological Chemistry*, 287(15), pp.12083–12097.

Hagmann, P. et al., 2008. Mapping the structural core of human cerebral cortex. *PLoS Biology*, 6(7), p.e159.

Hahn, A. et al., 2012. Differential modulation of the default mode network via serotonin-1A receptors. *Proceedings of the National Academy of Sciences of the United States of America*, 109(7), pp.2619–2624.

Hallmayer, J. et al., 2011. Genetic heritability and shared environmental factors among twin pairs with autism. *Archives of General Psychiatry*, 68(11), pp.1095–1102.

Hariri, A.R. et al., 2002. Serotonin transporter genetic variation and the response of the human amygdala. *Science*, 297(5580), pp.400–403.

Hariri, A.R. & Weinberger, D.R., 2003. Imaging genomics. *British Medical Bulletin*, 65, pp.259–270.

Hasler, G. et al., 2007. Reduced prefrontal glutamate/glutamine and gamma-aminobutyric acid levels in major depression determined using proton magnetic resonance spectroscopy. *Archives of General Psychiatry*, 64(2), pp.193–200.

Heffner, R.S. & Masterton, R.B., 1983. The role of the corticospinal tract in the evolution of human digital dexterity. *Brain, Behavior and Evolution*, 23(3-4), pp.165–183.

Heitland, I. et al., 2014. Genetic variability in the human cannabinoid receptor 1 is associated with resting state EEG theta power in humans. *Behavioural Brain Research*, 274, pp.344–348.

Hogart, A., Patzel, K.A. & LaSalle, J.M., 2008. Gender influences monoallelic expression of ATP10A in human brain. *Human Genetics*, 124(3), pp.235–242.

Homanics, G.E. et al., 1997. Mice devoid of gamma-aminobutyrate type A receptor beta3 subunit have epilepsy, cleft palate, and hypersensitive behavior. *Proceedings of the National Academy of Sciences of the United States of America*, 94(8), pp.4143–4148.

Honea, R.A. et al., 2008. Is gray matter volume an intermediate phenotype for schizophrenia? A voxel-based morphometry study of patients with schizophrenia and their healthy siblings. *Biological Psychiatry*, 63(5), pp.465–474.

Honea, R.A. et al., 2012. The neuroanatomy of genetic subtype differences in Prader-Willi syndrome. *American Journal of Medical Genetics. Part B, Neuropsychiatric Genetics*, 159B(2), pp.243–253.

Hulshoff Pol, H.E., Schnack, H.G., Posthuma, D., et al., 2006. Genetic contributions to human brain morphology and intelligence. *The Journal of Neuroscience*, 26(40), pp.10235–10242.

Hulshoff Pol, H.E., Schnack, H.G., Mandl, R.C.W., et al., 2006. Gray and white matter density changes in monozygotic and same-sex dizygotic twins discordant for schizophrenia using voxel-based morphometry. *NeuroImage*, 31(2), pp.482–488.

Hyvärinen, A., 1999. Fast and robust fixed-point algorithms for independent component analysis. *IEEE Transactions on Neural Networks*, 10(3), pp.626–634.

Inoue, H. et al., 2008. Association of the GABRB3 gene with nonsyndromic oral clefts. *The Cleft Palate-craniofacial Journal*, 45(3), pp.261–266.

Jacob, T.C. et al., 2005. Gephyrin regulates the cell surface dynamics of synaptic GABAA receptors. *The Journal of Neuroscience*, 25(45), pp.10469–10478.

Jacob, T.C., Moss, S.J. & Jurd, R., 2008. GABA(A) receptor trafficking and its role in the dynamic modulation of neuronal inhibition. *Nature Reviews Neuroscience*, 9(5), pp.331–343.

Jang, S.H., 2014. The corticospinal tract from the viewpoint of brain rehabilitation. *Journal of Rehabilitation Medicine*, 46(3), pp.193–199.

Jatoi, M.A. et al., 2014. EEG based brain source localization comparison of sLORETA and eLORETA. *Australasian physical & engineering sciences in medicine*, 37(4), pp.713–721.

Jenkinson, M. et al., 2002. Improved optimization for the robust and accurate linear registration and motion correction of brain images. *NeuroImage*, 17(2), pp.825–841.

Job, D.E. et al., 2005. Grey matter changes over time in high risk subjects developing schizophrenia. *NeuroImage*, 25(4), pp.1023–1030.

Job, D.E. et al., 2003. Voxel-based morphometry of grey matter densities in subjects at high risk of schizophrenia. *Schizophrenia Research*, 64(1), pp.1–13.

John, B. & Lewis, K.R., 1966. Chromosome variability and geographic distribution in insects. *Science* 152(3723), pp.711–721.

Jones, D.K. et al., 2005. The effect of filter size on VBM analyses of DT-MRI data. *NeuroImage*, 26(2), pp.546–554.

Jones, D.K., Knösche, T.R. & Turner, R., 2013. White matter integrity, fiber count, and other fallacies: the do's and don'ts of diffusion MRI. *NeuroImage*, 73, pp.239–254.

Jones, P. & Cannon, M., 1998. The new epidemiology of schizophrenia. *The Psychiatric Clinics of North America*, 21(1), pp.1–25.

Jung, T.P. et al., 2000. Removing electroencephalographic artifacts by blind source separation. *Psychophysiology*, 37(2), pp.163–178.

Jurd, R. et al., 2003. General anesthetic actions in vivo strongly attenuated by a point mutation in the GABA(A) receptor beta3 subunit. *FASEB Journal*, 17(2), pp.250–252.

Kakeda, S. & Korogi, Y., 2010. The efficacy of a voxel-based morphometry on the analysis of imaging in schizophrenia, temporal lobe epilepsy, and Alzheimer's disease/mild cognitive impairment: a review. *Neuroradiology*, 52(8), pp.711–721.

Kamali, A. et al., 2014. Tracing superior longitudinal fasciculus connectivity in the human brain using high resolution diffusion tensor tractography. *Brain structure & function*, 219(1), pp.269–281.

Kanchibhotla, S.C. et al., 2014. Genetics of microstructure of the corpus callosum in older adults. *PloS One*, 9(12), p.e113181.

Kapogiannis, D. et al., 2013. Posteromedial cortex glutamate and GABA predict intrinsic functional connectivity of the default mode network. *NeuroImage*, 64,

pp.112–119.

Karas, G.B. et al., 2004. Global and local gray matter loss in mild cognitive impairment and Alzheimer's disease. *NeuroImage*, 23(2), pp.708–716.

Karlson, P., 1960. [Nobel prize winners for medicine in 1959 (S. Ochoa and A. Kornberg)]. *Münchener medizinische Wochenschrift (1950)*, 102, pp.94–96.

Kash, T.L., Trudell, J.R. & Harrison, N.L., 2004. Structural elements involved in activation of the gamma-aminobutyric acid type A (GABAA) receptor. *Biochemical Society transactions*, 32(Pt3), pp.540–546.

Ke, Y. et al., 2000. Assessment of GABA concentration in human brain using two-dimensional proton magnetic resonance spectroscopy. *Psychiatry Research*, 100(3), pp.169–178.

Keller, S.S. & Roberts, N., 2008. Voxel-based morphometry of temporal lobe epilepsy: an introduction and review of the literature. *Epilepsia*, 49(5), pp.741–757.

Kim, Y.H. et al., 2011. Neuroimaging in identifying focal cortical dysplasia and prognostic factors in pediatric and adolescent epilepsy surgery. *Epilepsia*, 52(4), pp.722–727.

Klei, L. et al., 2012. Common genetic variants, acting additively, are a major source of risk for autism. *Molecular Autism*, 3(1), p.9.

Knyazev, G.G., 2007. Motivation, emotion, and their inhibitory control mirrored in brain oscillations. *Neuroscience and Biobehavioral Reviews*, 31(3), pp.377–395.

Kochunov, P., et al., 2010a. Genetics of microstructure of cerebral white matter using diffusion tensor imaging. *NeuroImage*, 53(3), pp.1109–1116.

Kochunov, P., et al., 2010b. Genetics of primary cerebral gyrification: Heritability of length, depth and area of primarysulci in an extended pedigree of

Papio baboons. *NeuroImage*, 53(3), pp.1126–1134.

Kochunov, P. et al., 2009. Loss of cerebral white matter structural integrity tracks the gray matter metabolic decline in normal aging. *NeuroImage*, 45(1), pp.17–28.

Koten, J.W. et al., 2009. Genetic contribution to variation in cognitive function: an FMRI study in twins. *Science*, 323(5922), pp.1737–1740.

Krystal, J.H. et al., 2006. Gamma-aminobutyric acid type A receptors and alcoholism: intoxication, dependence, vulnerability, and treatment. *Archives of General Psychiatry*, 63(9), pp.957–968.

Lachance-Touchette, P. et al., 2010. Screening of GABRB3 in French-Canadian families with idiopathic generalized epilepsy. *Epilepsia*, 51(9), pp.1894–1897.

Lancaster, J.L. et al., 2000. Automated Talairach atlas labels for functional brain mapping. *Human Brain Mapping*, 10(3), pp.120–131.

Lander, E.S. et al., 2001. Initial sequencing and analysis of the human genome. *Nature*, 409(6822), pp.860–921.

Laufs, H., 2012. A personalized history of EEG-fMRI integration. *NeuroImage*, 62(2), pp.1056–1067.

Laurie, D.J., Wisden, W. & Seeburg, P.H., 1992. The distribution of thirteen GABAA receptor subunit mRNAs in the rat brain. III. Embryonic and postnatal development. *The Journal of Neuroscience*, 12(11), pp.4151–4172.

Lawrie, S.M. et al., 2001. Brain structure, genetic liability, and psychotic symptoms in subjects at high risk of developing schizophrenia. *Biological Psychiatry*, 49(10), pp.811–823.

Leboyer, M. et al., 1998. Psychiatric genetics: search for phenotypes. *Trends in Neurosciences*, 21(3), pp.102–105.

Lee, T.-W. et al., 2012a. The influence of apolipoprotein E Epsilon4 polymorphism on qEEG profiles in healthy young females: a resting EEG study. *Brain Topography*, 25(4), pp.431–442.

Lee, T.-W. et al., 2012b. The influence of dopamine receptor d4 polymorphism on resting EEG in healthy young females. *The Open Neuroimaging Journal*, 6, pp.19–25.

Lee, T.W., Girolami, M. & Sejnowski, T.J., 1999. Independent component analysis using an extended infomax algorithm for mixed subgaussian and supergaussian sources. *Neural Computation*, 11(2), pp.417–441.

Leech, R. & Sharp, D.J., 2014. The role of the posterior cingulate cortex in cognition and disease. *Brain*, 137(Pt 1), pp.12–32.

Leemans, A. & Jones, D.K., 2009. The B-matrix must be rotated when correcting for subject motion in DTI data. *Magnetic Resonance in Medicine*, 61(6), pp.1336–1349.

Lehtovirta, M. et al., 1996. Spectral analysis of EEG in Alzheimer's disease: relation to apolipoprotein E polymorphism. *Neurobiology of Aging*, 17(4), pp.523–526.

Lewis, D.A. & Gonzalez-Burgos, G., 2006. Pathophysiologically based treatment interventions in schizophrenia. *Nature Medicine*, 12(9), pp.1016–1022.

Li, J., Zhang, Z. & Shang, H., 2012. A meta-analysis of voxel-based morphometry studies on unilateral refractory temporal lobe epilepsy. *Epilepsy Research*, 98(2-3), pp.97–103.

Li, Y. et al., 2006. Automatic removal of the eye blink artifact from EEG using an ICA-based template matching approach. *Physiological measurement*, 27(4), pp.425–436.

Lin, Y. et al., 2012. Investigating the metabolic changes due to visual stimulation using functional proton magnetic resonance spectroscopy at 7 T. *Journal*

of Cerebral Blood Flow and Metabolism, 32(8), pp.1484–1495.

Loo, S.K. et al., 2003. Functional effects of the DAT1 polymorphism on EEG measures in ADHD. *Journal of the American Academy of Child and Adolescent Psychiatry*, 42(8), pp.986–993.

Macdonald, R.L., Kang, J.-Q. & Gallagher, M.J., 2010. Mutations in GABAA receptor subunits associated with genetic epilepsies. *The Journal of Physiology*, 588(Pt 11), pp.1861–1869.

Maggioni, E. et al., 2014. Removal of Pulse Artefact from EEG Data Recorded in MR Environment at 3T. Setting of ICA Parameters for Marking Artefactual Components: Application to Resting-State Data. *PloS One*, 9(11), p.e112147.

Maier, M.A. et al., 2002. Differences in the corticospinal projection from primary motor cortex and supplementary motor area to macaque upper limb motoneurons: an anatomical and electrophysiological study. *Cerebral Cortex*, 12(3), pp.281–296.

Makeig, S. et al., 1997. Blind separation of auditory event-related brain responses into independent components. *Proceedings of the National Academy of Sciences of the United States of America*, 94(20), pp.10979–10984.

Markett, S. et al., 2013. The dopamine D2 receptor gene DRD2 and the nicotinic acetylcholine receptor gene CHRNA4 interact on striatal gray matter volume. *NeuroImage*, 64, pp.167–172.

Martinez, D., Broft, A. & Laruelle, M., 2001. Imaging neurochemical endophenotypes: promises and pitfalls. *Pharmacogenomics*, 2(3), pp.223–237.

Matura, S. et al., 2014. Differential effects of the ApoE4 genotype on brain structure and function. *NeuroImage*, 89, pp.81–91.

Maudsley, A.A. et al., 2005. Numerical simulation of PRESS localized MR spectroscopy. *Journal of Magnetic Resonance*, 173(1), pp.54–63.

Mazzotti, D.R. et al., 2012. Adenosine deaminase polymorphism affects sleep EEG spectral power in a large epidemiological sample. *PloS One*, 7(8), p.e44154.

McDonald, C. et al., 2006. Regional brain morphometry in patients with schizophrenia or bipolar disorder and their unaffected relatives. *The American Journal of Psychiatry*, 163(3), pp.478–487.

McGibney, G. & Smith, M.R., 1993. An unbiased signal-to-noise ratio measure for magnetic resonance images. *Medical Physics*, 20(4), pp.1077–1078.

Menke, R.A. et al., 2009. MRI characteristics of the substantia nigra in Parkinson's disease: a combined quantitative T1 and DTI study. *NeuroImage*, 47(2), pp.435–441.

Mesulam, M.M., 1998. From sensation to cognition. *Brain*, 121(Pt 6), pp.1013–1052.

Meyer-Lindenberg, A. et al., 2008. False positives in imaging genetics. *NeuroImage*, 40(2), pp.655–661.

Meyer-Lindenberg, A., 2012. The future of fMRI and genetics research. *NeuroImage*, 62(2), pp.1286–1292.

Mier, D., Kirsch, P. & Meyer-Lindenberg, A., 2010. Neural substrates of pleiotropic action of genetic variation in COMT: a meta-analysis. *Molecular Psychiatry*, 15(9), pp.918–927.

Miller, A.J. & Joseph, P.M., 1993. The use of power images to perform quantitative analysis on low SNR MR images. *Magnetic Resonance Imaging*, 11(7), pp.1051–1056.

Miralles, C.P. et al., 1999. Immunocytochemical localization of the beta(3) subunit of the gamma-aminobutyric acid(A) receptor in the rat brain. *The Journal of Comparative Neurology*, 413(4), pp.535–548.

Mullinger, K.J., Havenhand, J. & Bowtell, R., 2013. Identifying the sources

of the pulse artefact in EEG recordings made inside an MR scanner. *NeuroImage*, 71, pp.75–83.

Munafò, M.R., Attwood, A.S. & Flint, J., 2008. Bias in genetic association studies: effects of research location and resources. *Psychological Medicine*, 38(8), pp.1213–1214.

Muthukumaraswamy, S.D. et al., 2009. Resting GABA concentration predicts peak gamma frequency and fMRI amplitude in response to visual stimulation in humans. *Proceedings of the National Academy of Sciences of the United States of America*, 106(20), pp.8356–8361.

Mutirangura, A. et al., 1992. Dinucleotide repeat polymorphism at the GABAA receptor beta 3 (GABRB3) locus in the Angelman/Prader - Willi region (AS/PWS) of chromosome 15. *Human Molecular Genetics*, 1(1), p.67.

Napolitano, A., Kockenberger, W. & Auer, D.P., 2013. Reliable gamma aminobutyric acid measurement using optimized PRESS at 3 T. *Magnetic Resonance in Medicine*, 69(6), pp.1528–1533.

Neil, J. et al., 2002. Diffusion tensor imaging of normal and injured developing human brain - a technical review. *NMR in Biomedicine*, 15(7-8), pp.543–552.

Neuner, I. et al., 2014. Simultaneous EEG-fMRI acquisition at low, high and ultra-high magnetic fields up to 9.4T: Perspectives and challenges. *NeuroImage*, 102, pp.71–9.

Neuner, I. et al., 2010. White-matter abnormalities in Tourette syndrome extend beyond motor pathways. *NeuroImage*, 51(3), pp.1184–1193.

Niazy, R.K. et al., 2005. Removal of FMRI environment artifacts from EEG data using optimal basis sets. *NeuroImage*, 28(3), pp.720–737.

Noble, E.P. et al., 1998. D2 dopamine receptor and GABA(A) receptor beta3 subunit genes and alcoholism. *Psychiatry Research*, 81(2), pp.133–147.

Northoff, G. et al., 2007. GABA concentrations in the human anterior cingulate cortex predict negative BOLD responses in fMRI. *Nature Neuroscience*, 10(12), pp.1515–1517.

Nuwer, M.R. et al., 1999. IFCN standards for digital recording of clinical EEG. The International Federation of Clinical Neurophysiology. *Electroencephalography and Clinical Neurophysiology. Supplement*, 52, pp.11–14.

Oldfield, R.C., 1971. The assessment and analysis of handedness: the Edinburgh inventory. *Neuropsychologia*, 9(1), pp.97–113.

Olsen, R.W. & Sieghart, W., 2008. International Union of Pharmacology. LXX. Subtypes of gamma-aminobutyric acid(A) receptors: classification on the basis of subunit composition, pharmacology, and function. Update. *Pharmacological Reviews*, 60(3), pp.243–260.

Oostenveld, R. & Praamstra, P., 2001. The five percent electrode system for high-resolution EEG and ERP measurements. *Clinical Neurophysiology*, 112(4), pp.713–719.

Pascual-Marqui, R.D., Michel, C.M. & Lehmann, D., 1994. Low resolution electromagnetic tomography: a new method for localizing electrical activity in the brain. *International Journal of Psychophysiology*, 18(1), pp.49–65.

Peters, S.U. et al., 2011. Alterations in white matter pathways in Angelman syndrome. *Developmental Medicine and Child Neurology*, 53(4), pp.361–367.

Petrides, M. & Pandya, D.N., 2002. Comparative cytoarchitectonic analysis of the human and the macaque ventrolateral prefrontal cortex and corticocortical connection patterns in the monkey. *The European Journal of Neuroscience*, 16(2), pp.291–310.

Pirker, S. et al., 2000. GABA(A) receptors: immunocytochemical distribution of 13 subunits in the adult rat brain. *Neuroscience* 101(4), pp.815–850.

Pizzarelli, R. & Cherubini, E., 2011. Alterations of GABAergic signaling in

autism spectrum disorders. *Neural Plasticity*, 2011, p.297153.

Poline, J.-B. & Brett, M., 2012. The general linear model and fMRI: does love last forever? *NeuroImage*, 62(2), pp.871–880.

Price, S. et al., 2004. Voxel-based morphometry detects patterns of atrophy that help differentiate progressive supranuclear palsy and Parkinson's disease. *NeuroImage*, 23(2), pp.663–669.

Provencher, S.W., 2001. Automatic quantitation of localized in vivo 1H spectra with LCModel. *NMR in Biomedicine*, 14(4), pp.260–264.

Qiu, A. et al., 2010. Hippocampal-cortical structural connectivity disruptions in schizophrenia. *NeuroImage*, 52(4), pp.1181–1189.

Quarantelli, M. et al., 2013. Default-mode network changes in Huntington's disease: an integrated MRI study of functional connectivity and morphometry. *PloS One*, 8(8), p.e72159.

Raichle, M.E. et al., 2001. A default mode of brain function. *Proceedings of the National Academy of Sciences of the United States of America*, 98(2), pp.676–682.

Raichle, M.E. & Snyder, A.Z., 2007. A default mode of brain function: a brief history of an evolving idea. *NeuroImage*, 37(4), pp.1083–1089.

Rao, H. et al., 2007. Genetic variation in serotonin transporter alters resting brain function in healthy individuals. *Biological Psychiatry*, 62(6), pp.600–606.

Rasheed, T. et al., 2009. Attenuation of artifacts in EEG signals measured inside an MRI scanner using constrained independent component analysis. *Physiological Measurement*, 30(4), pp.387–404.

Reveley, A.M. et al., 1982. Cerebral ventricular size in twins discordant for schizophrenia. *Lancet*, 1(8271), pp.540–541.

Reveley, A.M., Reveley, M.A. & Murray, R.M., 1984. Cerebral ventricular enlargement in non-genetic schizophrenia: a controlled twin study. *The British Journal of Psychiatry*, 144, pp.89–93.

Ridgway, G.R. et al., 2008. Ten simple rules for reporting voxel-based morphometry studies. *NeuroImage*, 40(4), pp.1429–1435.

Rijsdijk, F. V et al., 2005. Brain MRI abnormalities in schizophrenia: same genes or same environment? *Psychological Medicine*, 35(10), pp.1399–1409.

Roosendaal, S.D. et al., 2009. Regional DTI differences in multiple sclerosis patients. *NeuroImage*, 44(4), pp.1397–1403.

Rosenberg, R.N., 2007. *The Molecular and Genetic Basis of Neurologic and Psychiatric Disease*, 4th ed. London: Lippincott Williams & Wilkins.

Rudolph, U. & Möhler, H., 2004. Analysis of GABAA receptor function and dissection of the pharmacology of benzodiazepines and general anesthetics through mouse genetics. *Annual Review of Pharmacology and Toxicology*, 44, pp.475–498.

Rueckert, D. et al., 1999. Nonrigid registration using free-form deformations: application to breast MR images. *IEEE Transactions on Medical Imaging*, 18(8), pp.712–721.

Saitoh, S. et al., 1992. Familial Angelman syndrome caused by imprinted submicroscopic deletion encompassing GABAA receptor beta 3-subunit gene. *Lancet*, 339(8789), pp.366–367.

Sanacora, G. et al., 2004. Subtype-specific alterations of gamma-aminobutyric acid and glutamate in patients with major depression. *Archives of General Psychiatry*, 61(7), pp.705–713.

Saunders, A.M. et al., 1993. Apolipoprotein E epsilon 4 allele distributions in late-onset Alzheimer's disease and in other amyloid-forming diseases. *Lancet*, 342(8873), pp.710–711.

Scapoli, L. et al., 2002. Linkage disequilibrium between GABRB3 gene and nonsyndromic familial cleft lip with or without cleft palate. *Human Genetics*, 110(1), pp.15–20.

Schaller, B. et al., 2014. Are glutamate and lactate increases ubiquitous to physiological activation? A (1)H functional MR spectroscopy study during motor activation in human brain at 7Tesla. *NeuroImage*, 93(Pt 1), pp.138–145.

Schmahmann, J.D. et al., 2008. Cerebral white matter: neuroanatomy, clinical neurology, and neurobehavioral correlates. *Annals of the New York Academy of Sciences*, 1142, pp.266–309.

Van der Schot, A.C. et al., 2009. Influence of genes and environment on brain volumes in twin pairs concordant and discordant for bipolar disorder. *Archives of General Psychiatry*, 66(2), pp.142–151.

Schroer, R.J. et al., 1998. Autism and maternally derived aberrations of chromosome 15q. *American Journal of Medical Genetics*, 76(4), pp.327–336.

Schutte, N.M. et al., 2013. Heritability of resting state EEG functional connectivity patterns. *Twin Research and Human Genetics*, 16(5), pp.962–969.

Selvaraj, S. et al., 2012. Grey matter differences in bipolar disorder: a meta-analysis of voxel-based morphometry studies. *Bipolar Disorders*, 14(2), pp.135–145.

Seunarine, K.K. & Alexander, D.C., 2014. 'Multiple Fibers: Beyond the Diffusion Tensor' in *Diffusion MRI*, 2nd edn, Elsevier, pp.105–123.

Shah, N.J. et al., 2013. Advances in multimodal neuroimaging: hybrid MR-PET and MR-PET-EEG at 3 T and 9.4 T. *Journal of Magnetic Resonance*, 229, pp.101–115.

Shao, Y. et al., 2003. Fine mapping of autistic disorder to chromosome 15q11-q13 by use of phenotypic subtypes. *American Journal of Human Genetics*, 72(3), pp.539–548.

Sheline, Y.I. et al., 2010. APOE4 allele disrupts resting state fMRI connectivity in the absence of amyloid plaques or decreased CSF Aβ42. *The Journal of Neuroscience*, 30(50), pp.17035–17040.

Shorvon, S.D., 2011. The causes of epilepsy: changing concepts of etiology of epilepsy over the past 150 years. *Epilepsia*, 52(6), pp.1033–1044.

Smit, D.J.A. et al., 2008. Heritability of "small-world" networks in the brain: a graph theoretical analysis of resting-state EEG functional connectivity. *Human Brain Mapping*, 29(12), pp.1368–1378.

Smith, S.A. et al., 1994. Computer Simulations in Magnetic Resonance. An Object-Oriented Programming Approach. *Journal of Magnetic Resonance*, Series A, 106(1), pp.75–105.

Smith, S.M. et al., 2004. Advances in functional and structural MR image analysis and implementation as FSL. *NeuroImage*, 23(Suppl 1), pp.S208–S219.

Smith, S.M. et al., 2009. Correspondence of the brain's functional architecture during activation and rest. *Proceedings of the National Academy of Sciences of the United States of America*, 106(31), pp.13040–13045.

Smith, S.M., 2002. Fast robust automated brain extraction. *Human Brain Mapping*, 17(3), pp.143–155.

Smith, S.M. et al., 2006. Tract-based spatial statistics: voxelwise analysis of multi-subject diffusion data. *NeuroImage*, 31(4), pp.1487–1505.

Snyder, A.Z. & Raichle, M.E., 2012. A brief history of the resting state: The Washington University perspective. *NeuroImage*, 62(2), pp.1–9.

Soher, B.J. et al., 1996. Quantitative proton MR spectroscopic imaging of the human brain. *Magnetic Resonance in Medicine*, 35(3), pp.356–363.

Sorg, C. et al., 2007. Selective changes of resting-state networks in individuals

at risk for Alzheimer's disease. *Proceedings of the National Academy of Sciences of the United States of America*, 104(47), pp.18760–18765.

Sturtevant, A.H., 1965. *A History of Genetics (Reprinted 2001)*, New York: Cold Spring Harbor Laboratory Press.

Suddath, R.L. et al., 1990. Anatomical abnormalities in the brains of monozygotic twins discordant for schizophrenia. *The New England Journal of Medicine*, 322(12), pp.789–794.

Takao, H., Hayashi, N. & Ohtomo, K., 2011. White matter asymmetry in healthy individuals: a diffusion tensor imaging study using tract-based spatial statistics. *Neuroscience* 193, pp.291–299.

Tanaka, M. et al., 2012. GABRB3, 'Epilepsy, and Neurodevelopment' in *Jasper's Basic Mechanisms of the Epilepsies*, 4th edn. National Center for Biotechnology Information (US).

Thompson, P.M., Martin, N.G. & Wright, M.J., 2010. Imaging genomics. *Current Opinion in Neurology*, 23(4), pp.368–373.

Tian, T. et al., 2013. Catechol-O-methyltransferase Val158Met polymorphism modulates gray matter volume and functional connectivity of the default mode network. *PloS One*, 8(10), p.e78697.

Tiwari, V.N. et al., 2012. Relationship between aberrant brain connectivity and clinical features in Angelman Syndrome: a new method using tract based spatial statistics of DTI color-coded orientation maps. *NeuroImage*, 59(1), pp.349–355.

Tomasi, D. & Volkow, N.D., 2010. Functional connectivity density mapping. *Proceedings of the National Academy of Sciences of the United States of America*, 107(21), pp.9885–9890.

Trachtenberg, A.J. et al., 2012. The effects of APOE on the functional architecture of the resting brain. *NeuroImage*, 59(1), pp.565–572.

Tretter, V. et al., 1997. Stoichiometry and assembly of a recombinant GABAA receptor subtype. *The Journal of Neuroscience*, 17(8), pp.2728–2737.

Ullsperger, M. & Debener, S., 2010. *Simultaneous EEG and fMRI: Recording, Analysis, and Application*, Oxford University Press, Oxford.

Vanderperren, K. et al., 2010. Removal of BCG artifacts from EEG recordings inside the MR scanner: a comparison of methodological and validation-related aspects. *NeuroImage*, 50(3), pp.920–934.

Venter, J.C. et al., 2001. The sequence of the human genome. *Science*, 291(5507), pp.1304–1351.

Vogt, B.A., Finch, D.M. & Olson, C.R., 1992. Functional heterogeneity in cingulate cortex: the anterior executive and posterior evaluative regions. *Cerebral Cortex*, 2(6), pp.435–443.

Vogt, B.A. & Laureys, S., 2005. Posterior cingulate, precuneal and retrosplenial cortices: cytology and components of the neural network correlates of consciousness. *Progress in Brain Research*, 150, pp.205–217.

Wacker, J. & Gatt, J.M., 2010. Resting posterior versus frontal delta/theta EEG activity is associated with extraversion and the COMT VAL158MET polymorphism. *Neuroscience Letters*, 478(2), pp.88–92.

Wagstaff, J. et al., 1991. Localization of the gene encoding the GABAA receptor beta 3 subunit to the Angelman/Prader-Willi region of human chromosome 15. *American Journal of Human Genetics*, 49(2), pp.330–337.

Wallner, M., Hanchar, H.J. & Olsen, R.W., 2003. Ethanol enhances alpha 4 beta 3 delta and alpha 6 beta 3 delta gamma-aminobutyric acid type A receptors at low concentrations known to affect humans. *Proceedings of the National Academy of Sciences of the United States of America*, 100(25), pp.15218–15223.

Wang, D. et al., 2013. KIBRA gene variants are associated with synchronization within the default-mode and executive control networks. *NeuroImage*, 69,

pp.213–222.

Wang, L. et al., 2012. Alzheimer disease family history impacts resting state functional connectivity. *Annals of Neurology*, 72(4), pp.571–577

Warrier, V., Baron-Cohen, S. & Chakrabarti, B., 2013. Genetic variation in GABRB3 is associated with Asperger syndrome and multiple endophenotypes relevant to autism. *Molecular Autism*, 4(1), p.48.

Wedeen, V.J. et al., 2005. Mapping complex tissue architecture with diffusion spectrum magnetic resonance imaging. *Magnetic Resonance in Medicine*, 54(6), pp.1377–1386.

Weinberger, D.R. et al., 1981. Familial aspects of CT scan abnormalities in chronic schizophrenic patients. *Psychiatry Research*, 4(1), pp.65–71.

Weinberger, D.R. et al., 2001. Prefrontal neurons and the genetics of schizophrenia. *Biological Psychiatry*, 50(11), pp.825–844.

Werner, C.J. et al., 2014. Altered resting-state connectivity in Huntington's disease. *Human Brain Mapping*, 35(6), pp.2582–2593.

Whitfield-Gabrieli, S. et al., 2009. Hyperactivity and hyperconnectivity of the default network in schizophrenia and in first-degree relatives of persons with schizophrenia. *Proceedings of the National Academy of Sciences of the United States of America*, 106(4), pp.1279–1284.

Wilson, B.J. et al., 2011. Abnormal language pathway in children with Angelman syndrome. *Pediatric Nneurology*, 44(5), pp.350–356.

Winkler, A.M. et al., 2010. Cortical thickness or grey matter volume? The importance of selecting the phenotype for imaging genetics studies. *NeuroImage*, 53(3), pp.1135–1146.

Wittchen, H.-U. & Pfister, H., 1997. *DIA-X-Interviews: Manual für Screening-Verfahren und Interview; Interviewheft.* Frankfurt: Swets & Zeitlinger.

Worsley, K.J. et al., 1996. A unified statistical approach for determining significant signals in images of cerebral activation. *Human Brain Mapping*, 4(1), pp.58–73.

Wright, I.C. et al., 1995. A voxel-based method for the statistical analysis of gray and white matter density applied to schizophrenia. *NeuroImage*, 2(4), pp.244–252.

Yang, A.C. et al., 2014. The APOE ϵ4 allele affects complexity and functional connectivity of resting brain activity in healthy adults. *Human Brain Mapping*, 35(7), pp.3238–3248.

Yang, J. et al., 2012. Voxelwise meta-analysis of gray matter anomalies in Alzheimer's disease and mild cognitive impairment using anatomic likelihood estimation. *Journal of the Neurological Sciences*, 316(1-2), pp.21–29.

Yoon, U. et al., 2011. Genetic and environmental influences on structural variability of the brain in pediatric twin: deformation based morphometry. *Neuroscience Letters*, 493(1-2), pp.8–13.

York, D.H., 1987. Review of descending motor pathways involved with transcranial stimulation. *Neurosurgery*, 20(1), pp.70–73.

Zeller, A. et al., 2007a. Identification of a molecular target mediating the general anesthetic actions of pentobarbital. *Molecular Pharmacology*, 71(3), pp.852–859.

Zeller, A. et al., 2007b. Mapping the contribution of beta3-containing GABAA receptors to volatile and intravenous general anesthetic actions. *BMC Pharmacology*, 7, p.2.

Zou, Q. et al., 2009. Static and dynamic characteristics of cerebral blood flow during the resting state. *NeuroImage*, 48(3), pp.515–524.